

Spring 2019

Suspended Sediment and Particulate Matter Transport in Mississippi Sound and Bight Assessed with Physical Modeling, Remote Sensing and In Situ Measurements

Stephan O'Brien
University of Southern Mississippi

Follow this and additional works at: <https://aquila.usm.edu/dissertations>



Part of the [Oceanography Commons](#)

Recommended Citation

O'Brien, Stephan, "Suspended Sediment and Particulate Matter Transport in Mississippi Sound and Bight Assessed with Physical Modeling, Remote Sensing and In Situ Measurements" (2019). *Dissertations*. 1665.

<https://aquila.usm.edu/dissertations/1665>

This Dissertation is brought to you for free and open access by The Aquila Digital Community. It has been accepted for inclusion in Dissertations by an authorized administrator of The Aquila Digital Community. For more information, please contact Joshua.Cromwell@usm.edu.

SUSPENDED SEDIMENT AND PARTICULATE MATTER TRANSPORT IN
MISSISSIPPI SOUND AND BIGHT ASSESSED WITH PHYSICAL MODELING,
REMOTE SENSING AND IN SITU MEASUREMENTS

by

Stephan Joel Myron O'Brien

A Dissertation
Submitted to the Graduate School,
the College of Arts and Sciences
and the School of Ocean Science and Engineering
at The University of Southern Mississippi
in Partial Fulfillment of the Requirements
for the Degree of Doctor of Philosophy

Approved by:

Dr. Jerry D. Wiggert, Committee Chair
Dr. Gregory A. Carter
Dr. Ian Church
Dr. Scott P. Milroy
Dr. Davin J. Wallace

Dr. Jerry D. Wiggert
Committee Chair

Dr. Jerry D. Wiggert
Associate Director of
School

Dr. Karen S. Coats
Dean of the Graduate School

May 2019

COPYRIGHT BY

Stephan Joel Myron O'Brien

2019

Published by the Graduate School



ABSTRACT

Tidal passes between Mississippi Sound (MS Sound) and Mississippi Bight (MS Bight) act as a transport pathway for the exchange of estuarine discharge and suspended particulate matter. A better understanding of sediment and particulate matter exchange can provide insights into turbidity, nutrient supply and aquatic ecosystem health for the region. This work examined the effects of different forcing factors (e.g. wind and tides) on the advection of suspended sediments and particulate matter in the study area.

Fieldwork included particle size distribution, Acoustic Doppler Current Profiler (ADCP) and conductivity-temperature-depth measurements in the MS Sound and MS Bight from summer 2015 through summer 2016 with the aim being to characterize the seasonal distribution of suspended sediments and particulate matter. A Moderate Resolution Imaging Spectroradiometer 645-nm suspended particulate matter anomaly (SPMa) expanded the spatial scale of the field measurements and extended the temporal coverage from winter 2014 to fall 2016. The physical and sediment component of a regional numerical model in addition to the ADCP's echo intensity were calibrated using in situ suspended sediment concentration (SSC), temperature, salinity and particle size data. SSC and SPMa were the final output of the model and remote sensing analysis used to investigate the exchange/transport of suspended sediments and particulate matter from the MS Sound to the MS Bight through the passes. Results provided information on changes in SSC/SPMa and timescales of the exchange. The exchange of coastal waters through the passes and the resulting shoreward advection of high salinity bottom water during a cold front caused increased SSC in MS Bight. The horizontal density gradient between the MS Sound and MS Bight in spring drives particulate matter exchange in the

surface water on a time scale of weeks. The results in this study have implications for pollutants transported by suspended sediments and particulate matter in the MS Sound and MS Bight.

ACKNOWLEDGMENTS

I am grateful for the support and guidance provided by my advisor, Dr. Jerry Wiggert. I would also like to thank my committee members, Dr. Gregory Carter, Dr. Ian Church, Dr. Scott Milroy and Dr. Davin Wallace for their advice throughout my dissertation research.

My study has benefitted from the assistance of the CONSortium for oil spill exposure pathways in Coastal River-Dominated Ecosystem research group.

This work would not have been possible without the funding provided by CONCORDE, Gulf of Mexico Research Initiative, The University of Southern Mississippi, National Science Foundation Established Program to Simulate Competitive Research, Mississippi Based RESTORE Act Center of Excellence, Environmental Protection Agency, Mississippi Department of Marine Resources, United States Geologic Survey and Marine Technology Society.

DEDICATION

I dedicate this dissertation to my parents, Hansen O'Brien and Carol Wren-O'Brien who have been a constant and invaluable source of support and encouragement.

TABLE OF CONTENTS

ABSTRACT ii

ACKNOWLEDGMENTS iv

DEDICATION v

LIST OF TABLES xv

LIST OF ILLUSTRATIONS xvi

LIST OF ABBREVIATIONS xxiii

CHAPTER I 1

 1.1 Introduction 1

 1.1.1 Sediment Transport 1

 1.1.2 Study Area 4

 1.1.3 Sediment and Particulate Matter Sources in the Study Area 6

 1.1.4 Transport Pathways in the Study Area 7

 1.2 Research Objectives 10

 1.3 Hypotheses 11

CHAPTER II 12

 2.1 Abstract 12

 2.2 Introduction 12

 2.3 Data and Methods 17

 2.3.1 Data 17

2.3.1.1 Coastal Relief Model	17
2.3.1.2 National Centers for Environmental Information Digital Elevation Models	17
2.3.1.3 National Ocean Service Hydrographic Surveys	19
2.3.2 Methods.....	20
2.3.2.1 Ingestion of NGCHC DEMs (Stage 1 Build)	20
2.3.2.2 Ingestion of NOS Surveys (Stage 2 Build).....	23
2.3.2.3 Assessment of BDDEM.....	26
2.4 Conclusion	30
CHAPTER III	31
3.1 Abstract.....	31
3.2 Introduction.....	31
3.3 Data and Methods	36
3.3.1 Data.....	36
3.3.1.1 Cruise and Sampling.....	36
3.3.2 Methods.....	37
3.3.2.1 In Situ Ichthyoplankton Imaging System	37
3.3.2.2 Scanfish.....	38
3.3.2.3 Hydrodynamic Model.....	38
3.3.2.4 Atmospheric Model	39

3.3.2.5 Wave Model.....	40
3.3.2.6 Sediment Model.....	40
3.3.2.7 National Data Buoy Center Buoy.....	42
3.3.2.8 Taylor Diagram.....	42
3.4 Results.....	43
3.4.1 Atmospheric and Wave Observations.....	43
3.4.2 In Situ Ichthyoplankton Imaging System and Scanfish in situ Observations..	44
3.4.3 Synthesis Model Verification.....	48
3.4.4 Synthesis Model Results: prefront to post front conditions.....	58
3.5 Discussion.....	62
3.6 Conclusion.....	66
CHAPTER IV.....	67
4.1 Abstract.....	67
4.2 Introduction.....	68
4.3 Data and Methods.....	70
4.3.1 Data.....	70
4.3.1.1 Cruise and Sampling.....	70
4.3.1.2 Remote Sensing MODIS Aqua Level 1 Files.....	73
4.3.1.3 Historical in situ and CONCORDE Synthesis Model Data.....	73
4.3.2 Methods.....	74

4.3.2.1 In situ Suspended Particulate Matter Concentration.....	74
4.3.2.2 LISST and CTD Data Processing	74
4.3.2.3 LISST Measurement Errors	75
4.3.2.4 Remote Sensing Suspended Particulate Matter Anomaly	75
4.4 Results.....	78
4.4.1 Characterization of Suspended Particulate Matter in MS Sound during winter, spring and summer using in situ CTD, SPM and LISST data	78
4.4.1.1 Summer 2015	78
4.4.1.2 Winter 2015	80
4.4.1.3 Spring 2016.....	84
4.4.1.4 Summer 2016.....	86
4.4.2 Characterization of Suspended Particulate Matter at the passes and MS Bight during winter, spring and summer using a remote sensing SPM algorithm	88
4.4.2.1 Main Pass	88
4.4.2.2 Petit Bois Pass.....	90
4.4.2.3 Horn Island Pass	92
4.4.2.4 Dog Key Pass	94
4.4.2.5 Ship Island Pass	96
4.4.2.6 MS Sound.....	97
4.5 Discussion.....	98

4.5.1 Characterization of Suspended Sediments in MS Sound during winter, spring and summer using in situ CTD, SPM and LISST data	98
4.5.1.1 Summer 2015	98
4.5.1.2 Winter 2015	99
4.5.1.3 Spring 2016.....	104
4.5.1.4 Summer 2016.....	106
4.5.2 Characterization of Suspended Particulate Matter at the passes and MS Bight during winter, spring and summer using a remote sensing algorithm	109
4.5.2.1 Main Pass	109
4.5.2.2 Petit Bois Pass.....	110
4.5.2.3 Horn Island Pass	112
4.5.2.4 Dog Key Pass	113
4.5.2.5 Ship Island Pass	114
4.5.2.6 Main Pass: summer 2015 and summer 2016	115
4.5.2.7 Horn Island Pass, Dog Key Pass and Ship Island Pass: summer 2015 and summer 2016.....	116
4.6 Conclusion	117
4.6.1 Characterization of Suspended Sediments in MS Sound during winter, spring and summer using in situ CTD, SPM and LISST data	117

4.6.2 Characterization of Suspended Particulate Matter at the passes and MS Bight during winter, spring and summer using a remote sensing algorithm	118
CHAPTER V	120
5.1 Abstract	120
5.2 Introduction.....	120
5.3 Data and Methods	122
5.3.1 Data	122
5.3.1.1 Cruise and Sampling.....	122
5.3.1.2 ADCP and Line Moorings	124
5.3.1.3 Historical in situ and CONCORDE Synthesis Model Data.....	125
5.3.2 Methods.....	125
5.3.2.1 In situ Suspended Particulate Matter Concentration.....	125
5.3.2.2 LISST and CTD Data Processing	126
5.3.2.3 Suspended Particulate Matter Concentration derived from ADCP Backscatter	126
5.3.2.4 Calibration of ADCP Echo Intensity to Estimate Suspended Sediment Concentration	131
5.3.2.5 Acoustic Sensitivity to Particle Size	134
5.4 Results.....	135
5.4.1 Wind at Station DPIA1: 1 April to 14 April	135

5.4.2 M4: In situ Alongshore and Across shore Velocity, Model Temperature and Salinity and Derived SPM Concentration.....	136
5.4.2.1 1 April to 3 April: Post Cold Front	136
5.4.2.1.1 In situ Alongshore and Across shore Velocity	136
5.4.2.1.2 Model Temperature, Model Salinity and Derived SPM Concentration	137
5.4.2.2 4 April to 8 April: Calm Wind Conditions	138
5.4.2.2.1 In situ Alongshore and Across shore Velocity	138
5.4.2.2.2 Model Temperature, Model Salinity and Derived SPM Concentration	139
5.4.2.3 April 10 to April 13: Pre Cold Front to Post Cold Front	140
5.4.2.3.1 In situ Alongshore and Across shore Velocity	140
5.4.2.3.2 Model Temperature, Model Salinity and Derived SPM Concentration	141
5.4.3 M5: In situ Alongshore and Across shore Velocity, Model Temperature and Salinity and Derived SPM Concentration.....	142
5.4.3.1 2 April to 3 April: Post Cold Front.....	142
5.4.3.1.1 In situ Alongshore and Across shore Velocity	142
5.4.3.1.2 Model Temperature, Model Salinity and Derived SPM Concentration	143

5.4.3.2 4 April to 8 April: Calm Wind Conditions	143
5.4.3.2.1 In situ Alongshore and Across shore Velocity	143
5.4.3.2.2 Model Temperature, Model Salinity and Derived SPM Concentration	145
5.4.3.3 April 10 to April 13: Pre Cold Front to Post Cold Front	146
5.4.3.3.1 In situ Alongshore and Across shore Velocity	146
5.4.3.3.2 Model Temperature, Model Salinity and Derived SPM Concentration	147
5.4.4 Effect of Tides and Wind Stress on Suspended Particulate Matter Concentration	147
5.4.4.2 SPM Concentration at M4 during Maximum Tidal Range and Maximum Wind Stress	150
5.4.4.3 SPM Concentration at M4 during Maximum Tidal Range and Minimum Wind Stress	153
5.5 Discussion	156
5.5.1 SPM Concentration variation at M4 and M5 during cold front events and calm wind conditions	156
5.5.2 SPM Concentration at M4 during Maximum Tidal Range and Minimum/Maximum Wind Stress	156
5.6 Conclusion	157
CHAPTER VI	158

6.1 Conclusions.....	158
6.1.1 Chapter III.....	158
6.1.2 Chapter IV.....	158
6.1.3 Chapter V.....	159
6.2 Summary.....	160
REFERENCES	161

LIST OF TABLES

Table 1.1 Sediment grain size classification.....	3
Table 2.1 Specifications for the DEMs in northern Gulf of Mexico	19
Table 3.1 Sediment model parameters of the cohesive and non-cohesive sediments present in the sediment model.....	41
Table 4.1 1 Dates of seasonal cruises in the MS Sound to characterize suspended particulate matter (SPM).....	71
Table 5.1 Twelve hundred kHz ADCP (M2) settings.....	124
Table 5.2 Six hundred kHz ADCP (M1, M3, M4 and M5) setting	124

LIST OF ILLUSTRATIONS

Figure 1.1 Mississippi and Alabama barrier islands 5

Figure 2.1 Gulf of Mexico ocean basin 13

Figure 2.2 Geographical limits of the 90-m Coastal Relief Model..... 15

Figure 2.3 Geographic limits of the Bathymetric Dynamic Digital Elevation Model
(BDDEM). 16

Figure 2.4 Digital Elevation Models (DEMs) developed by National Centers for
Environmental Information (NCEI)..... 18

Figure 2.5 Resampled the 90 m BDDEM and incorporated the 30 m NCEI NGC DEM 22

Figure 2.6 Updated the BDDEM with the 10 m NCEI DEMs 22

Figure 2.7 Overview of ingestion of National Ocean Service (NOS) surveys into
BDDEM 23

Figure 2.8 NOS surveys incorporated into the BDDEM 25

Figure 2.9 Location of NOS surveys conducted from 2002 through 2011 included in the
BDDEM 26

Figure 2.10 Location diagram and depth range of survey H11082 off the coast of
Alabama 27

Figure 2.11 Derivative of the depth with respect to the longitude after survey H11082
incorporated into the BDDEM..... 28

Figure 2.12 Depth difference between the 2009 and 2004 BDDEMs along coastline of
Louisiana..... 29

Figure 2.13 Depth difference between the 2009 and 2004 BDDEMs in MS Sound and
MS Bight..... 29

Figure 3.1 CONCORDE model domain and the locations of West Corridor (WCORR), Middle Corridor (MCORR), East Corridor (ECORR), The University of Southern Mississippi (USM) (42067) and Orange Beach (42012) buoys.....	35
Figure 3.2 Atmospheric pressure (AP), alongshore wind velocity (Al. Ve.), across shore wind velocity (Ac. Ve.) and significant wave height (SWH) at the Orange Beach (42012) and USM (42067) buoys during the passage of the cold front	44
Figure 3.3 In situ salinity (In Situ Ichthyoplankton Imaging System (ISIIS)), in situ temperature (ISIIS), in situ mean pixel gray level (ISIIS) and in situ particulate backscatter at 532 nm (Scanfish) measured along MCORR on 31 March.	46
Figure 3.4 In situ salinity (ISIIS), in situ temperature (ISIIS), in situ mean pixel gray level (ISIIS) and in situ particulate backscatter at 532 nm (Scanfish) measured along WCORR on 1 April	47
Figure 3.5 CMA model/in situ data comparison of the wind velocity at the Orange Beach (42012) and USM (42067) buoys	48
Figure 3.6 WWIII model/in situ data comparison of the SWH at the Orange Beach (42012) and USM (42067) buoys	49
Figure 3.7 Taylor diagram showing the CMA and WWIII model results/in situ data comparison between the atmospheric and wave data (SWH and wave orbital velocity: Wv. Orb.) at Orange Beach (42012) and USM Buoy (42067)	50
Figure 3.8 Comparison of in situ salinity measured by the ISIIS (top) and CONCORDE model salinity (bottom) along WCORR on 1 April.....	53
Figure 3.9 Comparison of in situ temperature measured by the ISIIS (top) and CONCORDE model temperature (bottom) along WCORR on 1 April	54

Figure 3.10 Taylor diagram showing CONCORDE model/in situ data comparison of the temperature and salinity measured by the ISIIS along WCORR, MCORR and ECORR	55
Figure 3.11 Comparison of in situ mean pixel gray level (ISIIS), in situ particulate backscatter at 532 nm (bbp (532)) (Scanfish) and synthesis model fine silt along WCORR on 1 April	57
Figure 3.12 Comparison of in situ mean pixel gray level (ISIIS) and synthesis model fine silt along MCORR on 2 April	58
Figure 3.13 Water advected shoreward at the surface during the prefront phase and higher salinity water at depth advected offshore on 30 March	60
Figure 3.14 Postfrontal northerly winds flushed the estuary and advected fresh water southwest through Main Pass and the tidal passes on 1 April	62
Figure 3.15 Southeasterly prefrontal winds generate shoreward bed shear and increased suspended sediments at WCORR due to the onshore Ekman transport of surface water and the offshore advection of high salinity bottom water	63
Figure 3.16 Southwesterly winds increased the depth of the fresh water plume by 1 m along WCORR and discharged fresh water into MS Bight	65
Figure 4.1 Location map showing Mobile Bay, the barrier islands and Lake Borgne enclosing MS Sound	68
Figure 4.2 Location of the stations at East and West Ship Island for the August 2015 cruise	72
Figure 4.3 Location diagram of the DMR stations in MS Sound sampled monthly in 2016	72

Figure 4.4 Workflow for converting a MODIS Aqua Level 1 file to estimated suspended particulate matter with a 500 m resolution	77
Figure 4.5 Surficial sediment map of the northern Gulf of Mexico	79
Figure 4.6 Particle size in situ data collected at the East (top left), West Ship (top right) Islands and Camille Cut (bottom left) on 19 August 2015	80
Figure 4.7 In situ particle size, temperature, salinity and SPM collected at MS Sound on 24 January 2016	81
Figure 4.8 In situ particle size, temperature and salinity collected at MS Sound on 31 January 2016	82
Figure 4.9 In situ particle size, temperature, salinity and SPM collected at MS Sound on 12 February 2016	83
Figure 4.10 In situ particle size, temperature, salinity and SPM collected at MS Sound on 22 April 2016	84
Figure 4.11 In situ particle size, temperature, salinity and SPM collected at MS Sound on 24 May 2016	85
Figure 4.12 In situ particle size, temperature, salinity and SPM collected at MS Sound on 8 June 2016	86
Figure 4.13 In situ particle size, temperature, salinity and SPM collected at MS Sound on 5 July 2016	87
Figure 4.14 In situ particle size, temperature, salinity and SPM collected at MS Sound on 2 August 2016	88
Figure 4.15 SPM anomaly at Main Pass	89
Figure 4.16 SPM anomaly at Petit Bois Pass	91

Figure 4.17 SPM anomaly at Horn Island Pass	93
Figure 4.18 SPM anomaly at Dog Key Pass.....	95
Figure 4.19 SPM anomaly at Ship Island Pass	97
Figure 4.20 In situ alongshore (blue) (positive east) and across shore (red) (positive north) wind velocity at Bay Waveland (MS) one week prior to the 19 August 2015 cruise at Ship Island.....	99
Figure 4.21 In situ alongshore (blue) (positive east) and across shore (red) (positive north) wind velocity at Bay Waveland one week prior to the 24 January 2016 cruise in MS Sound.....	100
Figure 4.22 Synthesis model output of surface ocean current superimposed on surface salinity on 23 January 2016	101
Figure 4.23 Synthesis model output of surface ocean current superimposed on surface salinity on 31 January 2016	102
Figure 4.24 Synthesis model output of surface ocean current superimposed on surface salinity on 12 February 2016	103
Figure 4.25 In situ time series of daily river discharge at Pearl River.....	103
Figure 4.26 In situ time series of daily river discharge at Pascagoula River.....	104
Figure 4.27 In situ alongshore (blue) (positive east) and across shore (red) (positive north) wind velocity at Bay Waveland one week prior to the 22 April 2016 cruise in MS Sound	105
Figure 4.28 In situ alongshore (blue) (positive east) and across shore (red) (positive north) wind velocity at Bay Waveland one week prior to the 24 May 2016 cruise in MS Sound	106

Figure 4.29 Synthesis model output of surface ocean current superimposed on surface salinity on 8 June 2016	107
Figure 4.30 Synthesis model output of surface ocean current superimposed on surface salinity on 5 July 2016	108
Figure 4.31 Synthesis model output of surface ocean current superimposed on surface salinity on 3 February 2016	112
Figure 5.1 Location map of the mooring stations (M1, M2, M3, M4 and M5) located in Mississippi Bight	123
Figure 5.2 LISST mean particle size and in situ suspended particulate matter (SPM) measurements at the ADCP stations in April 2016	130
Figure 5.3 Linear regression analysis of SPM _v and (E-Er) for the 614.4 kHz ADCPs..	131
Figure 5.4 M4 April 2016 time series	132
Figure 5.5 M5 April 2016 time series	133
Figure 5.6 Wind stress at NOAA Dauphin Island station, dpia1	148
Figure 5.7 Hourly averaged tidal heights at Dauphin Island station 8735180 during the ADCP deployment	149
Figure 5.8 M4 April 2016 time series on 2 April	151
Figure 5.9 Ekman pumping rate between M4 and M5 on 2 April during the third highest tidal range and maximum wind stress.....	151
Figure 5.10 River discharge at Tombigbee/Alabama River gauges 7-14 days before 2 April (i) Brunt Vaisala frequency at M4 on 2 April. (ii).	152
Figure 5.11 M4 April 2016 time series on 13 April	154

Figure 5.12 Ekman pumping rate between M4 and M5 on 13 April during the sixth
highest tidal range and second lowest wind stress..... 154

Figure 5.13 River discharge at Tombigbee/Alabama River gauges 7-14 days before 13
April (i) Brunt Vaisala frequency at M4 on 13 April. (ii). 155

LIST OF ABBREVIATIONS

<i>BDDEM</i>	Bathymetric Dynamic Digital Elevation Model
<i>CMA</i>	CONCORDE Meteorological Analysis
<i>COAWST</i>	Coupled Ocean-Atmosphere-Wave-Sediment Transport
<i>CONCORDE</i>	CONsortium for oil spill exposure pathways in Coastal River-Dominated Ecosystems
<i>CSTM</i>	Community Sediment Transport Modeling System
<i>CTD</i>	Conductivity, temperature and depth
<i>DEM</i>	Digital Elevation Model
<i>ISIS</i>	In Situ Ichthyoplankton Imaging System
<i>LISST</i>	Laser In-Situ Scattering and Transmissometry
<i>MLLW</i>	Mean Lower Low Water
<i>MODIS</i>	Moderate Resolution Imaging Spectroradiometer
<i>NAVD88</i>	North American Vertical Datum of 1988
<i>Scanfish</i>	EIVA ScanFish III Rocio
<i>SPM</i>	Suspended Particulate Matter
<i>SPMa</i>	Suspended Particulate Matter anomaly
<i>SSC</i>	Suspended Sediment Concentration

SWAN

Simulating WAves Near-shore

WWIII

WAVEWATCH III

CHAPTER I

1.1 Introduction

1.1.1 Sediment Transport

Sediment transport is a natural process that has occurred throughout the geologic time and is divided into different modes: bed load, suspended load and wash load. Bed load is the component of the total load in continuous contact with the bed during transport, and sediments roll and/or slide along the bed (Fredsoe & Deigaard, 1992; Imran, 2008). Suspended load is the component of the total load transported without continuous contact with the bed due to fluid turbulence and wash load consists of very fine particles transported by water and not represented in the bed (Fredsoe & Deigaard, 1992). Sediment properties are directly related to the mode of sediment transport.

The most relevant sediment properties with respect to morphodynamics are size, shape and specific gravity (Fredsoe & Deigaard, 1992). Diameter is used to describe grain size and defined using three different methods. Grain size greater than 16 mm represents the intermediate axis of the particle idealized as an ellipsoid. Grain sizes ranging from 0.0625 to 16 mm are defined as the smallest sieve size through which the particle can pass, and particle diameters less 0.0625 mm are measured by the settling velocity (Table 1.1) (Imran, 2008; Wentworth, 1922). Settling velocity is the terminal velocity reached when the grain is settling in an extended fluid under the action of gravity. Stokes' Law is commonly utilized to compute settling velocity as a function of grain diameter and specific gravity (Equation 1.1) (Stokes, 1850). Specific gravity of a sediment is the ratio of its weight to the weight of an equal volume of water and usually

close to 2.65 for natural sediments (Fredsoe & Deigaard, 1992). Sediments present on the seabed are subject to a number of different stabilizing and driving forces.

$$\omega_S = \sqrt{\frac{4 \times (s-1) \times g \times d}{3 \times c_D}} \quad \text{[Equation 1.1]}$$

where s is the specific gravity, g is the gravitational acceleration, d is the grain diameter and c_D is the drag coefficient.

Table 1.1 Sediment grain size classification

Wentworth Size Class	Grain Diameter (mm)
Clay	0.060 to 3.90×10^{-3}
Very fine silt	3.90 to 7.80×10^{-3}
Fine silt	7.80 to 15.6×10^{-3}
Medium silt	1.56 to 3.10×10^{-2}
Coarse silt	3.10 to 6.25×10^{-2}
Very fine sand	6.25 to 12.5×10^{-2}
Fine sand	1.25 to 2.50×10^{-1}
Medium sand	2.50 to 5.00×10^{-1}
Coarse sand	5.00 to 10.0×10^{-1}
Very coarse sand	1.00 to 2.00

Tractive stress and lift force are two driving forces acting on a sediment particle at rest. Movement of the water mass by ocean currents generates a horizontal drag and a pressure difference at the upstream and downstream sides of the grain due to flow separation. The water mass's streamlines generates a lifting force, which decreases the hydrostatic pressure at the top of the grains. The weight of the grain and friction between the grain and surrounding grains are the stabilizing forces acting on the grain (Fredsoe & Deigaard, 1992). Sediments remain at rest once the stabilizing force exceeds the driving force as shown in equations 1.2 and 1.3 (Shields, 1936). Sediment resuspension and bed load transport occurs when the driving force exceeds the stabilizing force.

$$\frac{U_{fc}^2}{(s-1) \times g \times d} = \frac{\mu_s}{c_D} \times \frac{4}{3 \times \alpha^2} \quad [\text{Equation 1.2}]$$

$$\theta_c = \frac{U_{fc}^2}{(s-1) \times g \times d} \quad [\text{Equation 1.3}]$$

where U_{fc} is the critical friction velocity, μ_s is the maximum friction between the grain and the surrounding grains, α is a non-dimensional coefficient and θ_c is the critical Shields parameter.

1.1.2 Study Area

Mississippi Sound (MS Sound) is a coastal lagoon with an average depth of 3 m, approximately 130 km long and 11-24 km wide. The area extends from Mobile Bay on the east to Lake Pontchartrain on the west and a series of barrier islands are located approximately 11 km south of the headland (Priddy et al., 1955). The tidal passes in the Sound are located between Petit Bois Island (Petit Bois Pass), Horn Island (Horn Island Pass), Ship Island (Dog Key Pass) and Cat Island (Ship Island Pass) (Figure 1.1). The

average depth of the passes is 5 m, and the depth of the two ship channels located in the passes (Pascagoula and Gulfport) is 20 m. Sediment type in the Sound is mostly soft clay/mud (80%), firm/sandy silt (15%) and sand (5%) (Priddy et al., 1955). Mobile Bay is 49 km in length and 37 km in width (Hummell, 1990). It has an average depth of 3 m and connects to MS Sound via Pass aux Herons and Mississippi Bight (MS Bight) via Main Pass (Figure 1.1). Main Pass is 5 km in width and consists of the 13-14 m deep Mobile Ship Channel (Dinnel et al., 1990; Hummell, 1990).

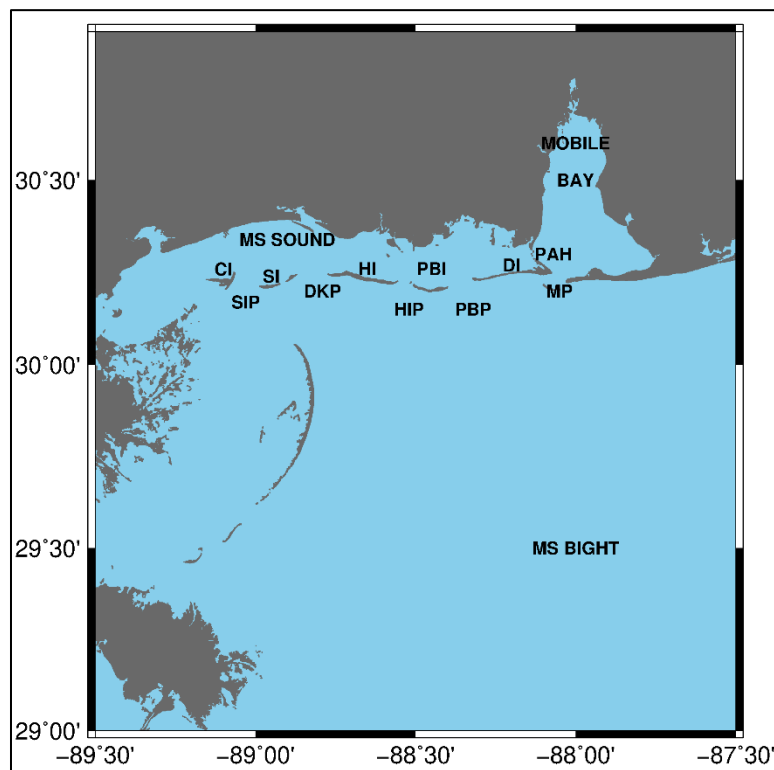


Figure 1.1 Mississippi and Alabama barrier islands

CI: Cat Island, SI: Ship Island, HI: Horn Island, PBI: Petit Bois Island, DI: Dauphin Island, SIP: Ship Island Pass, DKP: Dog Keys Pass, HIP: Horn Island Pass, PBP: Petit Bois Pass, MP: Main Pass and PAH: Pass aux Herons.

The diurnal tide is a major forcing factor in Mobile Bay and MS Sound (Kjerfve & Sneed, 1984). Tides in this region are microtidal (tidal range of 0-0.40 m) and tidal currents near the passes are approximately 0.15 m s^{-1} (Hummell, 1990). Main Pass tidal channel is classified as tide dominated due to the well developed ebb-tidal delta, poorly developed flood-tidal delta, and deep central channel through which tidal currents flow east of Pelican and Sand Islands. Sediment is transported towards the Bight through Main Pass by ebb-tidal currents (Hummell, 1990).

1.1.3 Sediment and Particulate Matter Sources in the Study Area

High volumes of fresh water, sediments and particulate matter from the Pearl River, Wolf River, Biloxi River, Pascagoula River, Alabama River and Tombigbee River discharge into MS Sound, Mobile Bay and MS Bight (Colson and Boswell, 1985; Kennicutt et al., 1995; Salisbury et al., 2004). The combined discharge rate of Alabama and Tombigbee rivers is approximately $2240 \text{ m}^3 \text{ s}^{-1}$ (Kennicutt et al., 1995). The sediment/particulate matter load entering Mobile River delta from Tombigbee River, Alabama River (combined rate of 134 kg s^{-1}) and uplands adjacent to the delta (3 kg s^{-1}) is estimated to be 137 kg s^{-1} . The river delta retains 35 kg s^{-1} of the load and discharges 102 kg s^{-1} into Mobile Bay. Approximately 45% of the average annual sediment/particulate matter load remains in Mobile Bay, 47 % exits into MS Bight and 8 % is discharged into MS Sound (Isphording et al., 1996; Ryan, 1969).

Fresh water discharge from Pascagoula River and Pearl River are comparable, with rates of 279 and $273 \text{ m}^3 \text{ s}^{-1}$, respectively. Wolf River has an average discharge rate of $19 \text{ m}^3 \text{ s}^{-1}$ and Biloxi River has a rate of $5 \text{ m}^3 \text{ s}^{-1}$ (Colson and Boswell, 1985).

Pascagoula River sediment/particulate matter load ranges from 10.0 kg s⁻¹ to 111 kg s⁻¹ (Burdin, 1992). The sediment/particulate matter discharge from Biloxi River, Wolf River and Pearl River are 0.374 kg s⁻¹, 1.89 kg s⁻¹ and 0.415 kg s⁻¹ respectively (Hudson & Mossa, 1997; Newcome et al., 1968).

1.1.4 Transport Pathways in the Study Area

Wind stress, a dominant forcing factor in the northern Gulf of Mexico, is characterized by a seasonal shift from northerly in the winter to southerly in the summer (De Velasco & Winant, 1996). Fresh water discharge is also seasonal with peak discharge in late winter/early spring and minimum discharge in late summer/early fall (Stumpf et al., 1993; Morey et al., 2005). A number of studies have identified sediment and particulate matter transport pathways in the northern Gulf of Mexico induced by the seasonal wind and river discharge in the region.

Zang et al. (2018) explored the sediment dynamics in coastal Louisiana during hurricane Gustav (2008) using the Coupled Ocean-Atmosphere-Wave-Sediment Transport (COAWST) modeling system. Approximately 1000 mg L⁻¹ of sediment was transported from the outer to the inner continental shelf. The seabed thickness near landfall decreased by 0.14 m due to erosion induced by the hurricane. Xu et al. (2016) studied the seabed erosion and deposition on the Louisiana shelf, before, during and after Hurricanes Katrina and Rita in 2005. The period of the frequency band in the wave spectrum with the most energy is defined as peak wave period. Wind-generated waves cause orbital motion below the surface of the water called wave orbital velocity (Wiberg & Sherwood, 2008). Peak wave periods, wave orbital velocities and significant erosion

for both storms was confined to the mid-continental shelf because wave energy dissipated over the inner shelf. Hurricane Katrina's path resulted in localized seabed disturbance along the eastern Louisiana shelf and Hurricane Rita affected the entire Louisiana shelf.

Researchers using data acquired by the Moderate Resolution Imaging Spectroradiometer (MODIS) (Walker et al., 2005; Huh et al, 2001) and in situ meteorological data investigated the effect of the wind stress on the transport and suspension of sediments along the Louisiana Gulf coast. The study provided evidence of a localized wind influence on the suspended sediment pattern along Louisiana Gulf coast during spring (Huh et al, 2001). Easterly winds (common in fall, winter and spring) generate a major pathway for the exchange of river and shelf waters between the Louisiana/Mississippi/Alabama shelf and the Louisiana/Texas shelf. Maximum sediment exchange occurs during northeasterly wind events (Walker et al., 2005).

Huh et al. (2001) and Walker & Hammack (2000) examined the suspended sediment transport along the Louisiana coastline using in situ meteorological data and Advanced Very High Resolution Radiometer (AVHRR) data. Walker and Hammack (2000) showed the wind direction and wind speed relative to the east/west orientation of the coastline were the major controlling factors for circulation, sediment transport and sediment concentration in Atchafalaya Bay. A single cold front event transports approximately 4×10^8 kg of sediments from the nearshore region to the inner shelf (Walker & Hammack, 2000).

Huh et al. (2001) and Walker & Hammack (2000) examined the suspended sediment transport along the Louisiana coastline using in situ meteorological data and Advanced Very High Resolution Radiometer (AVHRR) data. Walker and Hammack

(2000) showed the wind direction and wind speed relative to the east/west orientation of the coastline were the major controlling factors for circulation, sediment transport and sediment concentration in Atchafalaya Bay. A single cold front event transports approximately 4×10^8 kg of sediments from the nearshore region to the inner shelf (Walker & Hammack, 2000).

Ha et al. (2012) and Carlin et al. (2016) analyzed sediment resuspension in Mobile Bay (Alabama) and Galveston Bay (Texas) utilizing suspended sediment concentration (SSC) derived from Acoustic Doppler Current Profiler (ADCP) measurements. Ha studied the vertical and temporal variability of the SSC in the bottom boundary layer. The bottom boundary layer is the layer above the seabed where the flow influences the seabed and transfers physical, chemical and biological properties between the sediment flow and the seabed (Nielsen, 1992). Ha observed a high SSC in Mobile Bay during flood events due to the high fluvial input and reduced resistance to erosion. Carlin observed high SSC during the passage of cold front events that corresponded to increased wave height and wave periods related to the fetch of the bay relative to wind direction.

Understanding the processes affecting the transport pathways of sediments and particulate matter in the northern Gulf of Mexico are necessary for managing accident response efforts such as the 2010 Deepwater Horizon oil spill. Oil interacts with suspended sediments to form sinking aggregates, and particulate matter (e.g. marine snow) transports oil to deeper depths in the water column (Muschenheim & Lee, 2002, Khelifa et al., 2005; Passow et al., 2012). Deepwater Horizon disaster resulted in the release of approximately 5 million barrels of oil, 1.7×10^{11} g of methane, and the

transport of oil from MS Bight to the Louisiana, Mississippi, Alabama and Florida coastlines (Michel et al., 2013; Murawski et al., 2016; Reddy et al., 2012). The disaster produced significant environmental damage such as contaminated shorelines, mortality of marine mammals and bioaccumulation of hydrocarbons in fish (Bue et al, 1998; Sumaila et al., 2012).

The studies discussed in this section focused on the ocean currents and estuarine exchange between the nearshore region and MS Bight, but the effects on the transport of sediments and particulate matter remains under studied. This dissertation provides an overview of short term (hourly) and longer-term (monthly) sediment and particulate matter exchange between MS Sound, Mobile Bay and MS Bight. The work examines the effects of different forcing factors (e.g. wind, river discharge and tides) on the concentration and advection of sediments and particulate matter in the water column. The dataset covers a wide range of data types, spatial and temporal resolutions. Data analyses involved a combination of field methods, numerical modeling and remote sensing. The results from this study will improve the understanding of the mechanisms driving suspended sediments/particulate matter exchange between MS Sound, Mobile Bay and MS Bight through the tidal passes.

1.2 Research Objectives

Based on the physical, geological and bio-optical data collected in fall 2015, winter 2015, spring 2016 and summer 2016 in the MS Sound, MS Bight and Main Pass, the study focused on the following objectives:

1. To systematically examine the effects of a water mass's advection on the sediment concentration southwest of Horn Island Pass during a cold front.
2. To characterize the spatial and temporal pattern of suspended particulate matter and factors contributing to its variability in Mobile Bay, Mississippi Sound, the tidal passes and Mississippi Bight.
3. To investigate the effects of the diurnal tide and wind stress on vertical mixing and the sediment concentration southwest of Main Pass during a cold front.

1.3 Hypotheses

1. The elevated suspended sediment concentration during a 2016 cold front in Mississippi Bight was a result of episodic, advection-driven resuspension of sediments along the seafloor.
2. Increased river discharge in winter 2015 in Mobile Bay (referenced to the 2012-2016 mean) resulted in a positive suspended particulate matter anomaly occurring for a longer period in spring and summer 2016 at Main Pass compared to 2015.
3. Increased wind stress during the passage of a 2016 cold front south of Main Pass increases the concentration of suspended particulate matter in the surface and bottom waters via Ekman transport.

CHAPTER II

2.1 Abstract

Hydrodynamic models such as Regional Ocean Modeling System are commonly used to forecast the impacts of coastal hazards in the northern Gulf of Mexico. These models rely on bathymetric data discretized in space as a stretched terrain following vertical grid in the domain of interest. The Bathymetric Dynamic Digital Elevation Model (BDDEM) was originally developed using open source software, to support modeling systems operated as part of the Northern Gulf Coast Hazards Collaboratory (Twilley et al., 2014). Subsequently, the BDDEM has been applied to support the modeling and analyses of the CONSortium for oil spill exposure pathways in Coastal River-Dominated Ecosystems (CONCORDE) (Greer et al., 2018). The BDDEM's initial basis was obtained by merging five digital elevation models (DEMs) of the Northern Gulf region released by the National Centers for Environmental Information (NCEI). The final build of the BDDEM includes all of the National Ocean Service (NOS) hydrographic surveys conducted in western Florida, Alabama, Mississippi and Louisiana through 2011.

2.2 Introduction

The Gulf of Mexico is a small ocean basin covering an area of approximately $1.5 \times 10^6 \text{ km}^2$ (Balsam & Beeson, 2003). The inner shelf region extending from Florida to Louisiana consists of the following topographic features: West Florida Shelf, Upper Continental Slope, Mississippi Cone, De Soto Canyon and the Texas-Louisiana Shelf (Uchupi, 1967) (Figure 2.1). The width of the West Florida Shelf ranges from 155 km

north of the Keys to 55 km off Cape San Blas. The continental shelf between the De Soto Canyon and the Mississippi Trough is narrow in some areas and almost nonexistent in other regions (Uchupi, 1967). Reef-like mounds, ridges and shallow depressions (Sager et al., 1992) characterize the Mississippi-Alabama outer continental shelf. The width of the Texas-Louisiana Shelf is 180 to 240 km wide and extends from the continental shelf break to the continental rise south of the Sigsbee Escarpment (Bryant et al, 1990).

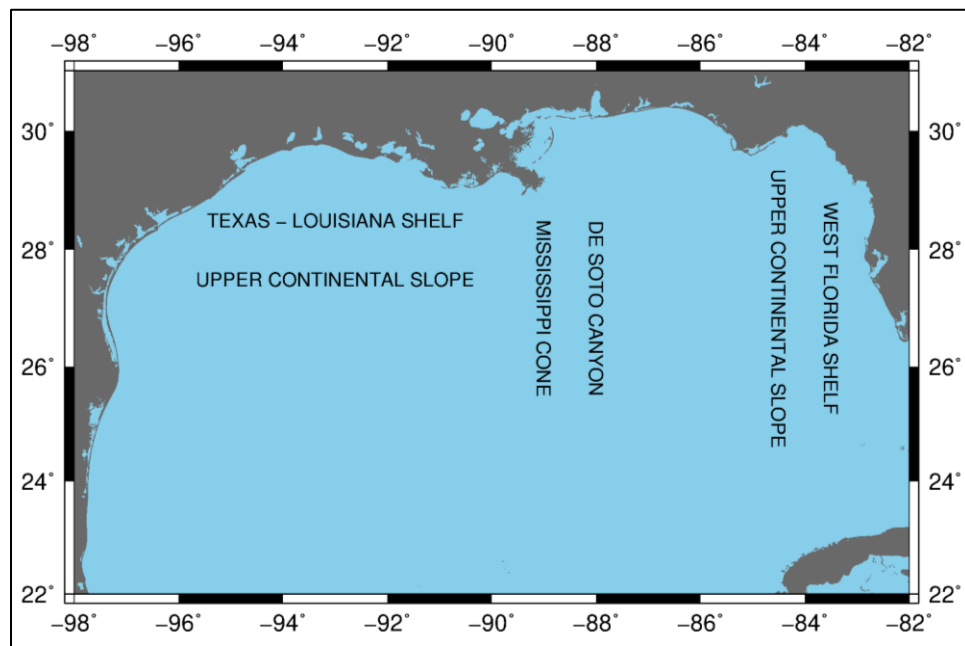


Figure 2.1 Gulf of Mexico ocean basin

Tropical storms and hurricanes adversely affect the coastlines along the northern Gulf of Mexico each year (Eisemann et al., 2018). Strong cyclonic winds generated by the storms and hurricanes result in extensive shoreline erosion and the loss of life and property (Gornitz et al., 1994). At least sixteen major hurricanes affected the north-

central Gulf of Mexico from 1941 to present (Bunya et al., 2010; Bell et al., 2011; Bell et al., 2012). Hurricane Katrina was one of the most severe hurricanes to hit the United States within this period and recorded as the costliest and one of the five deadliest hurricanes to strike the country (Knabb et al., 2005). Hurricane preparedness involves disaster management planning by federal and state agencies such as the Federal Emergency Management Agency (Kapucu, 2012).

Natural hazard management planning within the northern Gulf of Mexico utilize three-dimensional wind-wave and storm surge models. Chen et al. (2007) integrated the advanced surge model (ADvanced CIRculation (ADCIRC)) and a wind-wave model (Simulating WAVes Near-shore (SWAN)) to simulate the effects of hurricanes on flooding in the Mobile Bay estuary. The models successfully predicted the flood conditions along the low-lying areas including the hurricane evacuation routes. Dietrich et al. (2010) simulated the storm surges generated by hurricanes Rita and Katrina along the Louisiana and Mississippi coastlines. The difference in the geography of the locations affected by the two hurricanes resulted in significant differences between the heights of the storm surges. Bathymetry is one of the components required by these hydrodynamic models.

The Coastal Relief Model (CRM) is a DEM in the northern Gulf of Mexico produced by the NCEI (Figure 2.2). The CRM contains data compiled from NOS hydrographic surveys from 1888-2001 (NOAA National Centers for Environmental Information [NGDC], n.d.). The DEM is outdated and does not reflect the changes in the bathymetry from 2001 to 2011. The BDDEM was developed to provide updated bathymetry and support wind, wave and storm surge models in the northern Gulf of

Mexico (Twilley et al., 2014; Wiggert et al., 2018). The BDDEM extends from 27.50 °N to 30.89 °N and 84.00 °W to 94.00 °W (Figure 2.3). The latitude of 30.89° N was selected as the northern limit of the BDDEM to include Mobile Bay (Alabama) and Lake Pontchartrain (Louisiana) in the DEM. The bathymetry within the study area is variable, with maximum depths of approximately 3400 m south of the De Soto Canyon.

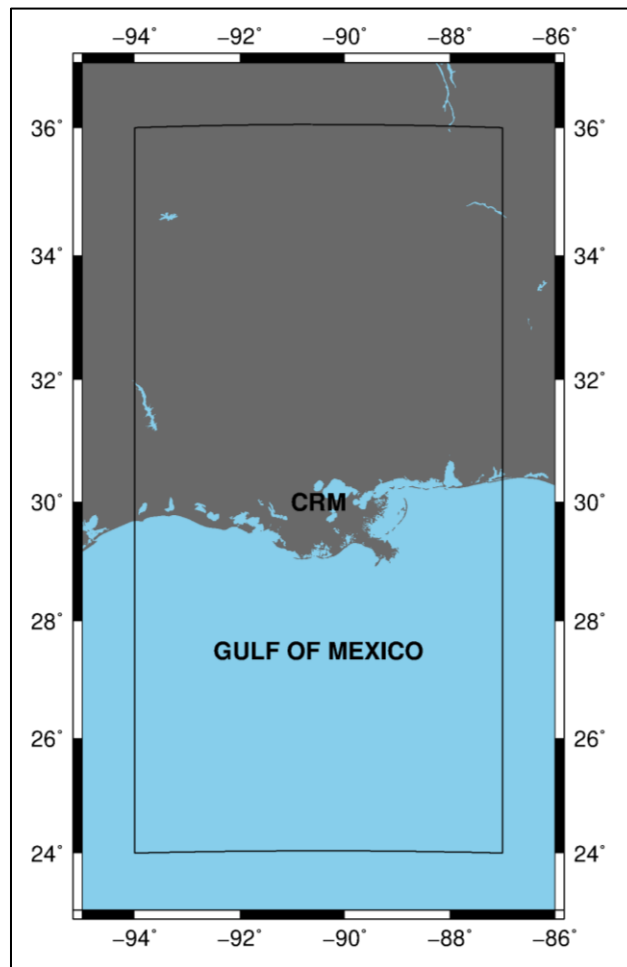


Figure 2.2 Geographical limits of the 90-m Coastal Relief Model

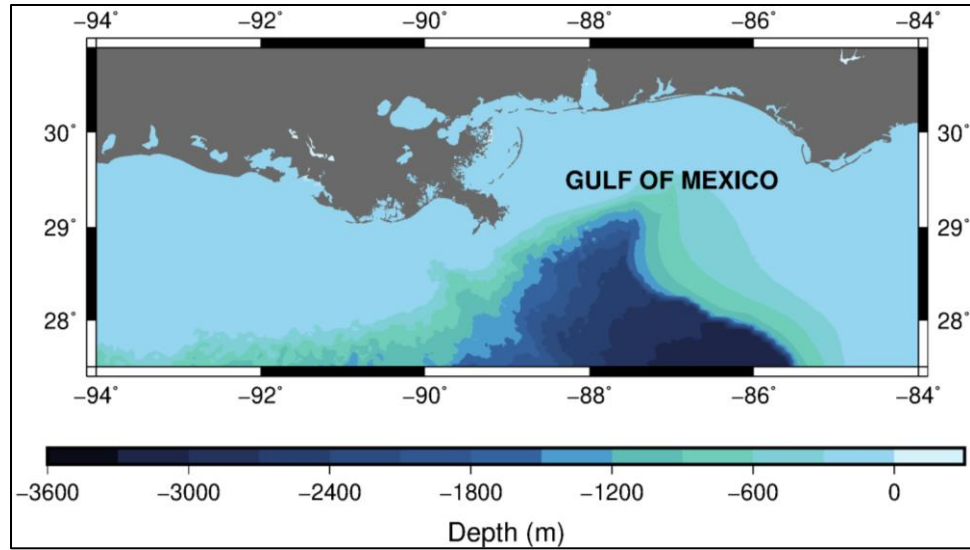


Figure 2.3 Geographic limits of the Bathymetric Dynamic Digital Elevation Model (BDDEM).

The method and tools utilized to develop the BDDEM are discussed in this chapter. In the first phase, open source tools consisting of NOAA Vertical Datum Transformation Tool (VDatum), Generic Mapping Tools (GMT) and MB-System Seafloor Mapping Software (MB) were utilized to update the CRM with the NCEI's 30 m Northern Gulf Coast (NGC) and 10 m Biloxi, Mobile, Southern Louisiana and New Orleans DEMs. The first stage of the development was evaluated by analyzing elevation plots along the edges of the NCEI DEMs. NOS surveys conducted in the northern Gulf of Mexico from 2001 to December 2011 were included in the BDDEM using the open source tools for the second stage of the project. This phase was assessed by computing the derivatives (dz/dx , dz/dy , $d^2z / dx dy$) within the area enclosed by the NOS surveys.

2.3 Data and Methods

2.3.1 Data

2.3.1.1 Coastal Relief Model

An extensive collection of bathymetric data was compiled for this project. The main data sources used for the BDDEM are the CRM, NCEI high resolution DEMs and the NOS bathymetric surveys conducted in the northern Gulf of Mexico from 2002 to 2011. The NCEI CRM volume 4 (Figure 2.2), released in 2001, has a horizontal resolution of 90 m with elevations resolved to 0.1 m. The CRM contains both topographic and bathymetric data; for the purposes of this study, only bathymetric data was extracted. The bathymetry represents a compilation of hydrographic data collected by NOS and a number of academic institutions. The surveys were conducted using a range of sounding methods including lead line, single beam echo sounders and multibeam sonars. A common vertical datum was not established for the CRM since the raw data from the hydrographic surveys are referenced to various tidal datums (e.g. Mean Lower Low Water (MLLW) and Mean Low Water (MLW)) (NGDC, n.d.).

2.3.1.2 National Centers for Environmental Information Digital Elevation Models

NCEI developed bathymetric-topographic DEMs for Biloxi, Mobile, New Orleans, NGC and Southern Louisiana from 2007 to 2010 (Figure 2.4). NOAA developed Mobile, New Orleans and NGC DEMs to evaluate VDatum, and established the Southern Louisiana and Biloxi DEMs as input for inundation models. A number of federal

agencies (NOS, Office of Coast Survey, Coastal Services Center, United States Geological Survey and the United States Army Corps of Engineers) collected the coastline, bathymetric and topographic datasets for the DEMs (Love et al., 2012; Love et al., 2011). Northern Gulf Coast, New Orleans, Southern Louisiana and Mobile DEMs were released with a vertical datum of the North American Vertical Datum of 1988 (NAVD88), and the Biloxi DEM was set at Mean High Water (MHW) tidal datum. The spatial resolution of all the DEMs is 10 m except for the NGC DEM, which has a resolution of 30 m (Table 2.1).

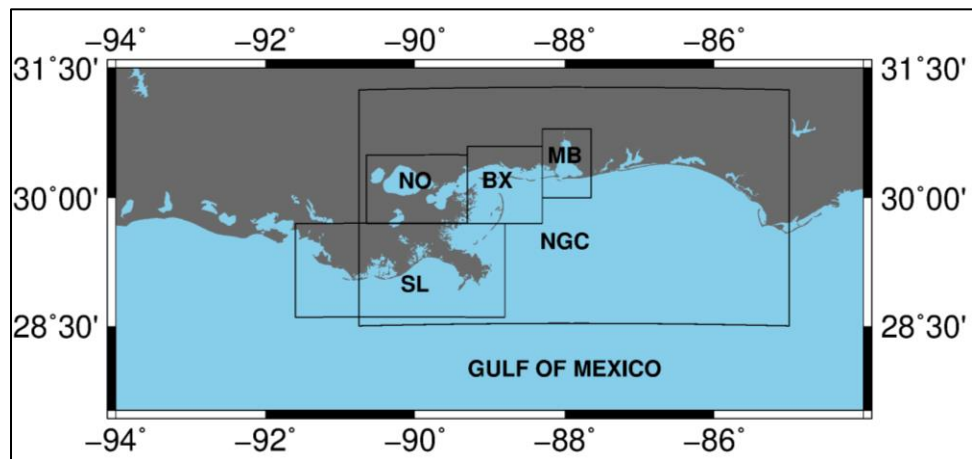


Figure 2.4 Digital Elevation Models (DEMs) developed by National Centers for Environmental Information (NCEI)

The five DEMs incorporated into the BDDEM are the 10 m Biloxi (BX), Mobile (MB), New Orleans (NO), Southern Louisiana (SL) and the 30 m Northern Gulf Coast (NGC)

Table 2.1 Specifications for the DEMs in northern Gulf of Mexico

Name	Geographic Extent	Date Completed	Spatial Resolution	Vertical Datum
Biloxi	89.30°W to 88.30°W, 29.70°N to 30.60°N	03/29/2007	10 m	MHW
Mobile	87.65°W to 88.30°W, 30.00°N to 31.00°N	11/30/2009	10 m	NAVD88
Northern Gulf Coast	90.75°W to 85.00°W, 28.50°N to 31.25°N	12/31/2010	30 m	NAVD88
New Orleans	90.65°W to 89.30°W, 29.70°N to 30.50°N	04/30/2010	10 m	NAVD88
Southern Louisiana	91.60°W to 88.80°W, 28.60°N to 29.70°N	12/31/2010	10 m	NAVD88

Amante et al., 2011; Love et al, 2012; Love et al. 2011; Taylor et al. 2008

2.3.1.3 National Ocean Service Hydrographic Surveys

One hundred and fifteen NOS surveys were completed in western Florida, Alabama, Mississippi and Louisiana nearshore and inner-shelf regions from 2001 through 2011. These additional surveys were identified by accessing the NCEI website (http://maps.ngdc.noaa.gov/viewers/nos_hydro/). The vertical datum of the NOS surveys is MLLW and included both multibeam and single beam surveys. The spatial resolution of these NOS surveys is lower than 10 m, with the multibeam surveys having a higher spatial resolution (at least 2 m) compared to the single beam surveys (at least 3 m) (National Ocean Service, 2017).

2.3.2 Methods

2.3.2.1 Ingestion of NGCHC DEMs (Stage 1 Build)

CRM bathymetry was converted from MLLW to NAVD88 in VDatum to make the data compatible with a topographic vertical datum (Love et al., 2012). VDatum transforms topographic and bathymetric data between different tidal, orthometric and ellipsoid based three dimensional reference systems (Xu et al., 2013). The tidal datums and NAVD88 stored in VDatum are defined relative to the local Mean Sea Level (MSL) (Yang et al., 2010). The grids developed in VDatum in the northern Gulf of Mexico extend from the coastline to the 46 km offshore limit, at approximately 29.90 °N (Xu et al., 2013).

For the development of the BDDEM, an 1800 m grid corresponding to the spatial extents of the CRM was first generated in Matlab. Each node was assigned an elevation of 0 m and converted from MLLW to NAVD88 in VDatum to develop the (NAVD88 - MLLW) grid. The (NAVD88 - MLLW) grid nodes located beyond VDatum's 46 km limit returned null values (no data). The null valued (NAVD88 - MLLW) nodes located along the southernmost latitude of the CRM (27.50 °N, or ~ 325 km offshore) were replaced with a value of 0 m in CARIS Bathy DataBase (CARIS BD), to reflect the inverse relationship between the MLLW to NAVD88 separation value and the depth. A linear interpolation algorithm was executed in CARIS BD between the nodes located at the 46 km limit and the nodes located at 325 km offshore in the CRM, to populate the null valued (NAVD88 - MLLW) nodes. The CRM surface was translated to NAVD88 in

CARIS BD and resampled to 30 m in GMT, to generate the NAVD88 BDDEM (Wessel et al., 2013; Wessel & Smith, 1998; Wessel & Smith, 1995; Wessel & Smith, 1991).

The northern extent of the 30 m NGC DEM (31.25 °N) extended beyond the northern boundary of the BDDEM (30.89 °N). Northern Gulf Coast DEM's northern border was modified from 31.25 °N to 30.89 °N to match the northern boundary of the BDDEM. The southern, western and eastern boundaries of the NGC DEM were revised to align with nodes present in the BDDEM. The BDDEM data was replaced with the data contained in the NGC DEM (Figure 2.5) and resampled from 30 m to 10 m in GMT.

Biloxi DEM bathymetry was converted from MHW to NAVD88 in VDatum to correspond to the vertical datums of Mobile, New Orleans and Southern Louisiana DEMs. The boundaries of the 10 m Biloxi, Mobile, New Orleans and Southern Louisiana DEMs were revised similar to the NGC DEM and incorporated into the BDDEM. The NCEI DEMs were incorporated into the BDDEM in the following order: New Orleans, Mobile, Southern Louisiana and Biloxi (Figure 2.6). Since the NCEI DEMs used the same NOS bathymetry data sources for its development, the order of ingesting the DEMs into the BDDEM was independent of the DEM's completion date.

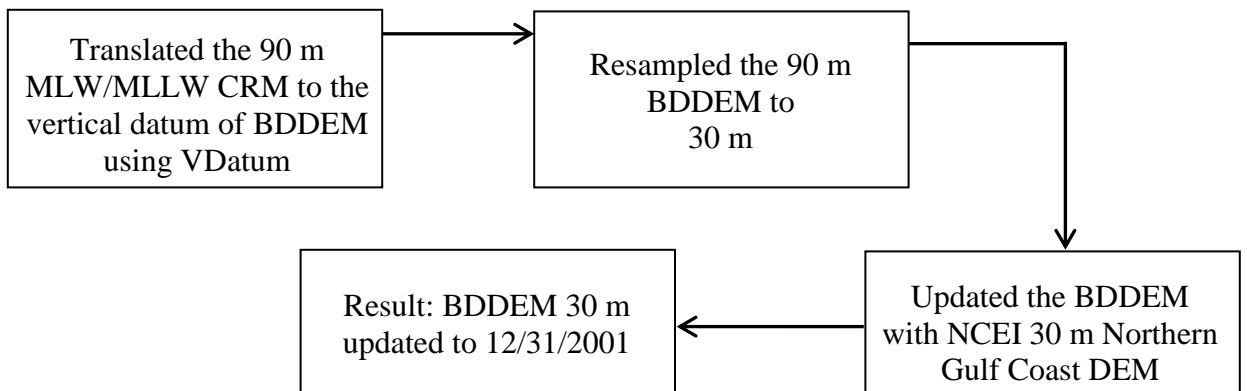


Figure 2.5 Resampled the 90 m BDDDEM and incorporated the 30 m NCEI NGC DEM

MLW is Mean Low Water, MLLW is Mean Lower Low Water, CRM is the Coastal Relief Model and VDatum is the National Oceanic and Atmospheric Administration Vertical Datum Transformation

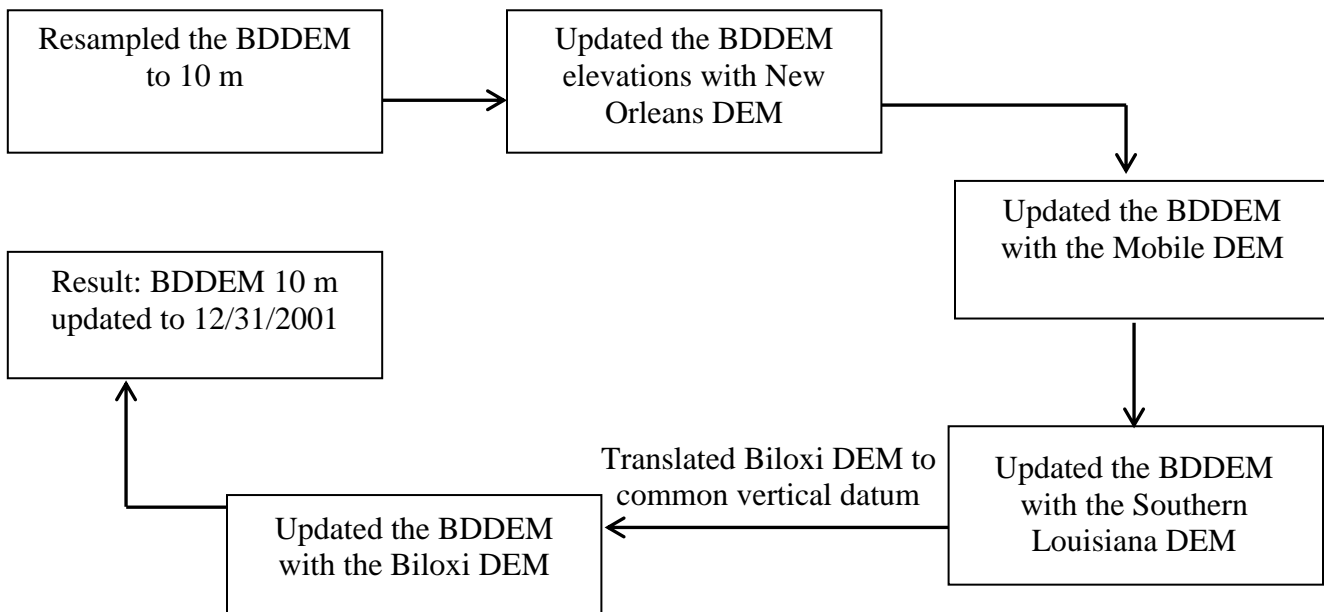


Figure 2.6 Updated the BDDDEM with the 10 m NCEI DEMs

2.3.2.2 Ingestion of NOS Surveys (Stage 2 Build)

NOS surveys in close proximity were included in the BDDEM in a single ingestion process in MB (Figure 2.7). NOS surveys were referenced to MLLW (NOAA standard for hydrographic surveys) and the BDDEM was referenced to NAVD88. The BDDEM was converted to MLLW to merge the NOS surveys and BDDEM at a higher resolution than 10 m. The merged NOS surveys were converted from MLLW to NAVD88 and incorporated into the final NAVD88 BDDEM product. This section explains these steps in further detail.

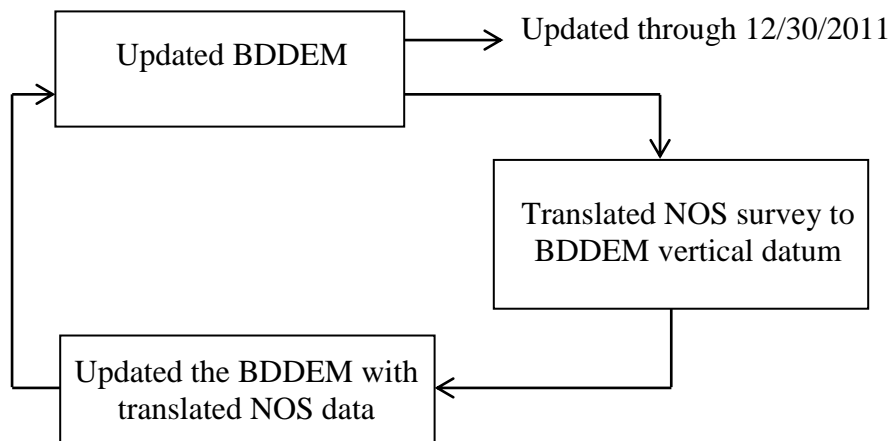


Figure 2.7 Overview of ingestion of National Ocean Service (NOS) surveys into BDDEM

A constant weight was assigned to each of the MLLW NOS surveys included in the ingestion process. The NOS surveys were merged using a spline interpolation in MB at 10 m grid spacing, and data gaps between the surveys remained as missing data. Spline interpolation was utilized because the multibeam surveys had a higher resolution than the BDDEM (Amante et al., 2011; Love et al., 2011; Taylor et al., 2008). The spline

interpolation was applied at a maximum radial distance of 12 grid cells (~ 120 m) from the swath data. The merged bathymetric data was plotted and analyzed to identify any data gaps. Data gaps present in the merged surveys were eliminated by repeating the merging procedure above and increasing the maximum radial distance of the spline interpolation.

The 1800 m (NAVD88 - MLLW) grid was resampled to a resolution of 10 m similar to the BDDEM. A region with an area equal to the ingested NOS surveys in close proximity was extracted from the (NAVD88 - MLLW) and BDDEM grids. The BDDEM was translated to the vertical datum of the NOS surveys (MLLW) and resampled from 10 to 3 m. NOS surveys were merged utilizing a spline interpolation at 3 m, with the BDDEM (MLLW) used to fill data gaps between the surveys. The merged NOS surveys containing no missing data between the surveys were resampled from 3 to 10 m. The downsampling (3 m) and resampling (10 m) of the grid was applied to reduce the edge effects in the merged NOS surveys (Figure 2.8) (Liu et al., 1999).

The merged NOS surveys without any grid included in the background were combined with the NOS surveys with a grid included in the background. The merged bathymetric data was converted from MLLW to NAVD88 to correspond to the datum of the BDDEM. The merged NOS surveys were incorporated into the BDDEM with GMT to generate an updated version of the BDDEM (Figure 2.8). Figures 2.9 highlights the location of the surveys included in the BDDEM yearly updates.

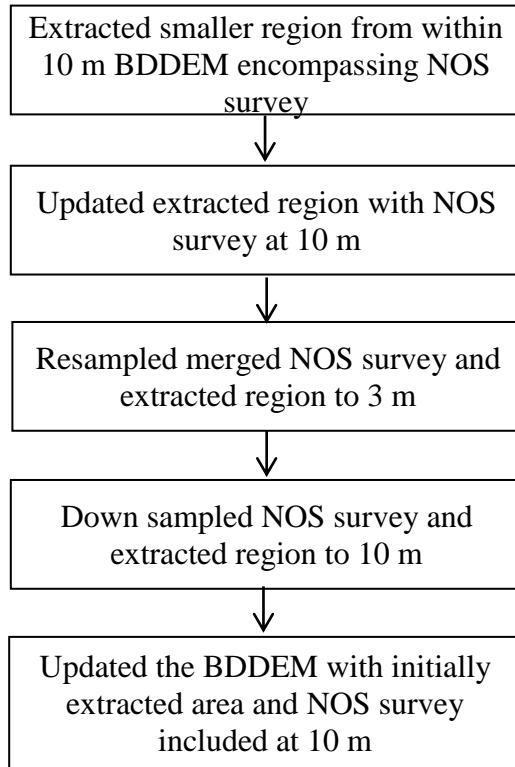


Figure 2.8 NOS surveys incorporated into the BDDEM

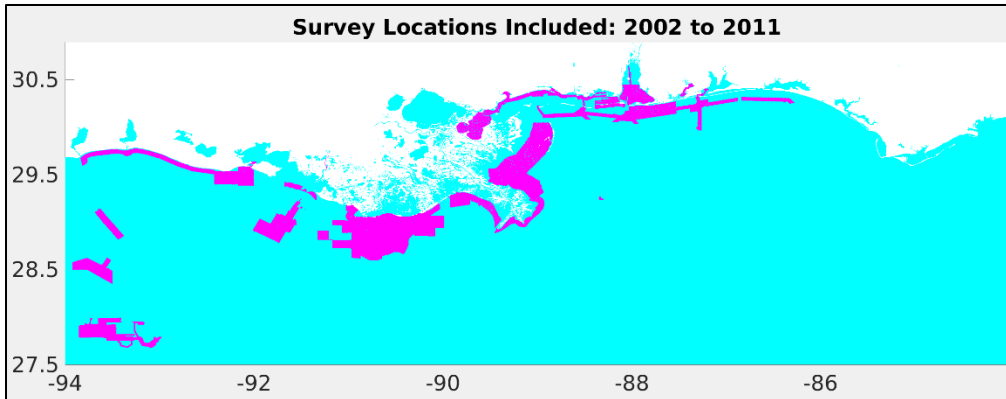


Figure 2.9 Location of NOS surveys conducted from 2002 through 2011 included in the BDDEM

2.3.2.3 Assessment of BDDEM

After the NOS surveys were included in the BDDEM, the derivatives of the updated BDDEM were determined in GMT. The first derivatives were computed in the longitudinal (dz/dx) and latitudinal (dz/dy) directions and the second derivative was calculated in the longitudinal direction followed by the latitudinal direction ($d^2z / dx dy$) (Jones, 1998). Derivative plots were mapped to assess how the natural variability of the bathymetry compared to the edge effects introduced in the BDDEM during the update process (i.e. how prominent were the borders of the newly ingested surveys in the updated BDDEM).

One of the NOS surveys included in the update of the BDDEM was H11082. This survey was selected as an example to highlight the derivatives along the edges of a survey and the natural bathymetry of the region. Survey H11082 is located within the proximity of an artificial fishing reef southwest of the Mobile Bay Main Shipping Channel (NOAA, 2002). The depth range of H11082 is approximately -21.0 to -17.0 m and the spatial extent of the survey area is shown in Figure 2.18. Derivative plots

confirmed artificial slopes were not present along the boundaries of the incorporated NOS surveys, similar to H11082 (Figure 2.10) (Amante et al., 2011; Love et al., 2011; Taylor et al., 2008).

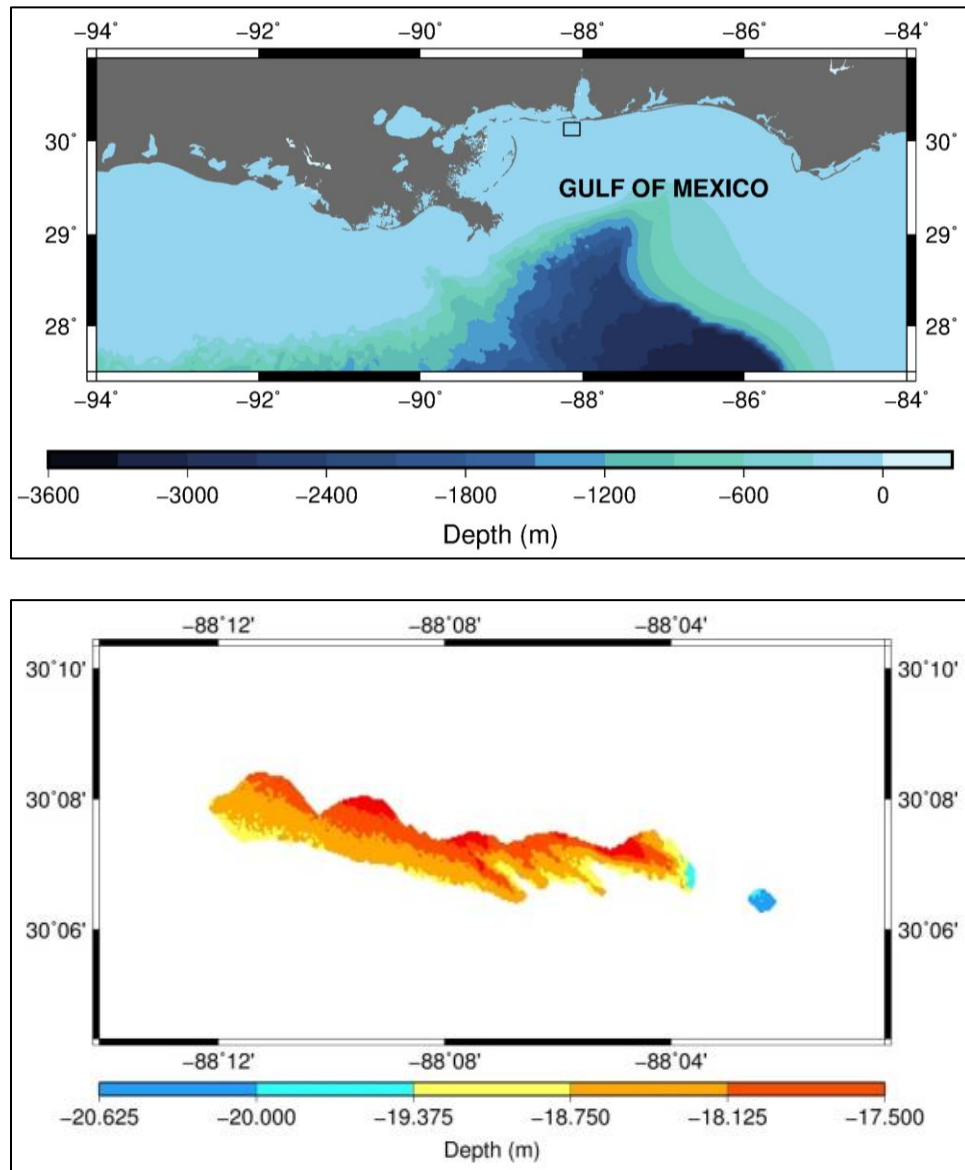


Figure 2.10 Location diagram and depth range of survey H11082 off the coast of Alabama

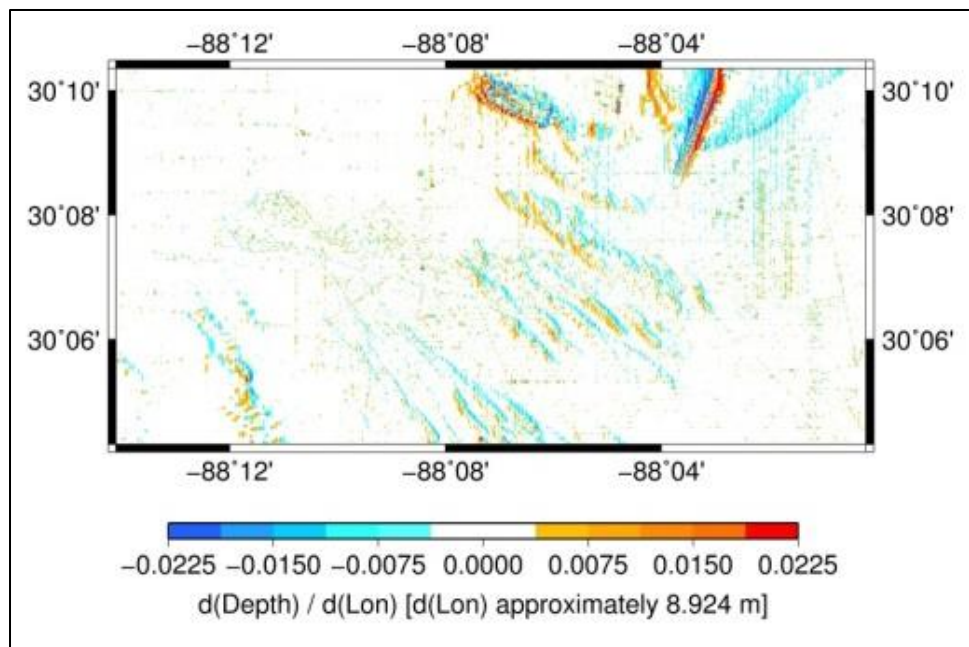


Figure 2.11 Derivative of the depth with respect to the longitude after survey H11082 incorporated into the BDDEM

Yearly difference plots were also generated from 2002 through 2011. The majority of surveys in Mississippi, Alabama and Louisiana nearshore regions were completed in the years following Hurricane Katrina (2005). The two most active years for conducting hydrographic surveys in the region were 2007 and 2009. Eighteen surveys were completed in 2007 and 30 surveys were executed in 2009. Depth differences between the 2009 and 2004 versions of the BDDEM ranged between -5.0 and 5.0 m along the coastline of Louisiana (Figure 2.12). Depth differences for the corresponding years ranged from -3.0 to 3.0 m in MS Sound and MS Bight (Figure 2.13). Depth differences between the BDDEM updates represent the depth change relative to the previous hydrographic survey in that region and not the change in the bathymetry from 2004 to 2009.

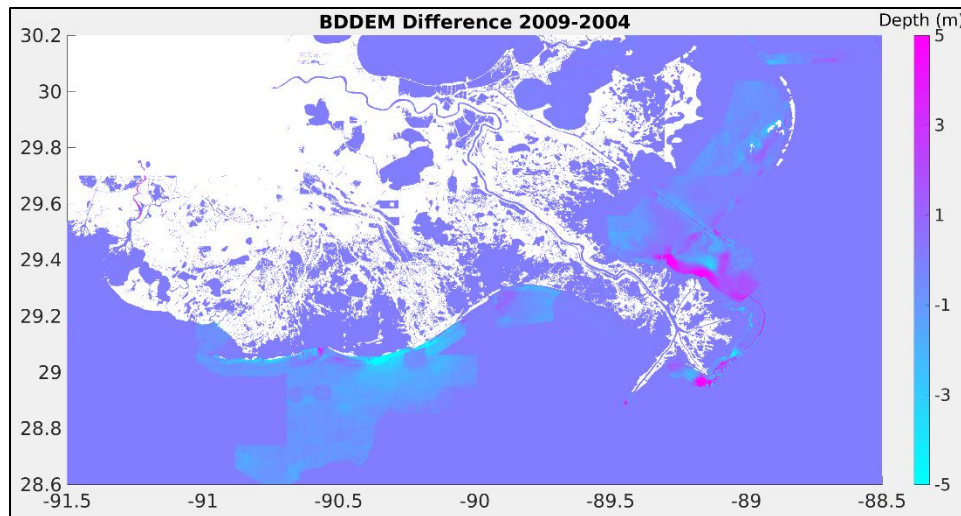


Figure 2.12 Depth difference between the 2009 and 2004 BDEMs along coastline of Louisiana

Differences of -5.0 to 5.0 m observed along the coastline.

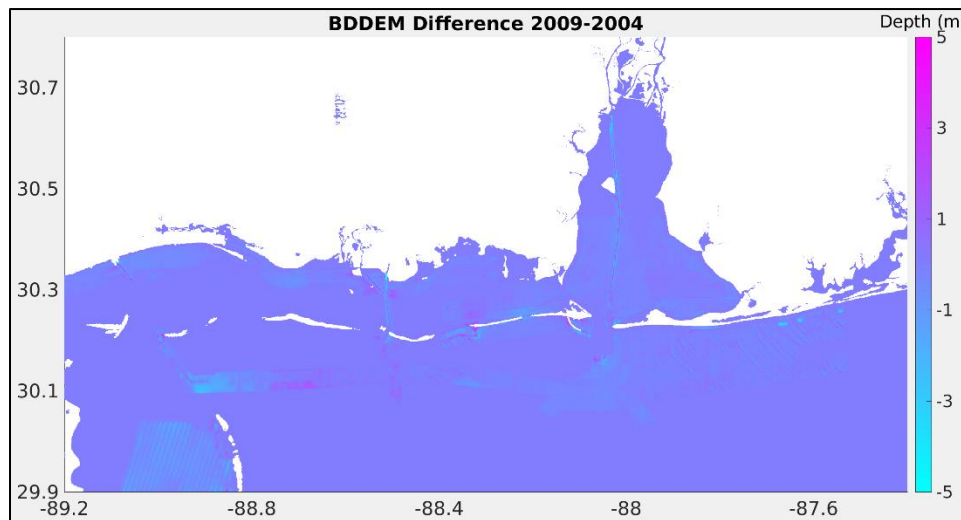


Figure 2.13 Depth difference between the 2009 and 2004 BDEMs in MS Sound and MS Bight

Differences ranged from - 3.0 to 3.0 m in MS Sound and MS Bight

2.4 Conclusion

A method was adopted to generate an updated DEM for the northern Gulf of Mexico using the open source tools GMT, MB-System and NOAA's VDatum. The derivatives of the updated BDDEM were computed to validate the BDDEM update process. Analysis of the BDDEM derivative plots indicated the ingestion procedure limited artificial slopes resulting from the inclusion of the NOS surveys in the BDDEM. The final BDDEM product is available at resolutions of 10, 30 and 90 m for the northern Gulf of Mexico (Wiggert et al., 2018a). The updated bathymetry was utilized in a synthesis model developed by CONCORDE.

CHAPTER III

3.1 Abstract

The physical forcing mechanisms affecting increased sediment concentration observed in the Mississippi Bight during a spring 2016 cold front event was investigated using CONsortium for oil spill exposure pathways in COastal River-Dominated Ecosystem's (CONCORDE) synthesis model, based on the Coupled Ocean-Atmosphere-Wave-Sediment Transport (COAWST) modeling system. The synthesis model was assessed using in situ gray scale images of particulate matter, atmospheric, temperature, salinity, wave and particulate backscatter data. Increased concentrations of suspended sediments in Mississippi Bight was caused mainly by the exchange of coastal waters through the tidal passes by Ekman transport and the resulting bottom shear generated by the shoreward and offshore advection of high salinity bottom water during the cold front. The sediment concentration in the Bight decreased, and sediments settled back to the seafloor during the dissipation of the cold front as the northerly wind velocity decreased.

3.2 Introduction

Mobile Bay (annual average of $\sim 2200 \text{ m}^3 \text{ s}^{-1}$) and the combined discharge from Lake Pontchartrain through the Rigolets, Biloxi, Pascagoula, Pearl and Wolf Rivers ($\sim 928 \text{ m}^3 \text{ s}^{-1}$) are major sources of fresh water and sediment load to Mississippi Sound (MS Sound) and Mississippi Bight (MS Bight) (Gelfenbaum & Stumpf, 1993; Sikora & Kjerfve, 1985). Regional discharge has a seasonal shift with maxima occurring in late winter/early spring and minima occurring in late summer/early fall (Stumpf et al., 1993;

Morey et al., 2005). Sediment type in the northern Gulf of Mexico consists of soft clay/mud (80%), firm/sandy silt (15%) and sand (5%) (Priddy et al., 1955).

Surface salinity annual range in the Bight is variable, approximately 7 to 12 psu (Dzwonkowski et al., 2011a). Summer months in the Bight have the greatest thermal stratification and vertical temperature gradient decreases in the winter. Winter months are usually characterized by warmer bottom temperatures than surface temperatures (Dzwonkowski et al., 2011a). Changes in the vertical density gradient due to salinity and temperature variations in the Bight affects vertical stratification and mixing of resuspended sediments within the water column (Knauss, 1997; Fredsoe & Deigaard, 1992). Fresh water discharge and winds affect the across shore transport of sediments in this region.

Both wind driven and buoyancy driven estuarine outflow are present in the northern Gulf of Mexico (Dzwonkowski & Park, 2010). Energy transfers from the wind to the ocean as wind blows along the surface of the ocean. Each water layer moves to the right (in the Northern Hemisphere) of the layer directly above it due to Coriolis force. Ekman transport of the water mass is 90° to the right of the wind in the Northern Hemisphere (Knauss, 1997). A geostrophic current is a current balanced by the pressure gradient and Coriolis forces (Knauss, 1997).

Fresh water outflow exits MS Sound/Mobile Bay into Mississippi Bight (MS Bight) in a westward direction due to buoyancy driven coastal currents and the Coriolis force. The buoyant outflow propagates down shelf as a coastal current (Whitney & Garvine, 2005). A horizontal density gradient develops between the fresh water discharge and the higher salinity offshore Bight waters and generates an across shelf

pressure gradient that supports the buoyancy driven coastal current (Garvine, 1995). Alongshelf winds generate wind driven across-shelf current flow via Ekman transport and geostrophic alongshelf flow (Mitchum and Clarke, 1986; Clarke & Brink, 1985). Upwelling favorable winds (alongshelf) drive offshore surface Ekman transport and water level decrease along the coast. Conversely, downwelling favorable alongshore winds causes onshore Ekman transport and water level rise (Whitney & Garvine, 2005). Morey et al. (2003) numerical model and drifter release experiment along Louisiana coastline showed southeasterly winds in the spring and summer drive Ekman transport of Mississippi River outflow eastward of the local wind stress vector. Transport within the buoyant surface layer of the stratified water is predominantly eastward and results in the advection of lower salinity water east of Mississippi River outflow.

Inner shelf circulation in the Northern Gulf of Mexico is upwelling favorable in winter/spring and downwelling favorable in summer/fall (Weisberg et al., 2005). A transition in the net surface heat flux from cooling to warming and warming to cooling initiates the switch in the circulation pattern in spring and fall (Virmani & Weisberg, 2003). The surface transport pathway in the nearshore region is mostly offshore although the predominant wind is a downwelling favorable easterly wind (Dzwonkowski et al., 2011b). In spring and summer, the flow has a strong asymmetric response characterized by upwelling favorable conditions and offshore surface transport (Dzwonkowski et al., 2011b).

The seasonal cycle in the fresh water discharge, vertical density structure, ocean circulation, wind and ocean current influence the sediment loadings in this region. CONCORDE was established to investigate the complex fine-scale biological, chemical

and physical interactions in MS Sound and MS Bight, controlled by pulsed river plume dynamics. This was accomplished by conducting small vessel (winter 2015 and spring 2016) and ship sampling (winter 2015, spring and summer 2016) in the MS Sound and MS Bight, and developing a synthesis model to integrate the measurements (Greer et al., 2018).

Small boat surveys were conducted at Main Pass (Alabama) to provide an overview of the physical dynamics in the nearshore region. Ship-based measurements collected data in the MS Bight along three transects (West Corridor (WCORR), Middle Corridor (MCORR) and East Corridor (ECORR) to characterize the biophysical and optical properties of the study area (Figure 3.1). The In Situ Ichthyoplankton Imaging System (ISIIS) acquired images of suspended particulate matter (SPM), and the EIVA ScanFish III Rocio (Scanfish) measured particulate backscatter (Cowen & Guigand, 2008).

A four-dimensional biogeochemical/lower trophic level synthesis model for MS Sound and MS Bight was developed, based on the Coupled Ocean-Atmosphere-Wave-Sediment Transport (COAWST) Modeling System and the Community Sediment Transport Modeling System (CSTM) (Warner et al., 2010; Warner et al., 2008a). This study utilized the synthesis model to investigate the origin of a cold saline water mass observed by the ISIIS and Scanfish during a cold front event in spring 2016 along CONCORDE's WCORR and the effects of advection on the sediment resuspension along the WCORR and MCORR.

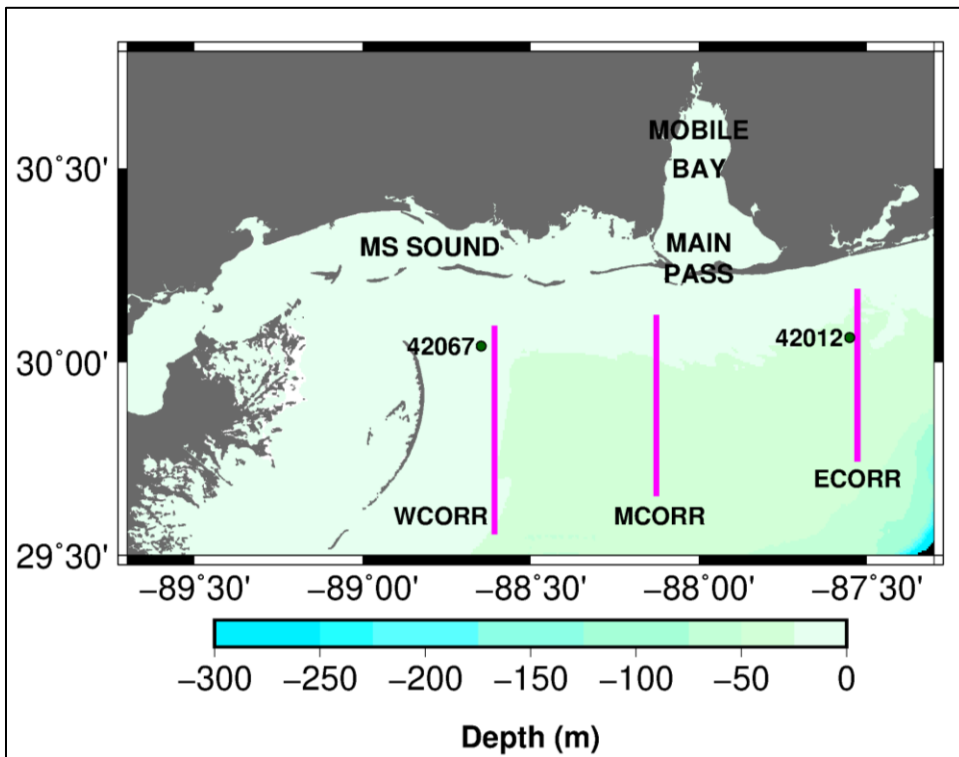
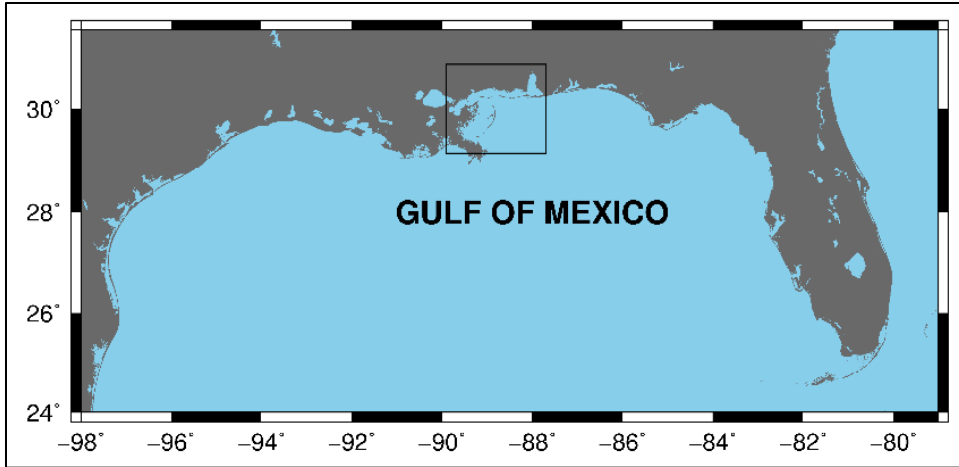


Figure 3.1 CONCORDE model domain and the locations of West Corridor (WCORR), Middle Corridor (MCORR), East Corridor (ECORR), The University of Southern Mississippi (USM) (42067) and Orange Beach (42012) buoys

3.3 Data and Methods

3.3.1 Data

3.3.1.1 Cruise and Sampling

In spring 2016 (28 March to 13 April), the R/V Pelican (Pelican) and R/V Point Sur (Point Sur) collected data in the MS Bight along WCORR, MCORR, ECORR (Figure 3.1). WCORR, MCORR and ECORR latitudinal limits are 29.55 to 30.09 ° N, 29.65 to 30.12 ° N and 29.74 to 30.19 ° N, located at -88.60 ° W, -88.12 ° W and -87.52 ° W. WCORR and MCORR were located within and outside of the fresh water plume exiting Horn Island Pass and Main Pass, and to the west of the tidal passes to capture the effects of the Coriolis force on the plumes. ECORR was located to the east of Main Pass and unaffected by large volumes of fresh water discharge.

Point Sur towed the ISIIS at a velocity of 2.5 ms⁻¹ and the optical sensor captured images of organic and inorganic matter within the water column. Wet Labs backscatter sensor (ECO-BB3) mounted on a Scanfish measured the particulate backscatter within the water column as the Pelican transited the research site. ISIIS transited MCORR on three occasions (31 March, 2 April and 4 April), ECORR on two occasions (30 March and 3 April) and WCORR on two occasions (1 April and 5 April). Scanfish collected data along MCORR on 31 March and WCORR on 1 April. ISIIS and Scanfish collected data simultaneously along WCORR on 1 April.

3.3.2 Methods

3.3.2.1 In Situ Ichthyoplankton Imaging System

The ISIIS provides a continual image with a pixel resolution of $\sim 68 \mu\text{m}$ and the ability to resolve particles ranging from fine scale (cm) to sub mesoscale features (Cowen et al., 2013). The imaging system's camera utilizes a combination of light emitting diode light source, altered by plano-convex optics to generate a collimated light field, which backlights a parcel of the water column and a high-resolution line scanning camera. The very high-resolution images capture zooplankton and particulate matter in their natural position and orientation (Cowen et al., 2008). This study utilized the small ISIIS camera (4.30 cm field of view and 8.90 cm depth of field) due to the high concentration of particulate matter present in the water column.

Background variation and vertical lines were removed from ISIIS's line scan imaging by applying a standard 'flat-fielding' procedure in ImageJ. Standard length was measured in pixel and converted to mm using the pixel resolution and field of view. Counts of particles were completed using a custom ImageJ macro, which thresholded the 8-bit gray scale image by converting pixels with a gray level ≤ 170 to black and ≥ 170 to white (Greer et al., 2015). Particles were grouped into three different size classes (0.25 to 1.00 mm², 1.00 to 3.00 mm² and 3.00 to 12.50 mm²) based on pixel area. The size classes were defined by running the particle counter on human identified images, and making size classes based on differences in taxon-specific size frequency histograms (Greer et al., 2015).

3.3.2.2 Scanfish

ECO-BB3 and conductivity, temperature and depth sensor (CTD) fitted to the Scanfish measured the particulate backscatter at a wavelength of 532 nm (bbp (532)), temperature and salinity. The ECO-BB3 measures the scattering by suspended particulates at an angle of 124 degrees. The signal measured by the sensor has a higher correlation with the size than the concentration of the particulate matter (Mobley, 1994). A 13-second time lag correction was applied to bbp (532), to account for the lag observed between the backscatter and CTD data.

3.3.2.3 Hydrodynamic Model

A four-dimensional biogeochemical/lower trophic level synthesis model was developed encompassing MS Sound and Bight with extents 29.00° N, - 89.96° W and 30.82° N, - 87.23° W (Figure 3.1) (Wiggert et al., 2018d; Wiggert et al., 2018e; Wiggert et al., 2018f; Wiggert et al., 2018h). The synthesis model has 24 vertical layers, higher vertical resolution near the surface and bottom to resolve boundary layer processes, and a 400 m horizontal resolution. The basis of the model is the Coupled Ocean-Atmosphere-Wave-Sediment Transport (COAWST) Modeling System (Warner et al., 2008a; Warner et al., 2010), and consists of two size classes of phytoplankton and detritus, three size classes of zooplankton, larval fish, dissolved organic nitrogen, nitrate, ammonium, and dissolved oxygen. The structure of the ecosystem model is similar to a Chesapeake Bay application (Wiggert et al., 2017).

The National Centers for Environmental Information (NCEI) Coastal Relief Model (CRM), released in 2001, was the basis for the synthesis model's bathymetry. The

90-m (horizontal resolution) CRM was updated utilizing NCEI's digital elevation models (DEMs) produced after 2001 and National Ocean Service bathymetric surveys completed from 2002 to 2011. The CRM data was updated with the Northern Gulf Coast, Biloxi, New Orleans, Mobile, Southern Louisiana DEMs and bathymetric surveys using MB System (Caress & Chayes, 1996) and Generic Mapping Tools (Wessel et al., 2013). The Bathymetric Dynamic Digital Elevation Model (BDDEM) represents the updated elevation model at resolutions of 10, 30 and 90 m. The updated 90 m bathymetry was interpolated onto the hydrodynamic model. The full details of the BDDEM are documented in chapter 2.

3.3.2.4 Atmospheric Model

Atmospheric forcing for the synthesis model is the CONCORDE Meteorological Analysis (CMA) field, which includes a variety of meteorological parameters run at 1 km horizontal resolution and 1-hour temporal resolution (Fitzpatrick & Lau, 2019). The 1 km atmospheric forcing grid was interpolated onto the 400 m hydrodynamic model grid. The Advanced Very High-Resolution Radiometer supplied daily sea surface temperature, and the Couple Ocean-Atmosphere Response Experiment flux algorithm provided the sensible heat flux and surface momentum stresses (Fairall et al., 2003). The North American Mesoscale Forecast System fields supplied the radiation parameters and total cloud cover percentage, and the Real-Time Mesoscale Analysis supplied the surface momentum and thermodynamic atmospheric data (De Pondca et al., 2011).

3.3.2.5 Wave Model

Surface waves interactions with the seabed are represented in terms of the wave-induced orbital fluid motion close to the seabed defined as wave orbital velocity. Near bottom wave orbital velocity is the wave orbital velocity just above the seabed (Wiberg & Sherwood, 2008). Bottom roughness, wave energy dissipation and sediment transport are essential parameters in hydrodynamic models for the coastal ocean (Wiberg & Sherwood, 2012). The National Oceanic and Atmospheric Administration (NOAA) WAVEWATCH III (WWIII), a third generation wave model, estimated the wave fields (Tolman & WAVEWATCH III Development Group [WDG], 2014). Wave parameters have a spatial resolution of approximately 7 km and a temporal resolution of 3 hours. The 7 km WWIII grid was interpolated onto the 400-m hydrodynamic model grid similar to Miles et al., 2015. Wave orbital velocity and bottom wave period were computed using a linear wave theory method utilizing an assumed Joint North Sea Wave Project spectrum, and interpolated onto the hydrodynamic model grid utilizing a bicubic interpolation method (Wiberg & Sherwood, 2008; Glover et al., 2011).

3.3.2.6 Sediment Model

The Community Sediment Transport Modeling System (CSTM) incorporates sediment transport and resuspension algorithms for erosion, bed load transport, suspended load transport and deposition of sediments. The sediment model consists of nine different classes ranging from clay to coarse sand (Table 3.1). Sediment transport calculations used the CSTM sediment routines outlined in Warner et al., 2008a. Mean grain diameter, porosity and sediment fraction were obtained from usSEABED, a data

repository consisting of discrete georeferenced data points with no fixed horizontal resolution. Mean grain diameter, porosity and sediment fraction were interpolated onto CONCORDE’s synthesis model grid utilizing a bicubic method (Buczowski et al., 2006; Glover et al., 2011). Biodiffusivity, mud mass, critical shear stress and erosion stress values were assigned based on previous studies and the settling velocity was computed from the mean grain diameter (Moriarty et al. 2014; Warner et al., 2008b; Knauss, 1997) (Table 3.1). The sediment parameters were used to generate an initial sediment bed for the CSTM.

Table 3.1 Sediment model parameters of the cohesive and non-cohesive sediments present in the sediment model

Moriarty et al. 2014; Warner et al., 2008b; Knauss, 1997

Wentworth Size Class	Grain Diameter (mm)	Density (kg/m ³)	Settling Velocity (mm/s)	Critical Shear Stress (Pa)
Clay	0.00006	2650	0.0000032	0.016
Very fine silt	0.0039	2650	0.013	0.019
Fine Silt	0.0078	2650	0.053	0.022
Medium Silt	0.0156	2650	0.22	0.038
Coarse Silt	0.031	2650	0.85	0.061
Very fine sand	0.0625	2650	3.4	0.090
Fine Sand	0.125	2650	13.8	0.140
Medium Sand	0.25	2650	55.3	0.190
Coarse Sand	0.5	2650	221.0	0.270

3.3.2.7 National Data Buoy Center Buoy

The synthesis model was validated using in situ atmospheric pressure, wind, significant wave height and wave orbital velocity data measured by the National Data Buoy Center's (NDBC) Orange Beach (42012) and The University of Southern Mississippi (USM) (42067) stations (Figure 3.1). Data is available for March and April 2016 at Orange Beach, and only April 2016 at the USM buoy. Station 42067 is located at 30.04° N and 88.64° W near the 20 m isobath, and station 42012 is located at 30.06° N and 87.55° W near the 25 m isobath.

3.3.2.8 Taylor Diagram

A Taylor diagram was generated to summarize the analysis of in situ data and synthesis model results (Taylor, 2001). Data comparison was conducted between ISIIS, Scanfish, NDBC buoys in situ data and synthesis model results. Root mean square difference, correlation coefficient and standard deviation were computed for the in situ and synthesis model results for meteorological and wave parameters (Glover et al., 2011). Root mean square difference and standard deviation of each synthesis model parameter were divided by the standard deviation of the corresponding in situ parameter to normalize and plot each variable on the same graph. Standard deviation of the in situ data is normalized by itself and therefore has a standard deviation of 1, correlation coefficient of 1 and root mean square difference of 0 (Taylor, 2001).

3.4 Results

3.4.1 Atmospheric and Wave Observations

A cold front affected MS Sound and MS Bight on 30 March 2016. The atmospheric pressure decreased from 1017 to 1008 hPa and there was a period of increasing southeast winds at the beginning of 30 March to 0200 Coordinated Universal Time (UTC) on 31 March (Figure 3.2). Significant wave height increased from 0.5 m to 1.5 m and zonal wind velocity increased from 5 to 9 ms^{-1} . Wind velocity was variable and rotated clockwise to northwesterly from 0300 UTC on 31 March to 0100 UTC on 2 April. Northerly wind decreased from 10 ms^{-1} at 0900 UTC to 3 ms^{-1} at 2200 UTC on 2 April as the cold front moved away from the region (Figure 3.2). The prefront is associated with southeasterly winds; the period of variable wind velocity and direction is characterized as the front, and reduced north winds as the post front (Kineke et al., 2006).

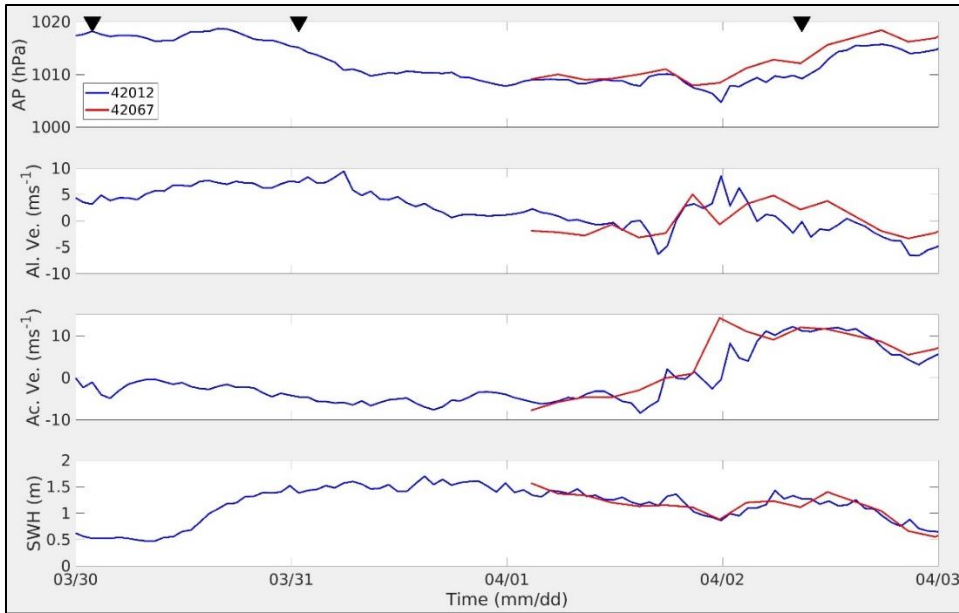


Figure 3.2 Atmospheric pressure (AP), alongshore wind velocity (Al. Ve.), across shore wind velocity (Ac. Ve.) and significant wave height (SWH) at the Orange Beach (42012) and USM (42067) buoys during the passage of the cold front

Atmospheric pressure started to decrease on 30 March (first black triangle) and maximum southeasterly winds occurred a few hours later on 31 March (second black triangle). Northerly winds started to decrease during the post cold front on 2 April (third black triangle)

3.4.2 In Situ Ichthyoplankton Imaging System and Scansfish in situ Observations

ISIIS and Scansfish observed temperature, salinity, particulate backscatter and gray scale images of particulate matter along the corridors during the front and post front periods. This section highlights observations at MCORR and WCORR during the front on 31 March (MCORR) and 1 April (WCORR). Lower salinity colder water was located in the surface water at the northern end (30.1 °C) of MCORR and higher salinity warm water was located at depths greater than 25 m between 29.7 and 29.9 °N (Figure 3.3). Fresh cooler estuarine discharge propagated from Mobile Bay and higher salinity MS Bight waters was present at deeper depths. Particulate backscatter along the entire

corridor was approximately 0.025 m^{-1} . D'sa et al. (2007) bbp (555) of 0.065 m^{-1} in Louisiana nearshore region, corresponded to an in situ SPM value of 0.160 kgm^{-3} .

Fresh water discharge was observed within the first 2 meters along the entire WCORR on 1 April (Figure 3.4). A cold high salinity water mass was present between 6 and 18 m at the northern end of the transect suggesting MS Bight waters propagated north along the transect. The cold water mass had minimum mean pixel gray level value of 120 and maximum bbp (532) of 0.15 m^{-1} (18 m and 29.9°N) along WCORR. The minimum mean pixel gray level and maximum bbp (532) values suggest the SPM concentration was maximum at this location (Cowen & Guigand, 2008; Greer et al., 2015; D'sa et al., 2006).

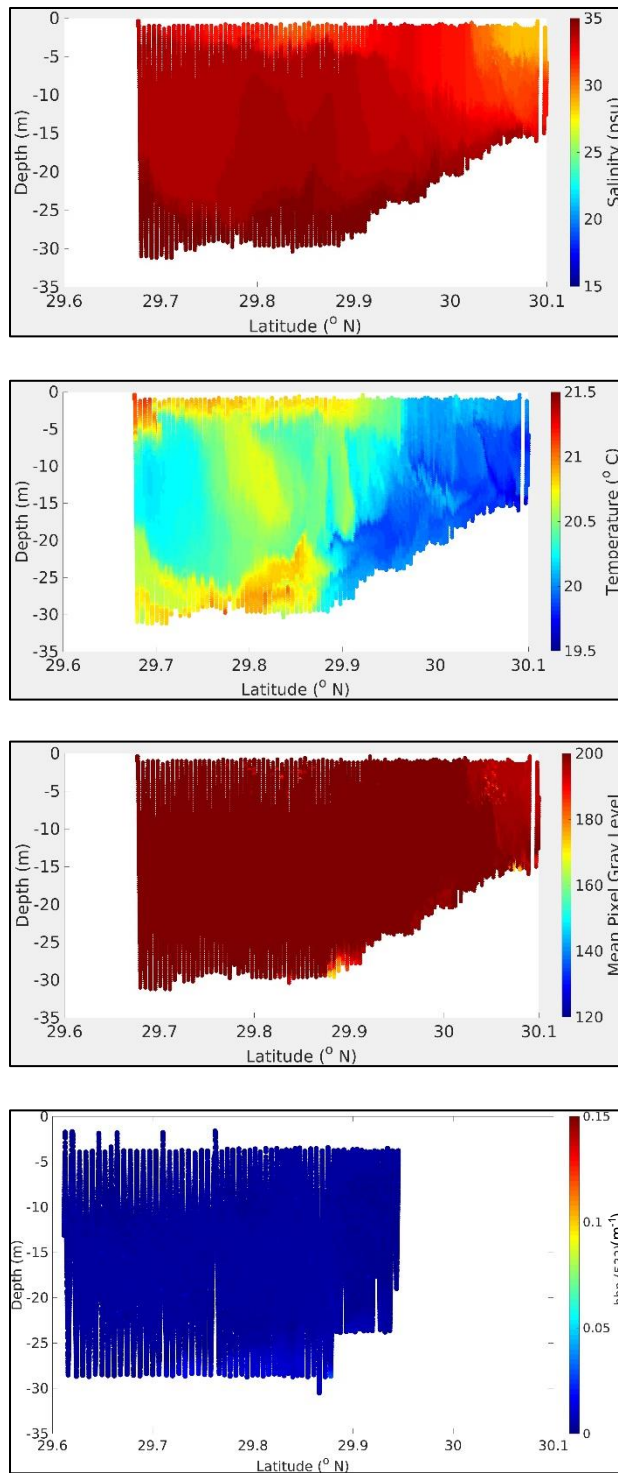


Figure 3.3 In situ salinity (In Situ Ichthyoplankton Imaging System (ISIIS)), in situ temperature (ISIIS), in situ mean pixel gray level (ISIIS) and in situ particulate backscatter at 532 nm (Scanfish) measured along MCORR on 31 March.

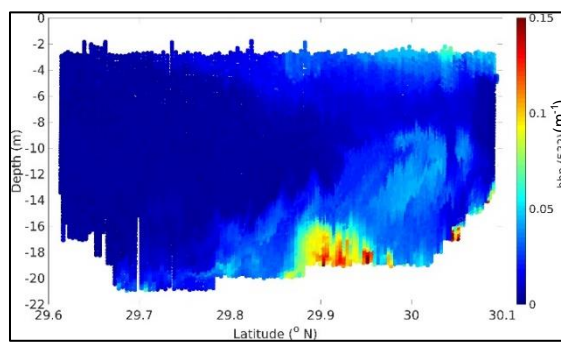
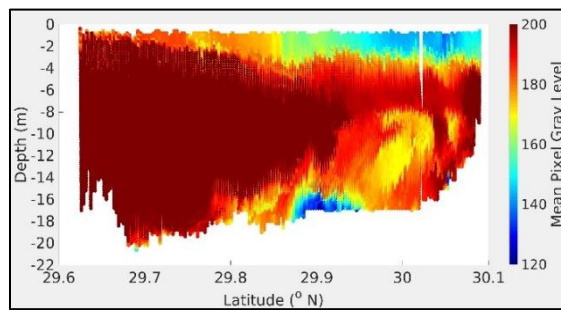
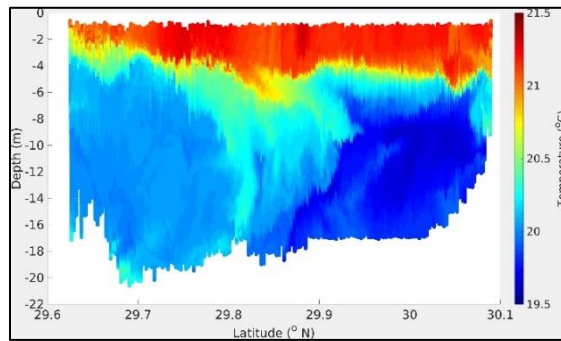
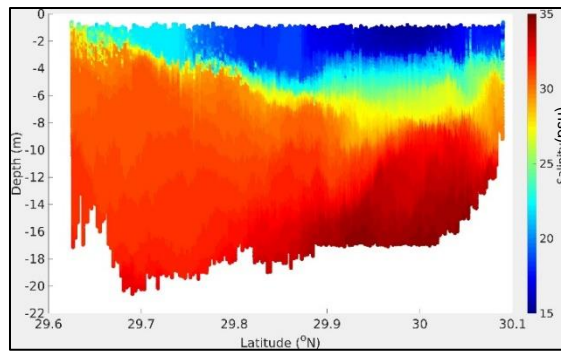


Figure 3.4 In situ salinity (ISIIS), in situ temperature (ISIIS), in situ mean pixel gray level (ISIIS) and in situ particulate backscatter at 532 nm (Scanfish) measured along WCORR on 1 April

The low mean pixel gray level and high particulate backscatter suggests suspended particulate matter concentration is maximum at this location along the transect

3.4.3 Synthesis Model Verification

In situ atmospheric pressure and wind velocity measured at NDBC buoys 42012 and 42067 from 18 March to 8 April 2016 were compared to the synthesis model's meteorological (CMA) results. Significant wave height and wave orbital velocity at NDBC buoys 42012 and 42067 were also computed for the same period and compared to WWIII outputs (Figures 3.5 and 3.6). Comparison of the in situ and synthesis model meteorological and wave results were summarized in a Taylor diagram (Figure 3.7).

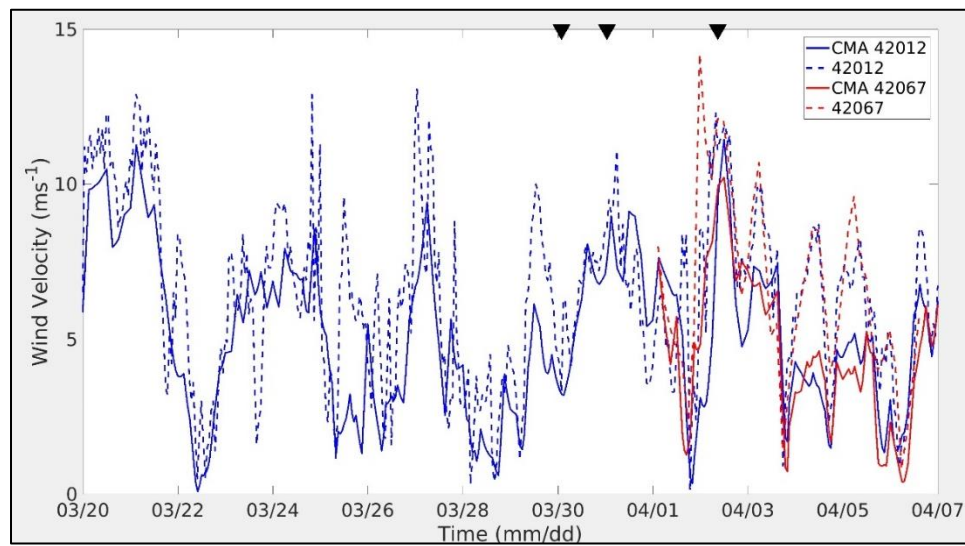


Figure 3.5 CMA model/in situ data comparison of the wind velocity at the Orange Beach (42012) and USM (42067) buoys

Prefrontal southerly winds increased for 18 hours on 30 March (first black triangle). Wind velocity was variable as the wind rotated clockwise from southeasterly to northwesterly on 31 March (second black triangle). Northerly post front winds started to decrease on 2 April (third black triangle).

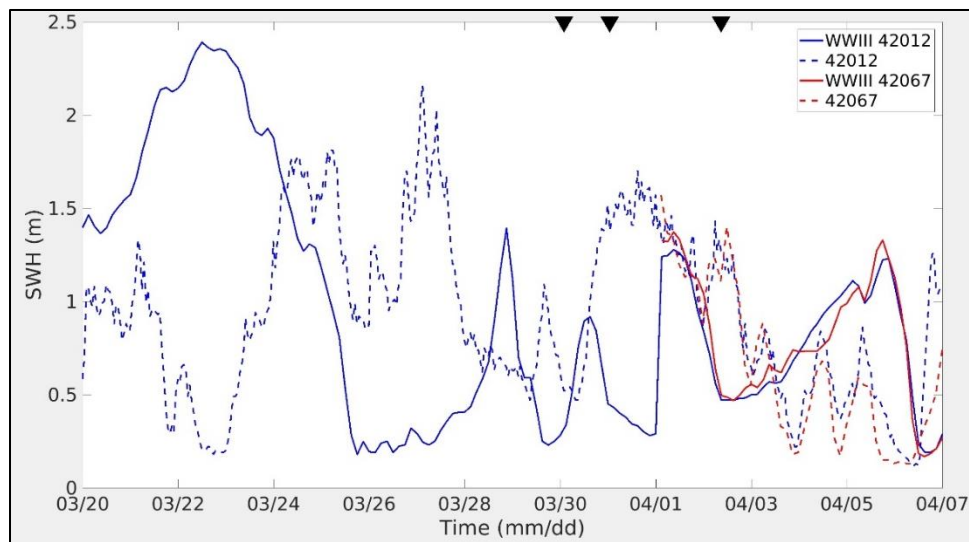


Figure 3.6 WWIII model/in situ data comparison of the SWH at the Orange Beach (42012) and USM (42067) buoys

In situ SWH increased as southerly winds increased on 30 March (first black triangle) and decreased as the wind rotated clockwise from southeasterly to northwesterly (second black triangle). SWH decreased at both buoys as the northerly velocity decreased.

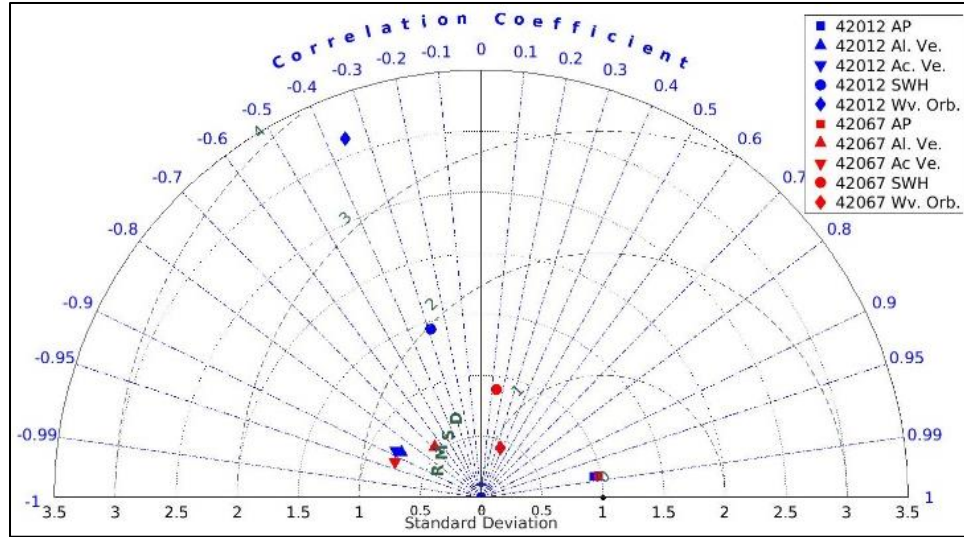


Figure 3.7 Taylor diagram showing the CMA and WWIII model results/in situ data comparison between the atmospheric and wave data (SWH and wave orbital velocity: Wv. Orb.) at Orange Beach (42012) and USM Buoy (42067)

Normalized CMA and WWIII model results are represented by the red (USM) and blue symbols (Orange Beach). Normalized in situ data is represented by the black circle with a standard deviation equal to 1 and root mean square difference of 0. The root mean square difference and standard deviation of the SWH and orbital velocity at Orange Beach (42012) was significantly higher than USM Buoy (42067).

CMA’s atmospheric pressure matched closely with stations 42012 and 42067 and had correlation coefficients of approximately 0.98 (Figure 3.7). CMA did not capture the peaks in the wind velocity and underestimated the winds at the USM and Orange Beach stations with maximum values of 5 ms^{-1} and 8 ms^{-1} . The across shore wind velocity’s root mean square difference (0.70), standard deviation (0.60) and correlation coefficient (-0.90) were similar at both locations (Figure 3.7).

Significant wave height at 42012 lagged WWIII data by approximately 36 hours and resulted in the model overestimating and underestimating the wave height at different times of the spring cruise (Figure 3.6). Station 42067 had a smaller root mean square difference (1.30 m) and standard deviation (0.20 m) compared to 42012 (1.90 m and 0.40

m). WWIII overestimated (~ 0.15 to 0.4 ms^{-1}) the near bottom wave orbital velocity at 42012 in the first 5 days of the model run, and the in situ data lagged the model output by approximately 24 hours for the remainder of the model run. The model near bottom wave orbital velocity had some agreement with station 42067 and had a much smaller root mean square difference (0.90 ms^{-1}) and standard deviation (0.20 ms^{-1}) than 42012 (3.70 ms^{-1} and 1.20 ms^{-1}) (Figure 3.7). The discrepancy in the significant wave height and near bottom wave orbital velocity are due to no spectral information provided with the WWIII model and the coarse resolution ($\sim 7200 \text{ m}$) compared to the synthesis model grid (400 m). Near bottom wave orbital velocity and significant wave height model values can be improved by coupling the Simulating WAVes Near-shore (SWAN) with the synthesis model instead of using WWIII and a linear wave theory method (Miles et al., 2015).

Sediment resuspension events are closely related to periods with high waves. Blas et al., 2007 sediment model study showed major resuspension events occurred when the significant wave height exceeded 1 m at a site located at approximately 20 m on a continental shelf similar to the NDBC buoys (42012 $\sim 26 \text{ m}$ and 42067 $\sim 20 \text{ m}$). Near bottom wave orbital motion due to surface waves is more critical than tidal motion to resuspend sediments in the nearshore region (Blass et al, 2007; Drake et al., 1985). Errors in the significant wave height and near bottom wave orbital velocity discussed above propagates to the synthesis model sediment resuspension results.

A Taylor diagram was also generated to compare the in situ temperature and salinity measured by the ISIIS and Scanfish along WCORR, ECORR and MCORR during the 2016 spring cruise. A qualitative comparison was completed between the in

situ mean pixel gray level, bbp (532) and the synthesis model sediment concentration. The model overestimated the salinity by approximately 2 psu and underestimated the temperature by approximately 0.50 °C along WCORR on 1 April (Figures 3.8 and 3.9). The model underestimated the salinity in the surface water by 2 and overestimated the temperature in the surface and bottom water by 0.25 to 0.75 °C at MCORR. The salinity in the fresh water plume was overestimated by 2 and the temperature above the thermocline was overestimated by 2.00 °C at ECORR. Salinity had a higher correlation coefficient and root mean square difference than the temperature along all the corridors (Figure 3.10). The dynamic nature of the Sound and Mobile Bay estuary in the spring involved vertical and horizontal mixing, advection and stratification processes, which occurred at different time and length scales (Greer et al., 2018; Jacobs, 2004). This contributed to the over estimation / underestimation of the temperature and salinity in the model.

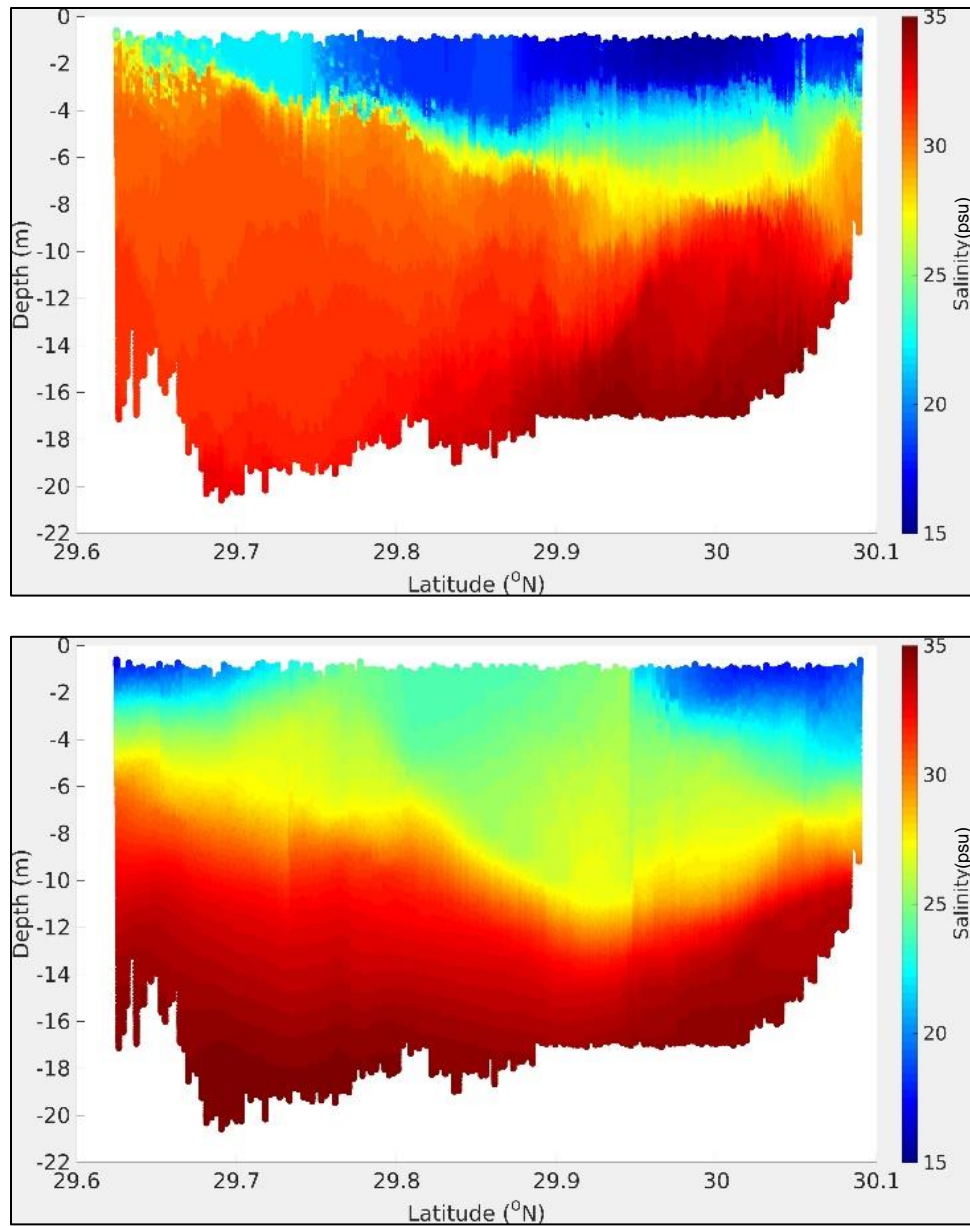


Figure 3.8 Comparison of in situ salinity measured by the ISIIS (top) and CONCORDE model salinity (bottom) along WCORR on 1 April

The model results overestimated the salinity by approximately 2 psu.

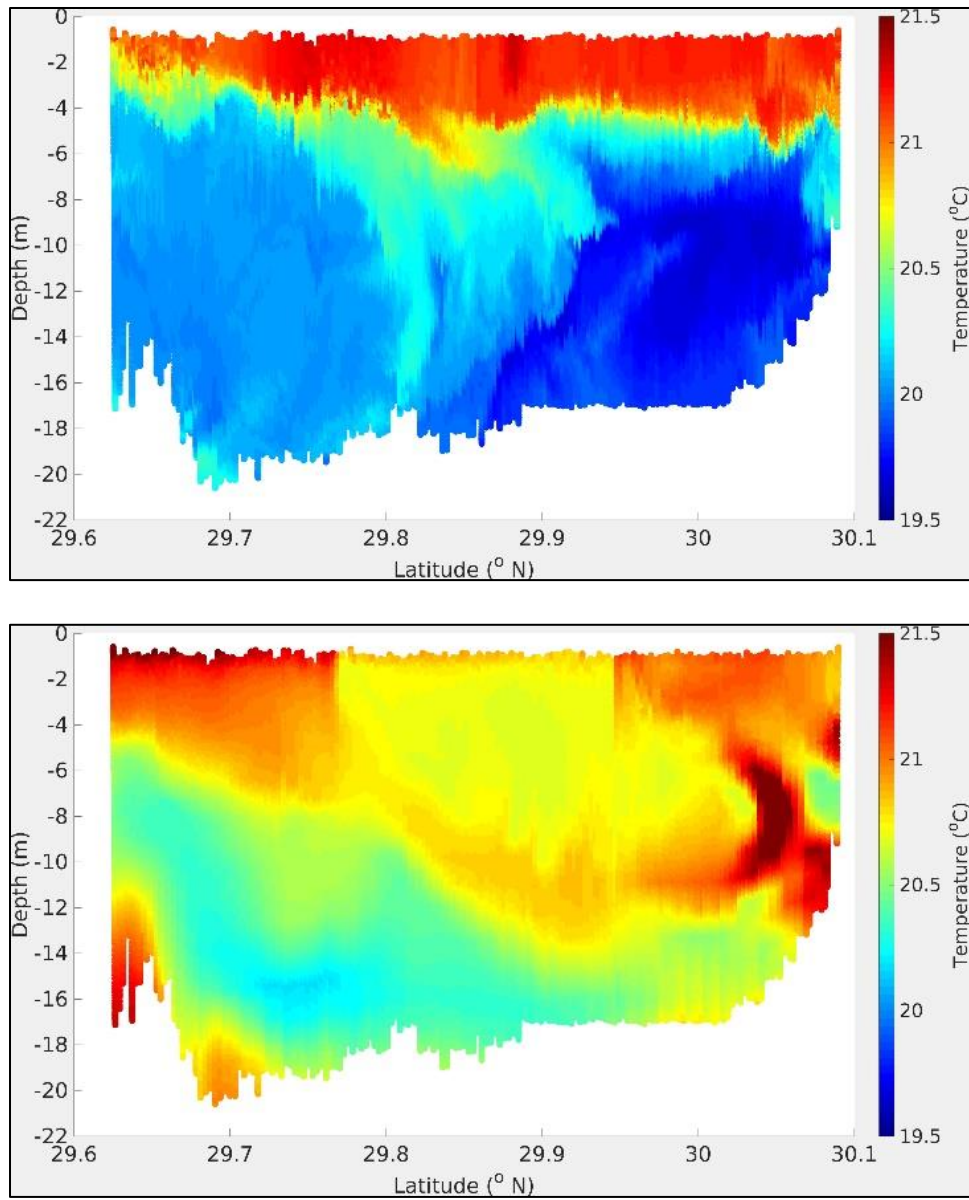


Figure 3.9 Comparison of in situ temperature measured by the ISIIS (top) and CONCORDE model temperature (bottom) along WCORR on 1 April

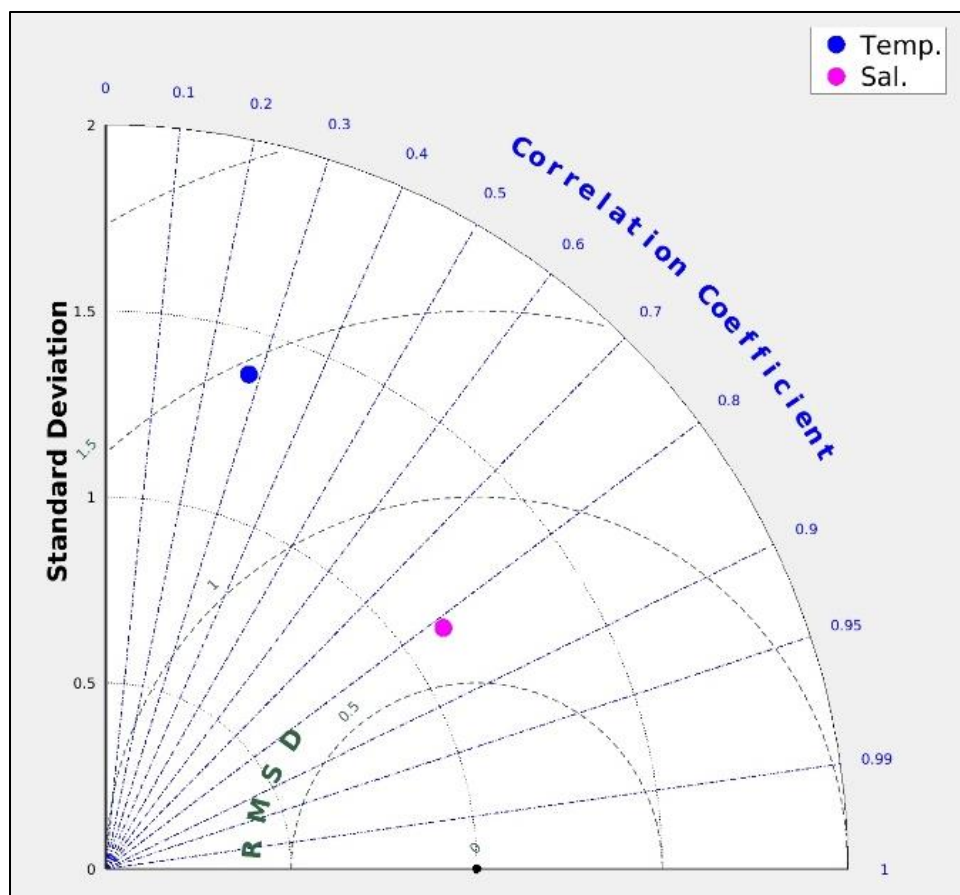


Figure 3.10 Taylor diagram showing CONCORDE model/in situ data comparison of the temperature and salinity measured by the ISIIS along WCORR, MCORR and ECORR

The model represented the salinity better than the temperature. Normalized in situ data is represented by the black circle with a standard deviation equal to 1 and root mean square difference of 0.

A qualitative comparison was completed between the mean pixel gray level, particulate backscatter and the synthesis model's fine silt concentrations. Fine silt was selected for the comparison because 95 % of the northern Gulf of Mexico consists of mud/silt and the critical shear stress required to resuspend fine silt is less than the larger silt classes (Moriarty et al. 2014; Warner et al., 2008b; Priddy et al., 1955). Minimum gray level value (120) and maximum particulate backscatter (0.15 m^{-1}) were observed at WCORR in the bottom water at 29.9°N on 1 April. The synthesis model's fine silt

concentrations of 1 kg m^{-3} were observed south of the minimum gray level and high particulate backscatter observations along the corridor (Figure 3.11). The mean pixel gray level of 170 was observed in the bottom water mass along MCOORR on 2 April, surrounded by a water mass with a mean pixel gray level of 200 (Figure 3.12). The synthesis model concentration of fine silt concentrations in the bottom water mass and fresh water plume were 1 kg m^{-3} .

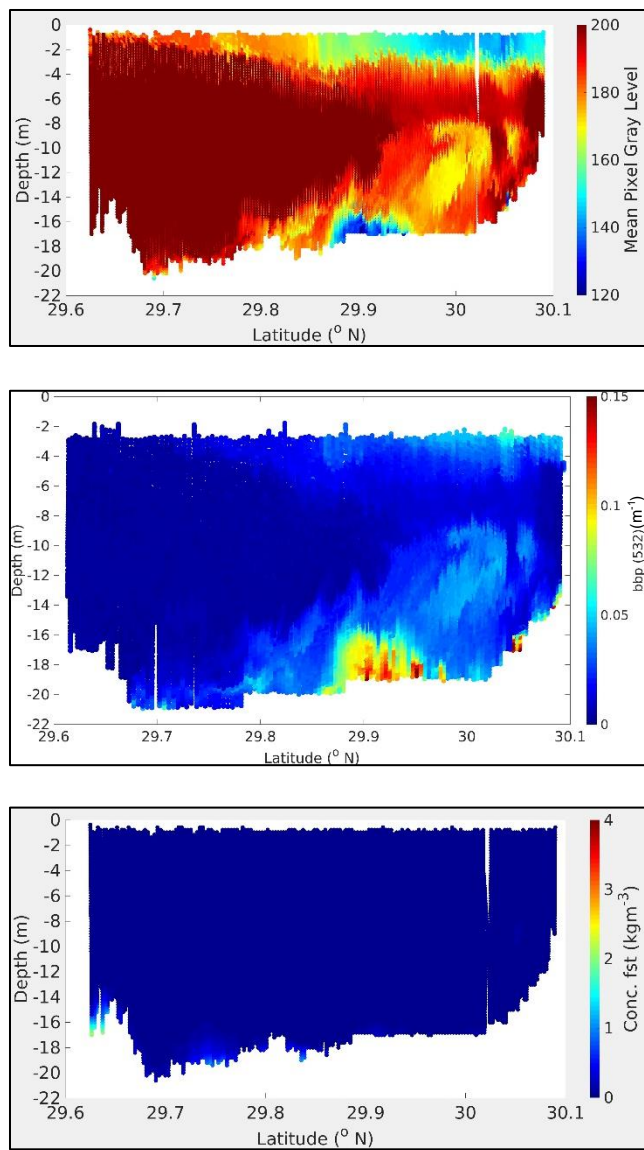


Figure 3.11 Comparison of in situ mean pixel gray level (ISIIS), in situ particulate backscatter at 532 nm (bbp (532)) (Scanfish) and synthesis model fine silt along WCORR on 1 April

Minimum gray level and maximum bbp (532) in the bottom water at 29.9 °N indicates maximum SPM concentration. Maximum synthesis model fine silt was located in the bottom water south of 29.9 °N.

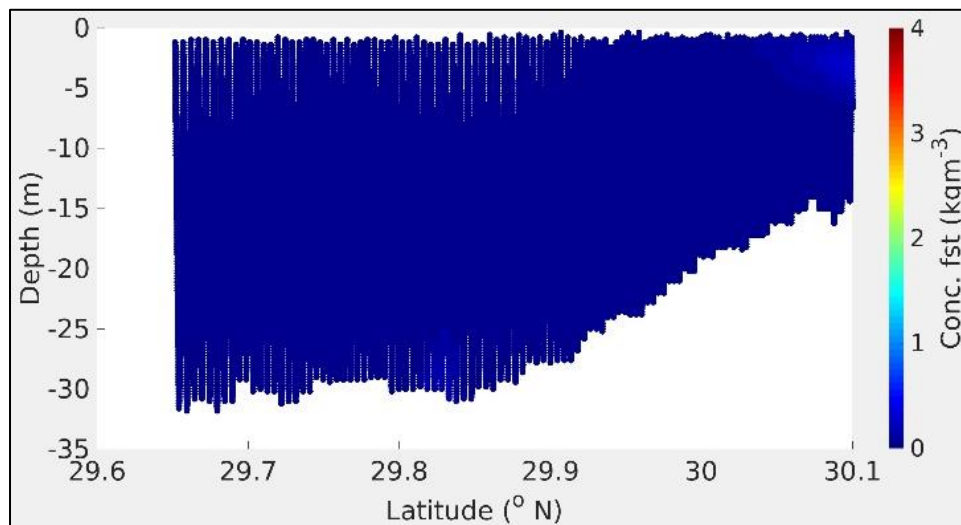
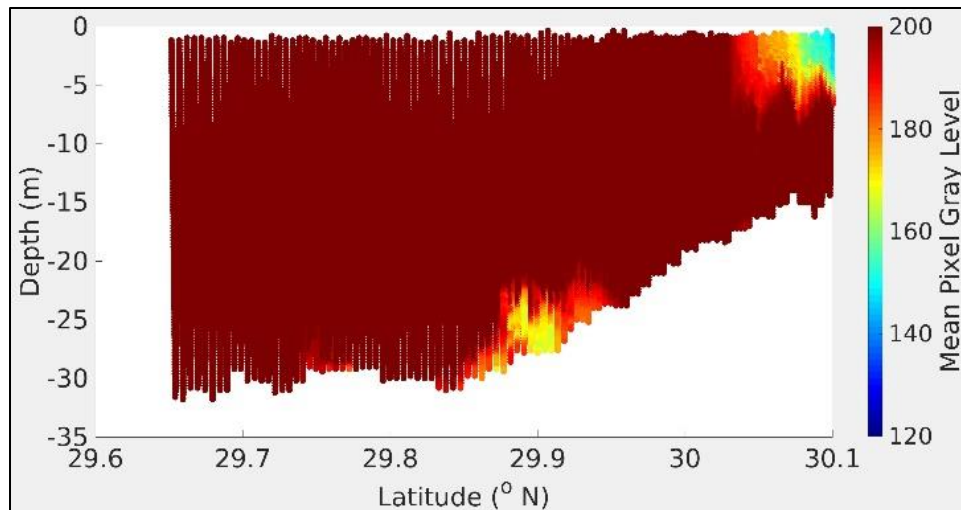


Figure 3.12 Comparison of in situ mean pixel gray level (ISIIS) and synthesis model fine silt along MCORR on 2 April

Minimum mean pixel gray level was located at approximately 29.90 °N at a depth of 30 m and maximum model concentration of fine silt was located at approximately 29.85 °N m at a depth of 30 m.

3.4.4 Synthesis Model Results: prefront to post front conditions

This section focuses on synthesis model results as the cold front system affected MS Sound and MS Bight. Synthesis model results focused on the advection of coastal waters between MS Sound, Mobile Bay and MS Bight in the proximity of WCORR and

MCORR during the cold front. At the start of 30 March, prefrontal winds in MS Sound and northern MS Bight were southeasterly and increased from 4.0 to 8.5 ms^{-1} for approximately 18 hours. The wind velocity decreased to 8.0 ms^{-1} and remained constant until 0200 UTC on 31 March. Maximum significant wave height in MS Bight was 1.3 m and decreased shoreward, and near bottom wave orbital velocity in the Bight was 0.1 ms^{-1} and increased northward. Near bottom wave orbital velocity at Main Pass and the barrier islands' coastline were similar (0.25 ms^{-1}), and 0.30 ms^{-1} at the Louisiana wetlands west of Chandeleur Island (Walker et al., 1989). Wind forcing resulted in northwestward ocean current advecting fresher (20 to 25 psu) surface water shoreward and higher salinity (25 to 32 psu) bottom water offshore due to the circulation of surface flow in the onshore/offshore direction and bottom flow in the opposite direction (Figure 3.13). Circulation of lower salinity surface water propagating onshore or offshore and a counter flow of higher salinity water at depth is a feature of estuarine circulation (Valle-Levinson, 2010).

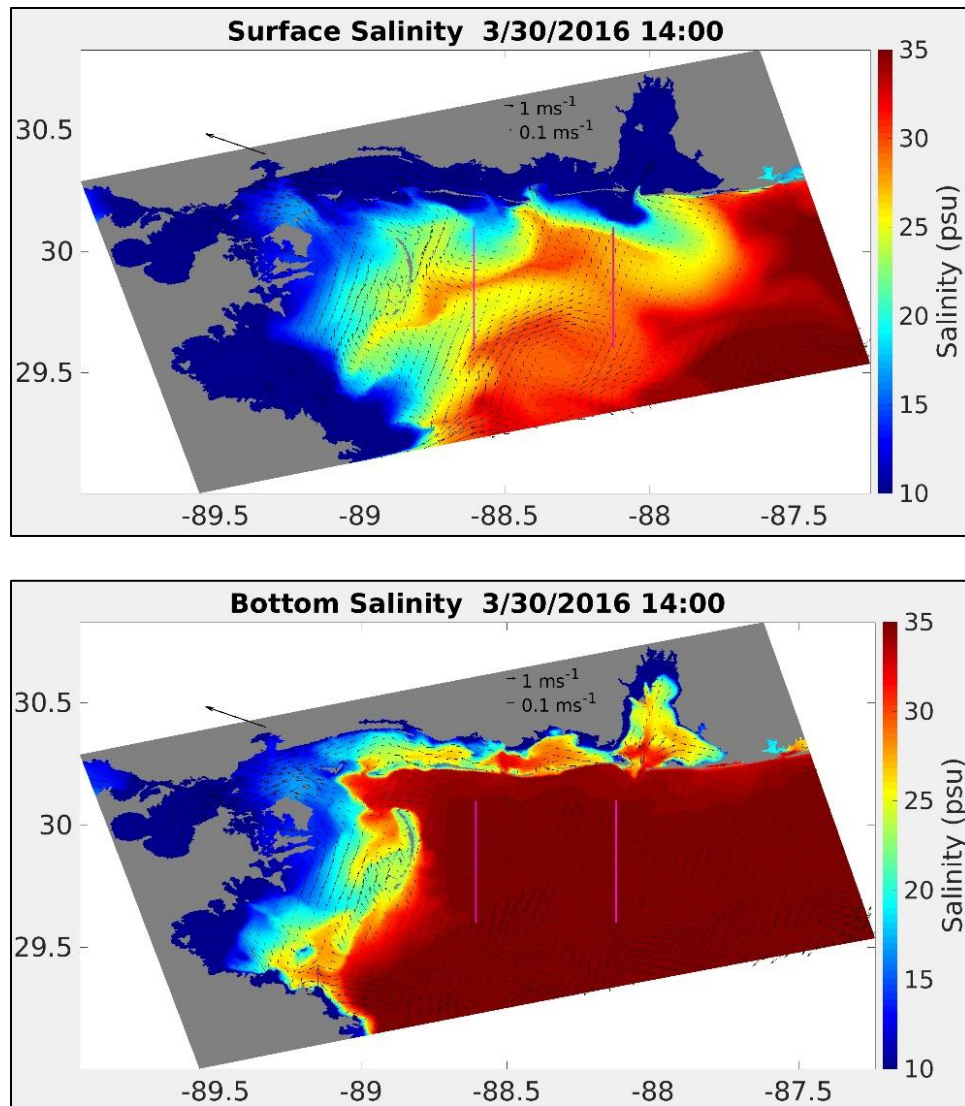


Figure 3.13 Water advected shoreward at the surface during the prefront phase and higher salinity water at depth advected offshore on 30 March

The thick black arrow shows the wind velocity, thin black arrows represents the surface current velocity. The locations of WCORR and MCORR transects are highlighted by the magenta lines.

Synthesis model results showed variability in the current circulation as the cold front system affected the northern Gulf of Mexico. The passage of the cold front from 31 March to 2 April was associated with clockwise rotation of the wind from southeasterly to northwesterly and variable wind velocity ranging from 1.5 to 6.0 ms^{-1} . Significant

wave height varied from 0.2 to 1.5 m with maximum values just south of the barrier islands, and the near bottom wave orbital velocity in the MS Sound and MS Bight increased from 0.05 to 0.3 ms⁻¹. The ocean current transported surface water in the MS Sound and northern MS Bight eastward and bottom water in the Sound and Bight moved westward opposite to the fresher surface waters.

Post frontal northerly winds decreased from 8.0 to 4.0 ms⁻¹ on 2 April from 1000 to 2200 UTC. Southward wind driven ocean current flushed the fresh estuarine surface water from MS Sound and Mobile Bay through the tidal passes and Main Pass. Coriolis force shifted the fresh water to the west as it exited Mobile Bay and the Sound (Figure 3.14). The change in wind velocity reduced the significant wave height in the Bight from 1.2 m to 0.3 m, and the near bottom wave orbital velocity in the Sound and Bight reduced from 0.3 ms⁻¹ to less than 0.2 ms⁻¹.

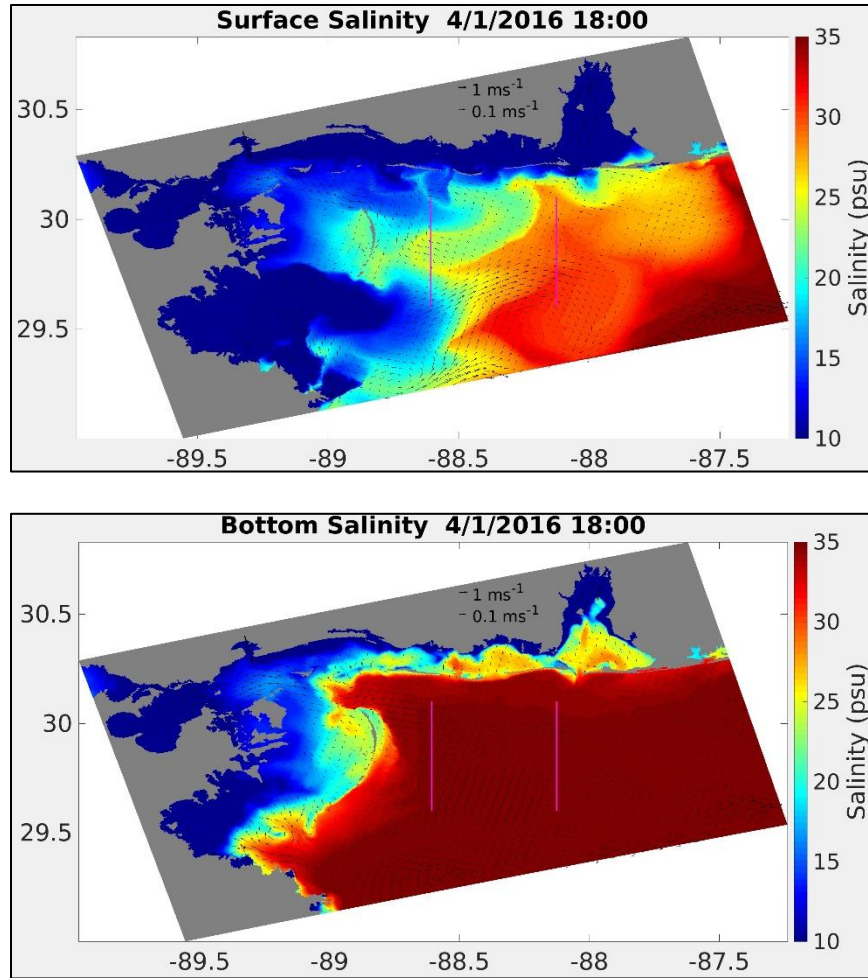


Figure 3.14 Postfrontal northerly winds flushed the estuary and advected fresh water southwest through Main Pass and the tidal passes on 1 April

The thick black arrow shows the wind velocity and the thin black arrows represents the surface current velocity. The locations of WCORR and MCORR transects are highlighted by the magenta lines.

3.5 Discussion

Sediment concentration model results during the cold front are discussed in this section. The fresh water plume along WCORR had a depth of approximately 5 m, and the depth of the fresh water plume along MCORR sloped shoreward from a depth of 3 m (offshore) to 5 m (inshore). Bottom shear generated by the Ekman transport of surface

water and the resulting advection of high salinity bottom water offshore suspended fine silt along the entire length of WCORR and the middle and southern sections of MCORR. Stratification along both corridors limited the resuspended sediments to depths below the fresh water plume. The concentration of fine silt was less than 0.5 kg m^{-3} within the fresh water plume along WCORR, and had maximum concentrations of 1 kg m^{-3} below the plume (Figure 3.15). The maximum concentration of fine silt along MCORR was 0.5 kgm^{-3} .

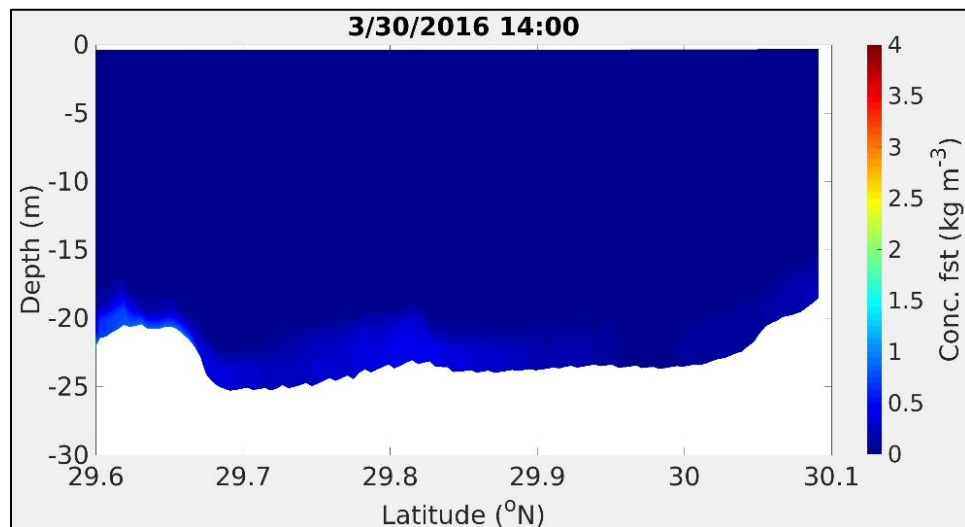


Figure 3.15 Southeasterly prefrontal winds generate shoreward bed shear and increased suspended sediments at WCORR due to the onshore Ekman transport of surface water and the offshore advection of high salinity bottom water

Suspended sediment model results were compared to two cold front studies in Louisiana estuary. Perez et al. (2000) studied suspended sediment concentration for three months in winter. Maximum in situ suspended sediment concentration (clay to coarse sand) was 1.5 kg m^{-3} and mainly due to resuspension of benthic sediments by increased wind velocity. A second study from October 1997 through March 2001 examined the

relationship between sediment transport and cold front events. Peak in situ surface sediment concentration of 0.26 kg m^{-3} occurred during increased northerly winds (Kineke et al., 2006). Sediment concentration model results along MCORR and WCORR exceeded the in situ maximum sediment concentration observed in these two studies. This indicates the synthesis model overestimated sediment concentration along WCORR during the cold front event. Lag time in the significant wave height, underestimation/overestimation of significant wave height and overestimation of the bottom orbital velocity in the synthesis model contributed to the over estimation of the suspended sediment concentration during the cold front event. The goal of this study was not to estimate the sediment concentration observed on 1 April along MCORR and WCORR, but to assess the physical processes contributing to the resuspension event.

As the winds rotated clockwise, water level and salinity at the northern end of WCORR and MCORR decreased due to Ekman processes and the draining of the coastal waters into MS Bight before the arrival of the post frontal northwesterly winds (Walker and Hammack, 2000; Dzwonkowski et al., 2017). Decreased salinity increased the depth of the fresh water plume at the northern section of WCORR and MCORR by 1 and 2 m respectively. The maximum concentration of fine silt increased by 300 % along WCORR due to the bottom shear caused by the greater volume of surface water moving offshore and bottom water moving inshore (Figure 3.16).

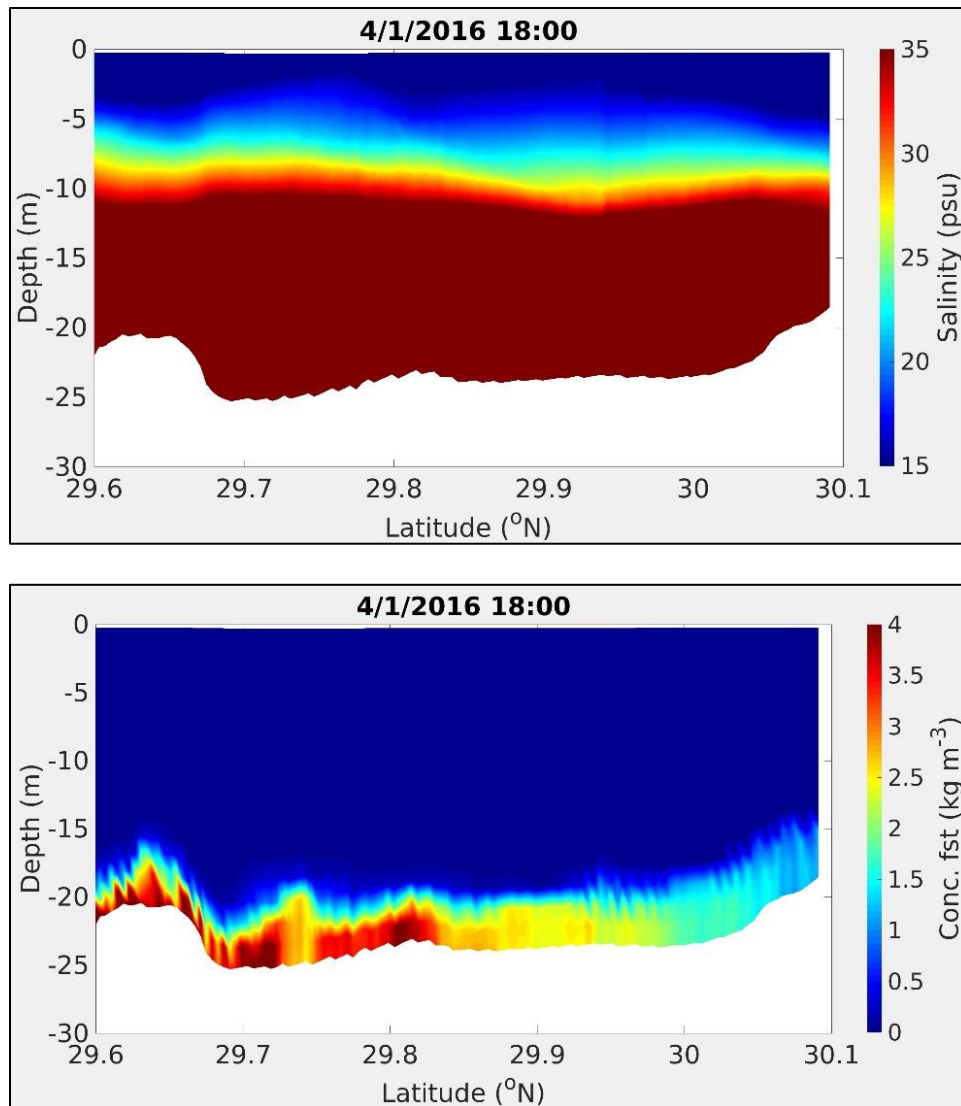


Figure 3.16 Southwesterly winds increased the depth of the fresh water plume by 1 m along WCOOR and discharged fresh water into MS Bight

The shoreward advection of the bottom water resuspended fine silt along the seabed.

The discharge of water from the coastal environment through the tidal passes continued, and advected further south into MS Bight during the post frontal northwesterly and northerly winds. Fine silt were transported southward by longshore drift from MS Sound and northern Chandeleur Sound to southern Chandeleur Sound. Southward

longshore drift along the eastern side of Chandeleur Island could act as a sediment source for WCORR during westerly winds (Keen, 2002). The concentration fine silt along WCORR and MCORR decreased as the wind velocity decreased and the sediments settled to the seabed.

3.6 Conclusion

This study used CONCORDE's COAWST based synthesis model and CSTM to investigate the changes in the ocean conditions and sediment dynamics in MS Sound and Bight during a cold front in spring 2016. Model results/in situ data analysis for the atmospheric pressure, salinity, temperature, wind velocity, optical backscatter, significant wave height and near bottom wave orbital velocity were conducted during calm conditions and the cold front event. Bottom shear produced by Ekman transport suspended sediments along WCORR and MCORR during the prefront, and stratification limited the suspended sediments to the high salinity bottom water. Maximum suspended sediment concentration along the corridors occurred during the passage of the front as high salinity bottom water moved onshore/offshore and increased the shear stress along the seabed. Decreased wind velocity in the post frontal phase reduced sediment concentration along the corridors as the sediments settled towards the seabed.

CHAPTER IV

4.1 Abstract

Mississippi Sound is low-lying coastline composed of marsh and wetland areas. It is characterized by turbid waters because of high input of organic and inorganic matter from several major sources (Mobile Bay, Pascagoula River and Pearl River) and the resuspension of silt-sized bottom sediments. Tidal passes in the Sound act as pathways for the exchange of estuarine discharge and suspended particulate matter (SPM) with Mississippi Bight. Particle size distribution, water samples and conductivity-temperature-depth (CTD) measurements were obtained in the Sound from August 2015 to August 2016, in support of the CONsortium for oil spill exposure pathways in COastal River-Dominated Ecosystems (CONCORDE) research effort to characterize the physical fields influenced by pulsed river discharge. To support the field measurements and provide spatio-temporal variability context at 500 m resolution, a SPM anomaly (SPMa) remote sensing algorithm was applied to Moderate Resolution Imaging Spectroradiometer (MODIS) measurements of 645 nm remote sensing reflectance. Surface velocity, salinity and temperature provided by CONOCRDE's synthesis model were used to analyze the changes in the SPM in the Sound, Bight and tidal passes after a period of increased fresh water input in winter 2015. Results show there is a sink of finer particles (31-63 μm) in western MS Sound in summer 2016, and the timing of the peak winter/spring river discharge in the Sound and Mobile Bay has a greater effect on the concentration of particulate matter in summer than the volume of the river discharge.

4.2 Introduction

Mississippi Sound is 4,792 km² and has an average depth of approximately 3 m (Arnone et al., 1983; Engle et al., 2009) (Figure 4.1). Pearl River, Pascagoula River and Mobile Bay estuarine discharge through Pass aux Herons are the major sources of fresh water input in the Sound. Eighty percent of the Sound is soft clay/mud, 15% is firm silt or sandy silt and 5% is sand (Priddy, 1955). Mobile Bay (east), the barrier islands (south) and MS Sound (west) borders MS Sound. This region encompasses CONCORDE's study area in the northern Gulf of Mexico.

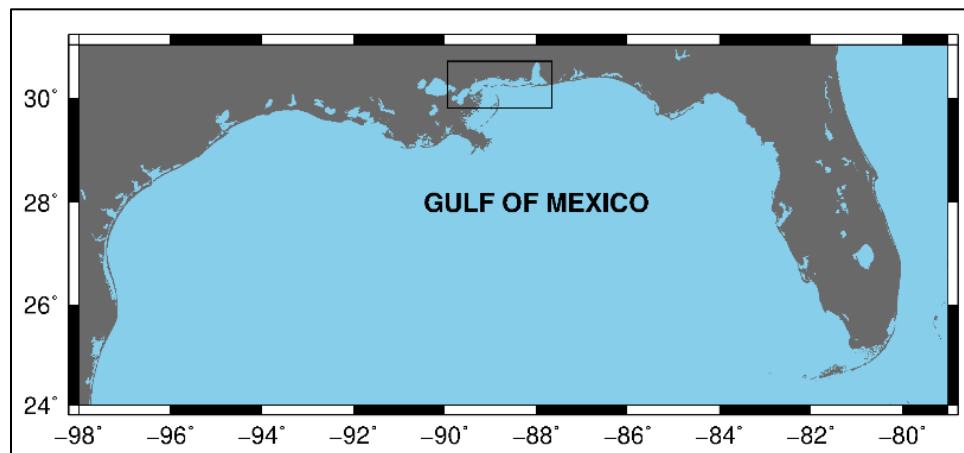


Figure 4.1 Location map showing Mobile Bay, the barrier islands and Lake Borgne enclosing MS Sound

Mobile Bay ebb-tidal estuary is 49 km in length from Main Pass to the Mobile delta, and 37 km at its widest point from Bon Secour Bay to Mississippi Sound (Hummell, 1990). The average depth of Mobile Bay is 3 m and has a volume of approximately 3.48 billion m³ (Jarrell, 1981). Main Pass has a width of 5 km between the eastern end of Dauphin Island and Mobile Point, and a deep 13-14 m ship channel

(Mobile Ship Channel) (Dinnel et al, 1990; Hummell, 1990). Approximately 85% of the river system discharge enters MS Bight through Main Pass and 15% enters the Sound through Pass aux Herons (Ryan, 1969). The MS barrier islands are located southwest of Mobile Bay.

The MS barrier islands from east to west are Petit Bois, Horn, Ship (East and West) and Cat. The tidal passes (Petit Bois Pass, Horn Island Pass, Dog Keys Pass and Ship Island Pass) between the islands act as a medium for the exchange of sediments between MS Sound and Bight. Petit Bois Pass is approximately 8 km wide and separated from Dauphin Island by the channel and a system of shoals. Horn Island Pass is approximately 5.5 km and consists of the Pascagoula Shipping Channel. Dog Key Pass is located between Horn and Ship Islands and has ebb tidal shoals. Ship Island Pass is located west of West Ship and encompasses Gulfport Ship Channel. The average depth within the passes is approximately 5 m, and the navigation channels have a maximum depth of 20 m (Byrnes et al., 2013).

Lake Borgne covers an area of approximately 550 km², and connects to MS Sound at the northeast end (Ischen, 2009). Pearl River is located north of Lake Borgne and is a source of fresh water discharge to the lake. Lake Borgne receives outflow from Lake Pontchartrain at the Rigolets and Chef Menteur natural tidal passes (Sikora & Kjerfve, 1985). Fresh water discharge entered Lake Borgne via the Rigolets and Chef Menteur during the 23-day Bonnet Carre spillway opening from 10 January to 1 February 2016. Peak discharge of 5,748 m³ s⁻¹ at the spillway occurred 8 days after the initial opening on 17 January (USACE, 2018).

Suspended particulate matter consists of organic fractions and minerals (Sackett, 1978). In coastal waters such as MS Sound and Mobile Bay, eroded terrestrial material may be an important source of particulate matter (Degens & Ittekkot, 1985). A combination of in situ, CONCORDE's synthesis model and remote sensing data sets were utilized to investigate the spatial and temporal changes in the SPM in MS Sound and MS Bight, the tidal passes and Main Pass. A remote sensing derived SPM anomaly (SPMa) and in situ particle size data provided an overview of the SPM distribution in 2015 and 2016. These two years were corresponded to CONCORDE's oceanographic cruises in the study area in fall 2015, spring 2016 and summer 2016. The 2015 and 2016 SPMa data sets were compared to identify differences due to the increased fresh water discharge in MS Sound and Mobile Bay in winter 2015 and spring 2016.

4.3 Data and Methods

4.3.1 Data

4.3.1.1 Cruise and Sampling

Small boat research cruises were conducted to characterize the SPM in the MS Sound in summer 2015, winter 2015, spring 2016 and summer 2016 (Table 4.1). In situ Sea-Bird CTD profiles, discrete water samples and Laser In-Situ Scattering and Transmissometry (LISST) profiles were collected in August 2015 at Ship Island, and monthly at the Mississippi Department of Marine Resources (DMR) stations from January to August 2016 (except March 2016) (Figures 4.2 and 4.3). Surface (within the

first meter) and bottom (approximately 1 meter from the seabed) water samples were collected to measure the SPM concentration at the stations.

Table 4.1 1 Dates of seasonal cruises in the MS Sound to characterize suspended particulate matter (SPM)

Season	Cruise Dates
Summer 2015	19 August 2015
Winter 2015	24 January, 31 January and 12 February 2016
Spring 2016	22 April, 24 May and 8 June 2016
Summer 2016	5 July and 2 August 2016

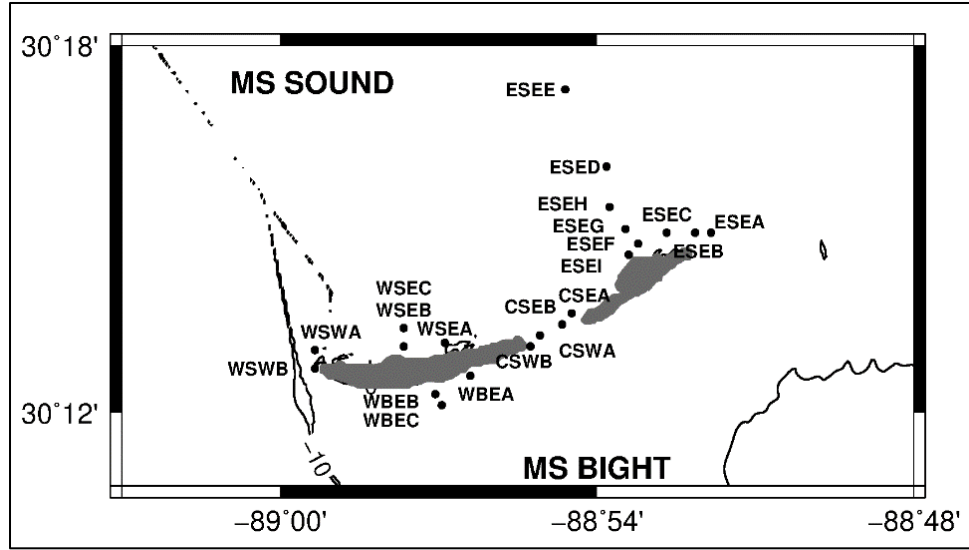


Figure 4.2 Location of the stations at East and West Ship Island for the August 2015 cruise

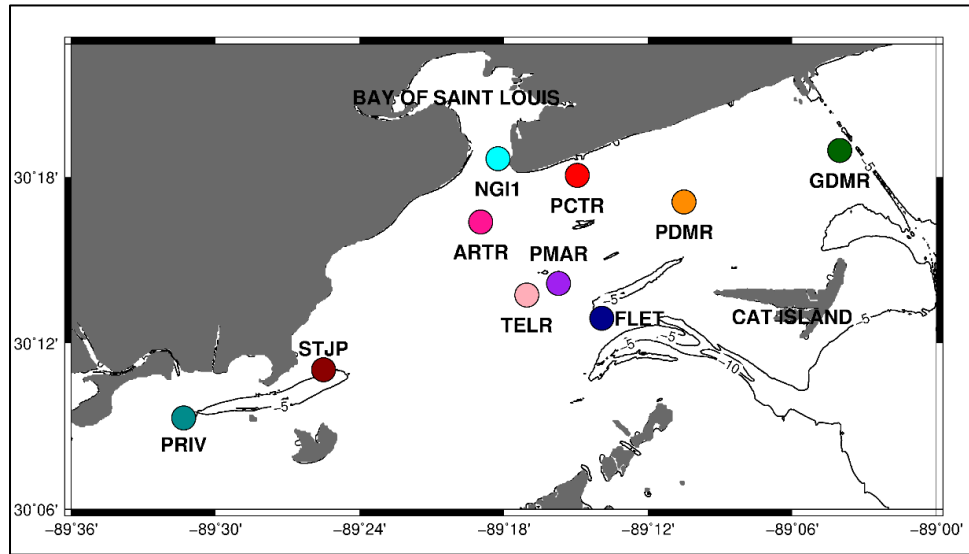


Figure 4.3 Location diagram of the DMR stations in MS Sound sampled monthly in 2016

4.3.1.2 Remote Sensing MODIS Aqua Level 1 Files

A list of partially cloud free MODIS Aqua Level 2 files were downloaded from National Aeronautics and Space Agency (NASA) Ocean Biology Processing Group in the geographic region defined by 89.70° W, 87.50° W, 29.50° N and 30.67° N (NASA, 2016). Matlab and bash scripts were used to convert the name of the Level 2 files to the corresponding Level 1 files, and the Level 1 files were downloaded from NASA Ocean Color Web for the period January 2012 to December 2016.

4.3.1.3 Historical in situ and CONCORDE Synthesis Model Data

Daily temperature, salinity and ocean current were extracted from CONCORDE's synthesis model from December 2014 to December 2016 and utilized in the SPMa analysis at the passes (Greer et al., 2018; Wiggert et al., 2018a; Wiggert et al., 2018b; Wiggert et al., 2018c). The synthesis model is based on the Coupled Ocean-Atmosphere-Wave-Sediment Transport (COAWST) Modeling System, and has a resolution of 400 m (Warner et al., 2008; Warner et al., 2010). Daily river discharge (United States Geological Survey) and six-minute wind velocity (National Oceanic and Atmospheric Association) were downloaded for the Alabama/Tombigbee Rivers (02428400 and 02469761), Pascagoula River (02479000), Pearl River (02489500), Dauphin Island (dpia1c), Katrina Cut (kata1), Petit Bois Island (ptbm6) and Bay Waveland (wycm6). These data sets were also included in the analysis of the SPMa.

4.3.2 Methods

4.3.2.1 In situ Suspended Particulate Matter Concentration

Whatman 1.5 μm pore size GF/F filters were prepared with 20 mL of Nanopure water and oven dried at 103-105 $^{\circ}\text{C}$ for 90 minutes. The filter was oven dried until the weight change was less than 4% of the previous weight (U.S. EPA, 1982). The SPM calculation is listed in equation 4.1.

$$SPM = \frac{(FPR - FP)}{V_s} \quad [\text{Equation 4.1}]$$

where FPR is the combined weight of the filter, petri dish and residue (mg), FP is the combined weight of the filter and petri dish and V_s is the volume of seawater sample filtered.

4.3.2.2 LISST and CTD Data Processing

CTD salinity and temperature profiles were processed with Sea-Bird Scientific software. LISST diffraction angles were processed in Matlab and transformed to total volume concentration, mean particle size and median particle size (Sequoia, 2013). Particle size measured by the LISST represented the inorganic and organic particulate matter in the MS Sound and Bight in this experiment. In this study, the average particle size (mean particle size) was computed by averaging the mean particle size depth profile at each station. Since the LISST is an optical sensor, density differences in the surface and bottom water results in measurement biases. The next section discusses these errors in further detail.

4.3.2.3 LISST Measurement Errors

Salinity and temperature anomalies in the coastal environment result in the disturbance of the optical path due to small differences in the refractive index known as schlieren (Topler, 1867; Schardin, 1942; Karpen et al., 2004). Schlieren in the pycnocline introduces artifacts in LISST measurements and erroneously records an increase in mean particle size due to the refraction of the light wave as it travels from one density layer to another. Lowering the LISST through a density gradient generates turbulence and mixing within the water column, and contributes to the effects of schlieren such as overestimating particle size measurements (Mikkelsen et al., 2008). High concentration of particulate matter causes multiple scattering of light and increases the scattering angle measured by the LISST. Since particle size is inversely proportional to the scattering angle measured by the detector, the LISST will underestimate the diameter of the particle (Agrawal & Pottsmith, 2000).

4.3.2.4 Remote Sensing Suspended Particulate Matter Anomaly

A Level 1 MODIS Aqua file was converted to a Level 1b file in SeaDAS using a geolocation file. The geolocation and Level 1b files were used to generate daily 500 m resolution Level 2 and Level 3 remote sensing reflectance files at 645 nm (Rrs (645)). The remote sensing reflectance product provides an estimate of the surface spectral reflectance measured at ground level when atmospheric scattering and absorption are negligible (Jensen, 2007). Level 3 Rrs (645) daily files were binned over a 1-month period and the georeferenced 500 m resolution image files were generated in SeaDAS 7.1 (Wiggert et al., 2018d).

In this study, a modified version of Zhao (2011) remote sensing SPM algorithm (equation 4.2) was applied to the monthly binned Level 3 Rrs (645) files in Generic Mapping Tools (GMT) to estimate the SPM in MS Sound and Bight from January 2012 to December 2016 (Wessel et al., 2013; Wessel & Smith, 1998; Wessel & Smith, 1995; Wessel & Smith, 1991; Wiggert et al., 2018g) (Figure 4.4).

$$SPM = 2.12 \times e^{(45.92 \times Rrs(645))} \quad \text{[Equation 4.2]}$$

where Rrs (645) is the remote sensing reflectance at 645 nm

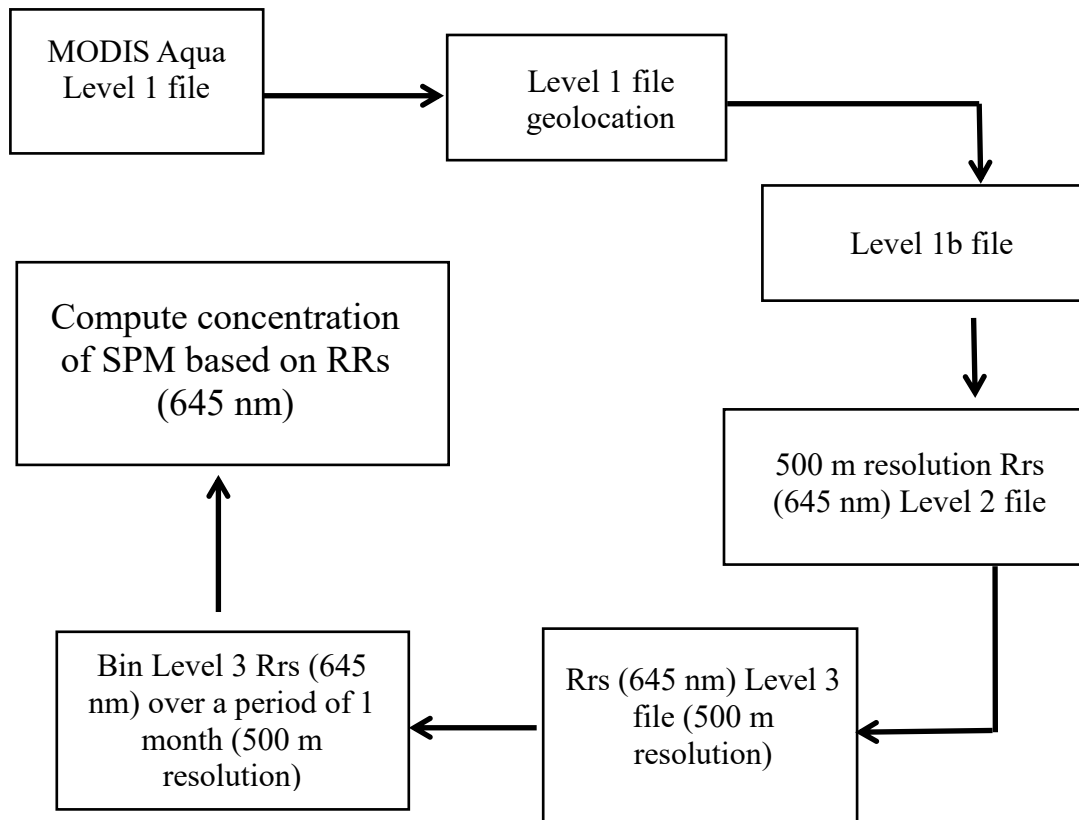


Figure 4.4 Workflow for converting a MODIS Aqua Level 1 file to estimated suspended particulate matter with a 500 m resolution

A monthly SPM climatology and SPMa were computed for the observational period. Climatology was defined as the 5-year mean (2012-2016) at each time step for each location as follows (Woodard, 2014):

$$SPM\ Climatology(\chi, \psi, t) = \frac{\sum_{t=2012}^{t=2016} SPM_{\chi, \psi, t}}{5} \quad \text{[Equation 4.3]}$$

where χ is the latitude, ψ is the longitude and t is the month. For each monthly composite at every coordinate in the data set, there would be five different SPM concentrations (e.g. January 2012, January 2013, January 2014, January 2015 and January 2016) that would be averaged to compute the SPM climatology.

$$SPM \text{ Anomaly} = SPM \text{ monthly mean} - SPM \text{ Climatology} \quad [\text{Equation 4.4}]$$

Missing data values in the climatological files were replaced with the coincident monthly climatological mean to generate a gap free SPM climatology. Missing data values were removed from the data set to remove any bias in the SPMa analysis.

Hovmoller diagrams of the SPMa were generated in the tidal passes and Main Pass to determine the effects of the hydrographic (temperature and salinity), wind and river discharge on the sediment exchange between Mobile Bay, MS Sound and MS Bight.

Hovmoller diagrams were generated by extracting the longitudinal section of each tidal pass in Matlab and plotting December 2014 to December 2016 time series. Coincident alongshore and across shore current, temperature and salinity were extracted from the synthesis model and included in the analysis. In situ wind and river discharge in the tidal passes and Main Pass were also included with the Hovmoller diagrams.

4.4 Results

4.4.1 Characterization of Suspended Particulate Matter in MS Sound during winter, spring and summer using in situ CTD, SPM and LISST data

4.4.1.1 Summer 2015

This section outlines in situ temperature, salinity, particle size and SPM concentration collected in MS Sound. East and West Ship Island consists of sediment types ranging from medium silt to coarse silt, and medium silt to very fine sand (Buczowski et al., 2006) (Figure 4.5). Seventy seven percent of the stations at East Ship

Island had a mean particle size between 20 and 30 μm and 33% of the stations had a mean particle size between 40 and 50 μm on 19 August (Figure 4.6). Stations with a larger particle size were located along the back-barrier shoreline of East Ship Island. Surface and bottom SPM at ESEH, located along the back barrier beach of East Ship Island was 32 mgL^{-1} and 84 mgL^{-1} respectively.

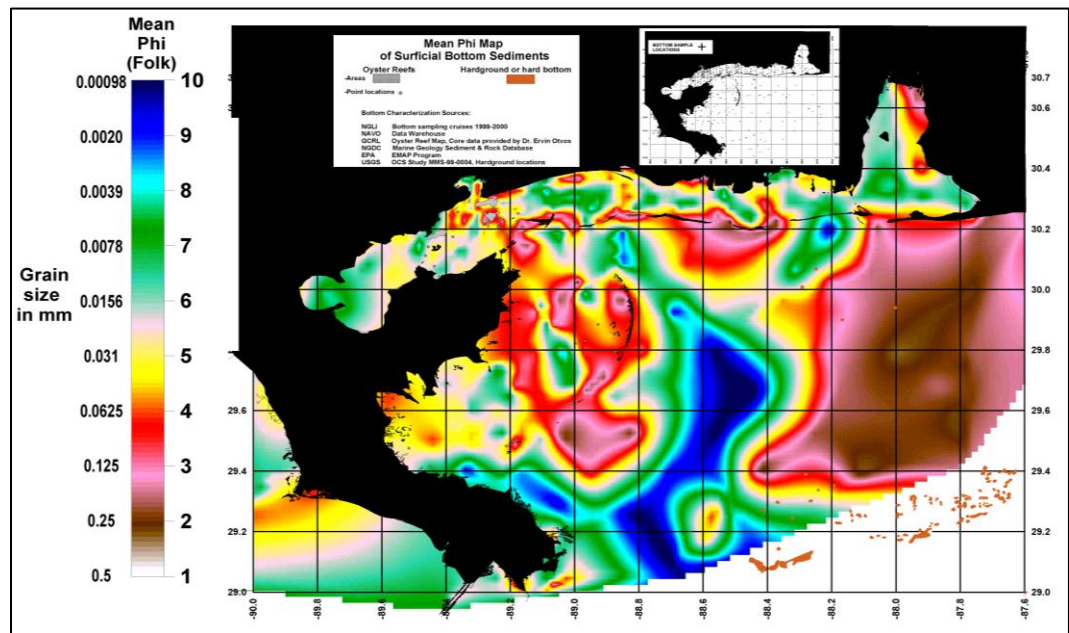


Figure 4.5 Surficial sediment map of the northern Gulf of Mexico

Sawyer et al., 2001. Sediments ranging from medium silt to coarse silt characterize East Ship Island and sediments ranging from medium silt and very fine sand characterize West Ship Island.

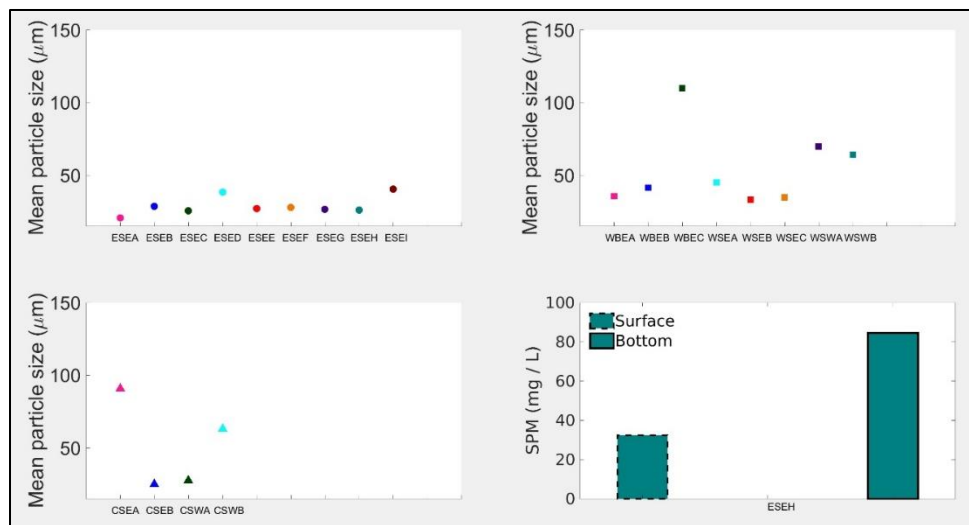


Figure 4.6 Particle size in situ data collected at the East (top left), West Ship (top right) Islands and Camille Cut (bottom left) on 19 August 2015

SPM was measured at station ESEH near East Ship Island (bottom right).

The majority of stations (63%) at West Ship Island consisted of a mean particle size between 30 and 50 µm. Two stations located along the back barrier of West Ship Island had a mean particle size between 60 and 80 µm and one station located along the Bight shoreline had a mean particle size of 110 µm (Figure 4.6). Two stations (CSWA and CSEB) situated in the center of Camille Cut had a particle size between 20 and 30 µm, and two stations located closer to the western and eastern ends of East Ship Island and West Ship Island had a larger particle size (60 to 100 µm).

4.4.1.2 Winter 2015

Surface and bottom in situ water temperature in the MS Sound ranged between 11 to 13 °C on 24 January (Figure 4.7). The water column was well mixed at PCTR and FLET, and a halocline was present at GDMR with a salinity of 17 psu in the bottom

water. The particle size between 40 and 50 μm was the most prevalent at the stations (FLET, PDMR, PMAR, PRIV and STJP). A particle size of 20 μm was observed at TELR and a range of 70 to 90 μm was observed at GDMR and PCTR. Surface and bottom SPM ranged between 10 and 20 mgL^{-1} at FLET, GDMR, PCTR, PDMR, PMAR, PRIV and TELR. STJP had the highest bottom SPM with a concentration of 91 mgL^{-1} .

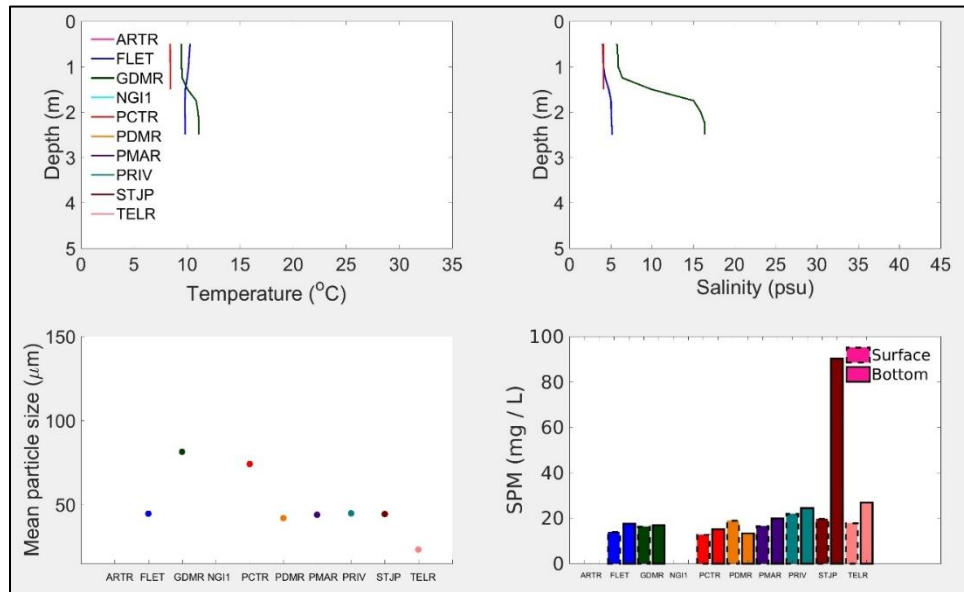


Figure 4.7 In situ particle size, temperature, salinity and SPM collected at MS Sound on 24 January 2016

In situ salinity of the bottom water at GDMR increased from 18 to 23 between 24 and 31 January (Figure 4.8). Stations STJP and PRIV were well mixed on 31 January and had a salinity of approximately 3 psu. A mixed layer with a depth of 1.0 m, a halocline and bottom water layer were present at the other stations. The mixed layer, halocline and bottom water had salinity ranges of 5 to 10 psu, 10 to 20 psu and 20 to 27 psu. Stations south of Bay of Saint Louis (PMAR, TELR, FLET and GDMR)

represented the highest bottom water salinities measured in the Sound. Particle size increased from less than 50 μm to a range of 50 to 140 μm at FLET, PDMR, PMAR, GDMR and TELR, and the particle size changed by less than 10 μm at PCTR and STJP between 24 and 31 January.

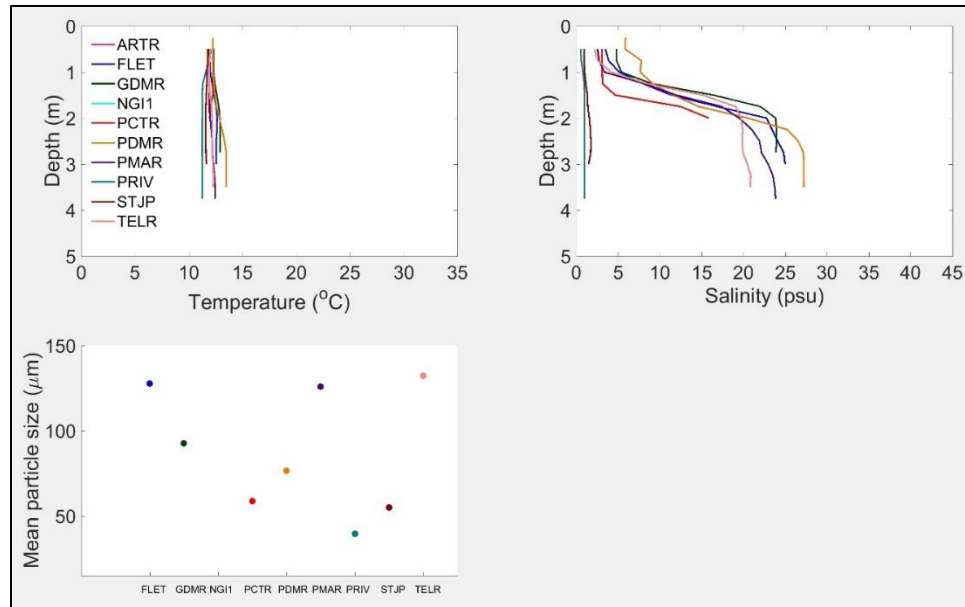


Figure 4.8 In situ particle size, temperature and salinity collected at MS Sound on 31 January 2016

In situ salinity remained highest south of Bay of Saint Louis (PMAR, TELR, FLET and GDMR) in February, and the range of the bottom water salinity increased to a minimum of 23 and a maximum of 33 (Figure 4.9). Mean particle size at PMAR and TELR decreased from 120 and 130 μm to less than 90 μm . Bottom SPM concentration increased between 24 January and 12 February at the west and central regions of the study area (GDMR, PDMR and PCTR), and surface SPM increased at PRIV, STJP and TELR. The high concentration of bottom SPM at STJP in January was not observed in February.

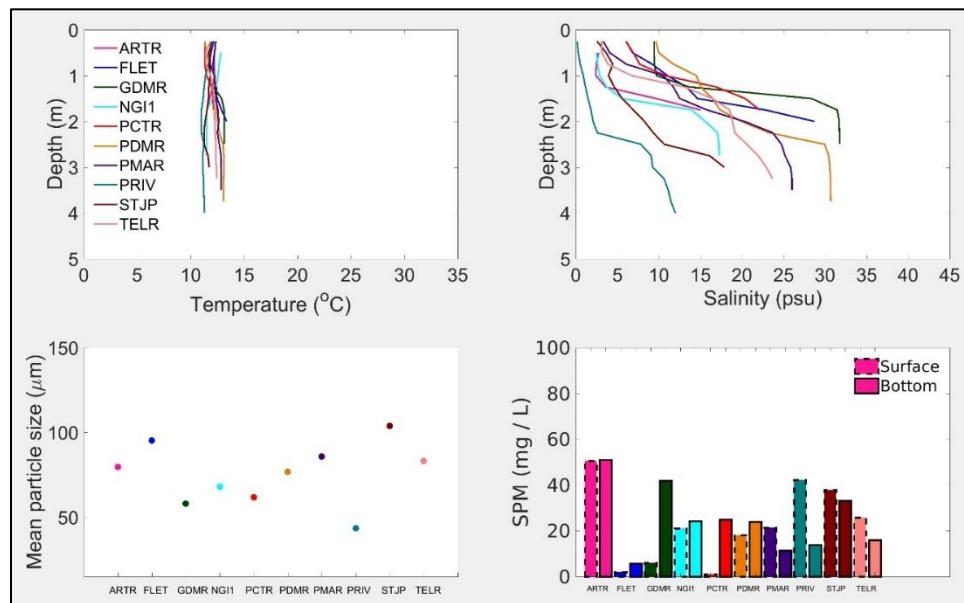


Figure 4.9 In situ particle size, temperature, salinity and SPM collected at MS Sound on 12 February 2016

4.4.1.3 Spring 2016

In situ temperature of the water column in the study area ranged between 21 to 23 °C on 22 April (Figure 4.10). The mixed layer increased from 1.0 m in February to 2.5 m at PMAR and FLET, and 3.0 m at PDMR and STJP. ARTR, FLET, GDMR, NGI1, PCTR, PDMR and PRIV had a particle size between 40 to 50 μm , and all other stations (PMAR and TELR) had a particle size of 80 μm . Surface SPM concentration was highest at PRIV (29 mgL^{-1}) and STJP (21 mgL^{-1}), and the SPM concentration was lowest at FLET (9 mgL^{-1}).

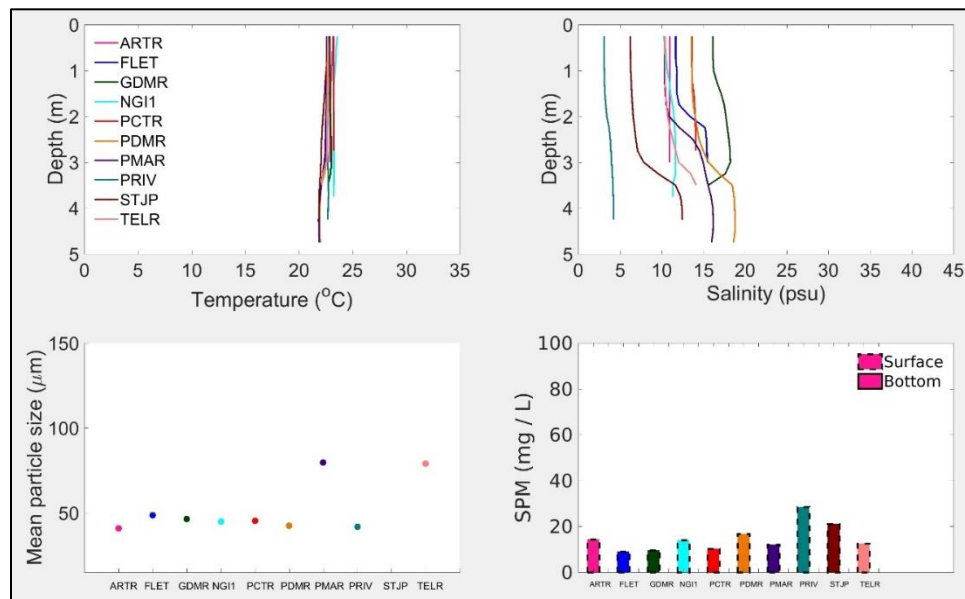


Figure 4.10 In situ particle size, temperature, salinity and SPM collected at MS Sound on 22 April 2016

In situ water temperature increased at all stations with a range of 25 to 27 °C on 24 May, and the water column was well mixed at PRIV, STJP, PCTR, TELR, PMAR and FLET (Figure 4.11). A fresh water plume with a salinity of 13 psu was present in the

first meter at PDMR and the bottom water had a salinity of approximately 19 psu. The surface water had a salinity of 23 psu at GDMR and the bottom water had a salinity of 28 psu. High salinity bottom water observed at STJP in April was not present in May. Surface SPM concentration increased from 22 to 40 mgL⁻¹ at STJP in May and was relatively unchanged at the other stations, suggesting a steady river discharge. Mean particle size decreased from 80 μm to less than 50 μm at TELR and PMAR, and the stations closest to the shoreline (PRIV, ARTR and PCTR) had a constant particle size (40 to 50 μm) during both spring cruises.

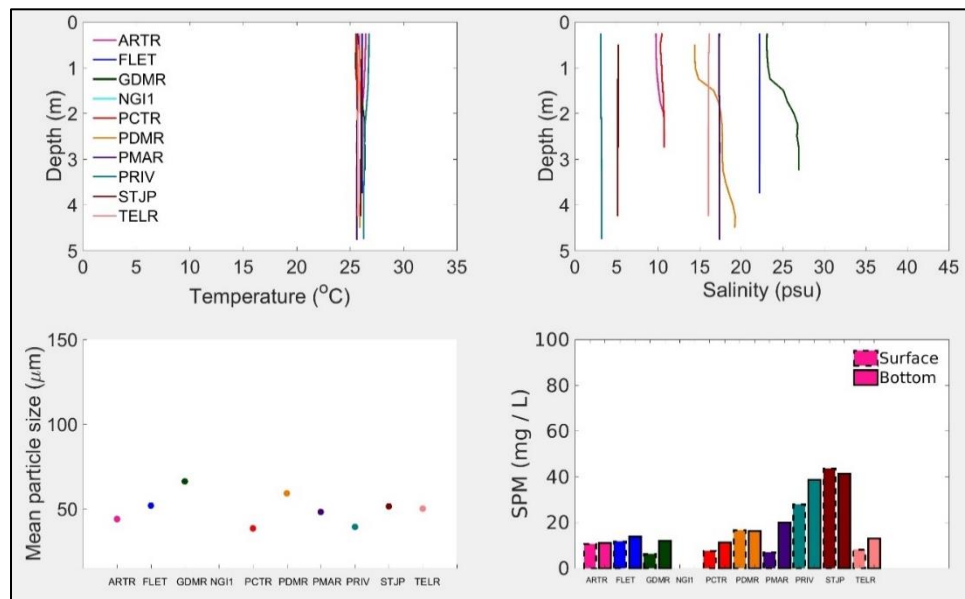


Figure 4.11 In situ particle size, temperature, salinity and SPM collected at MS Sound on 24 May 2016

4.4.1.4 Summer 2016

The water column was well mixed in the Sound and had an in situ temperature of approximately 28 °C on 8 June (Figure 4.12). Stations closest to the coast (PRIV, STJP, NGI1, ARTR and PDMR) had in situ salinity values of 9 to 13 psu, and ranged between 18 and 23 psu at the stations located offshore. Bottom SPM at PMAR and PRIV decreased by 11 and 31 mgL⁻¹ respectively, and bottom SPM at STJP increased by 30 mgL⁻¹.

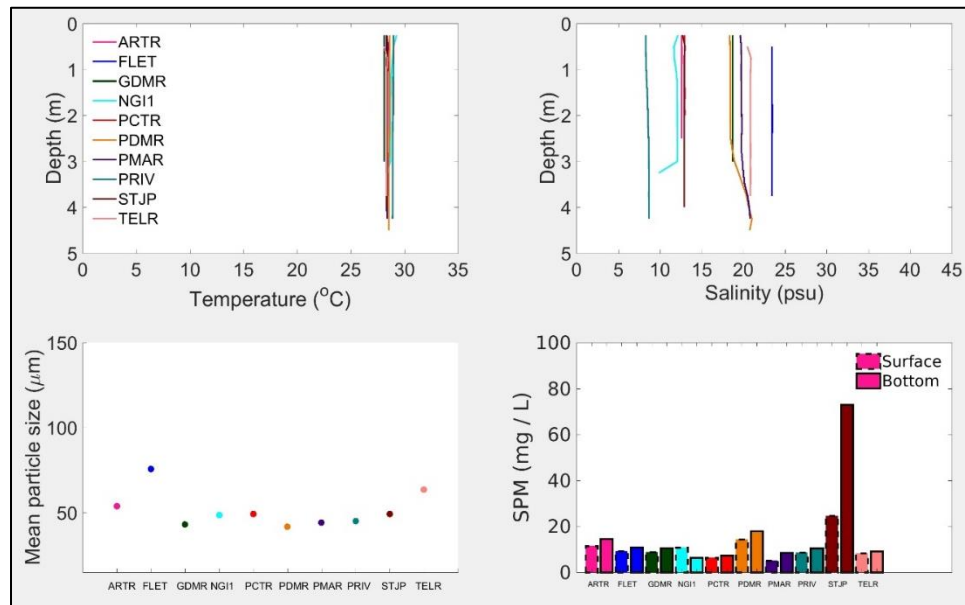


Figure 4.12 In situ particle size, temperature, salinity and SPM collected at MS Sound on 8 June 2016

In situ temperature of the water column ranged from 28 to 33 °C in the Sound on 5 July (Figure 4.13). Minimum and maximum in situ salinity at stations closest to the coastline (PRIV, STJP, NGI1, ARTR and PDMR) was 13 to 26 psu, and the salinity range at the offshore stations was 33 to 42 psu. Mean particle size at the stations

increased from less than 55 μm to a range between 60 and 90 μm . Bottom SPM concentration decreased at STJP, and surface and bottom concentrations increased at the other nine stations.

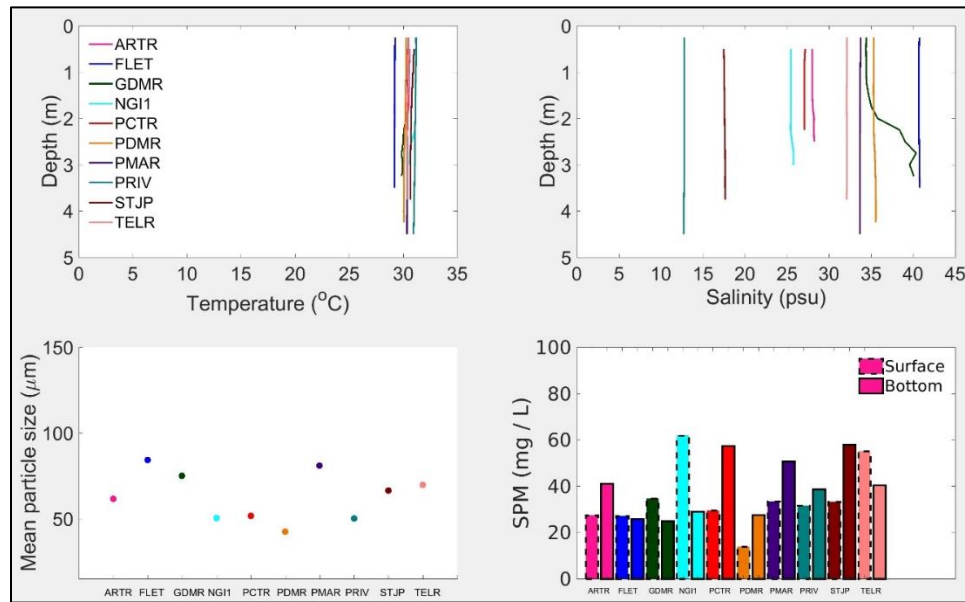


Figure 4.13 In situ particle size, temperature, salinity and SPM collected at MS Sound on 5 July 2016

A halocline was observed at stations PCTR (depth of 0.5 m), PDMR (depth of 1.0 m) and GDMR (depth of 1.5 m) on 2 August (Figure 4.14). In situ temperature of the water column was approximately 32 $^{\circ}\text{C}$. Particle size increased (20 to 70 μm) at ARTR, GDMR, NGI1, PRIV, STJP and TELR. Surface and bottom SPM concentration returned to the pre-July summer values between 10 and 30 mgL^{-1} , but STJP surface and bottom concentrations was lower in August compared to June.

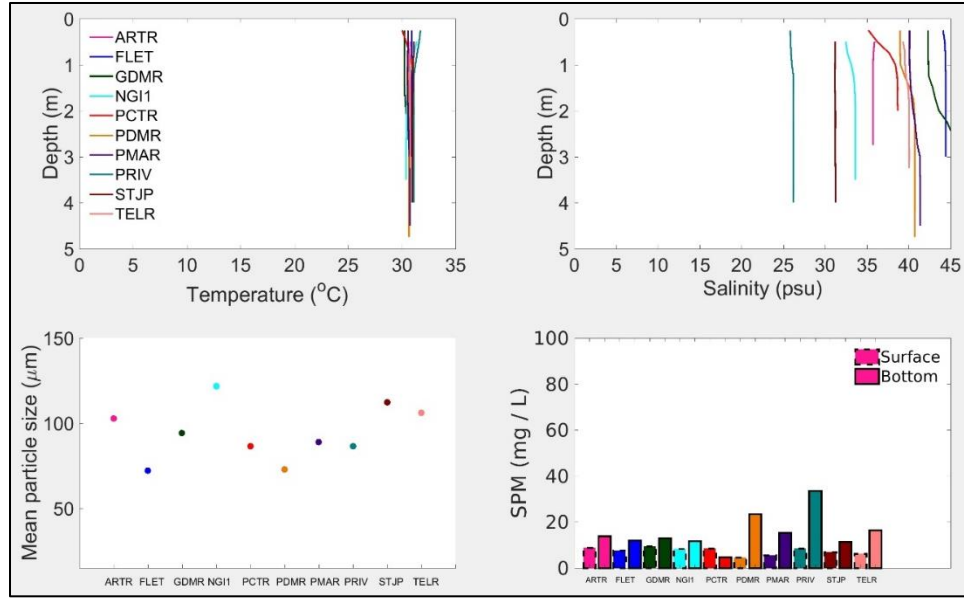


Figure 4.14 In situ particle size, temperature, salinity and SPM collected at MS Sound on 2 August 2016

4.4.2 Characterization of Suspended Particulate Matter at the passes and MS Bight during winter, spring and summer using a remote sensing SPM algorithm

4.4.2.1 Main Pass

In this section, the river discharge and wind data are in situ measurements. Surface current velocity (alongshore and across shore), temperature and salinity were extracted from CONCORDE’s synthesis model. A positive SPMa (feature 1) travelled southward at Main Pass in spring 2015 (Figure 4.15). The positive anomaly feature was associated with a low salinity (12 psu), low temperature (24 °C) river discharge propagating southwestward from Mobile Bay into the Bight. A positive SPMa (feature 2) propagated northward in April 2015 a few weeks after the formation of feature 1, driven by southeasterly winds (4.0 to 8.0 ms⁻¹). The northeastward surface ocean current

advected high salinity (31 psu), high temperature (30 °C) waters northward from the Bight into the Sound.

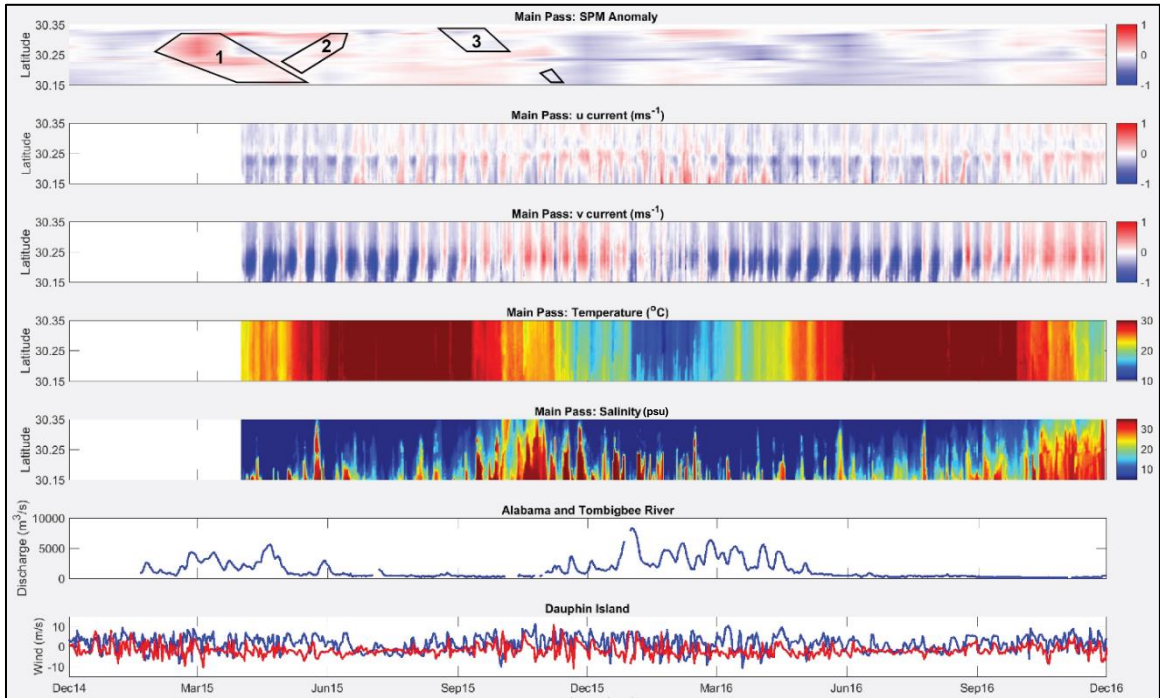


Figure 4.15 SPM anomaly at Main Pass

Synthesis model alongshore current, synthesis model across shore current, synthesis model temperature, synthesis model salinity, in situ discharge at Alabama/Tombigbee Rivers and in situ alongshore and across shore wind at Dauphin Island. Features 1, 2 and 3 are highlighted in the figure.

A negative SPMa feature (feature 3) propagated southward from the northern end of Pass aux Herons to Main Pass for approximately two months at the end of summer 2015. The surface ocean current was southwestward during the southward movement of feature 3. Warm fresh water (31 °C and 15 psu) was initially present at Main Pass at the start of fall 2015. Increased southeasterly winds (2.0 to 6.0 ms⁻¹) moved a lower temperature (24 °C), high salinity (31) water mass shoreward in September and October

2015. The high salinity water mass reached the northern latitude of 30.25 °N by the end of October, and prevented the negative SPMa from propagating further southward until the middle of November.

4.4.2.2 Petit Bois Pass

A negative SPMa (feature 4) propagated southward from MS Sound towards the Bight at the end of spring 2015 (Figure 4.16). The along shore current was westward and the across shore current was southward (30.25 to 30.35 °N), driving the movement of the negative anomaly. At the start of July, southeasterly winds with a mean velocity of 5.6 ms⁻¹ generated northeastward ocean current via Ekman transport. The northeastward current transported a high salinity (31 psu), high temperature (30 °C) water mass shoreward between the latitudes of 30.15 to 30.25 °N, and hindered feature 4 from moving further southward into the Bight.

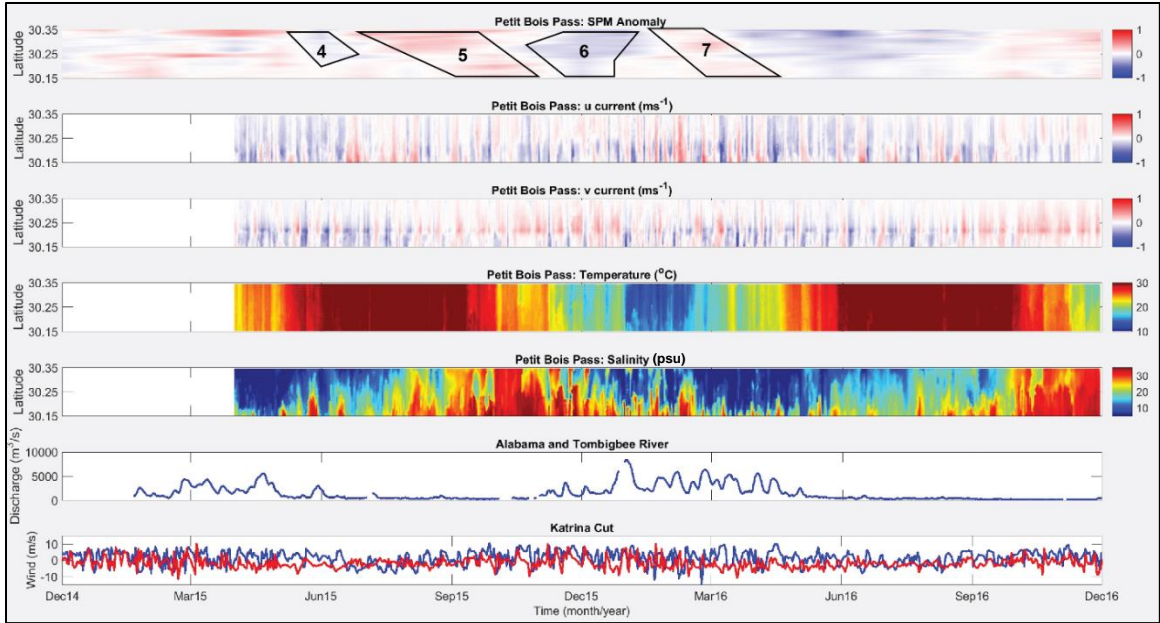


Figure 4.16 SPM anomaly at Petit Bois Pass

Synthesis model alongshore current, synthesis model across shore current, synthesis model temperature, synthesis model salinity, in situ discharge at Alabama/Tombigbee Rivers and in situ alongshore and across shore wind at Katrina Cut. Features 4, 5, 6 and 7 are highlighted in the figure.

Westerly alongshore winds were present at Petit Bois Pass in mid-July and mid-August 2015 for a cumulative total of approximately 1 month. The westerly wind initiated and propagated a positive SPMa (feature 5) southward towards the Bight. Southeasterly winds with a mean velocity of 6.5 ms^{-1} advected a high salinity (31 psu), high temperature ($31 \text{ }^{\circ}\text{C}$) water mass northeastward towards the Sound, at the end of summer 2015. The high salinity water mass moved northward and prevented further southward movement of feature 5. Southeasterly winds and the resulting northeastward current transported a negative SPMa (feature 6) northward across Petit Bois Pass from November 2015 to January 2016.

Alabama/Tombigbee River discharge increased from 2,100 to 8,400 m³ s⁻¹ between December 2015 and January 2016. In early February 2016, a southward current moved a fresh (10 psu), low temperature (10 °C) water mass from the Sound towards the Bight. The southward current also transported a positive SPMa (feature 7) in an offshore direction. The fresh water discharge advected into the Bight displaced the high salinity (24 to 30 psu) water present at the southern end of the pass in February 2016.

4.4.2.3 Horn Island Pass

Horn Island Pass experienced westerly alongshore wind in July and August 2015. Southward Ekman transport by the alongshore wind propagated a positive SPMa (feature 8) offshore in August 2015 for 10 weeks (Figure 4.17). The water mass exiting the Sound had a substantial salinity range (10 to 29 psu) and limited temperature range (29 to 30 °C). The ocean current switched to northwestward in October and transported the surface water towards the Sound. The shoreward movement of the water mass dissipated the positive SPMa located at the pass.

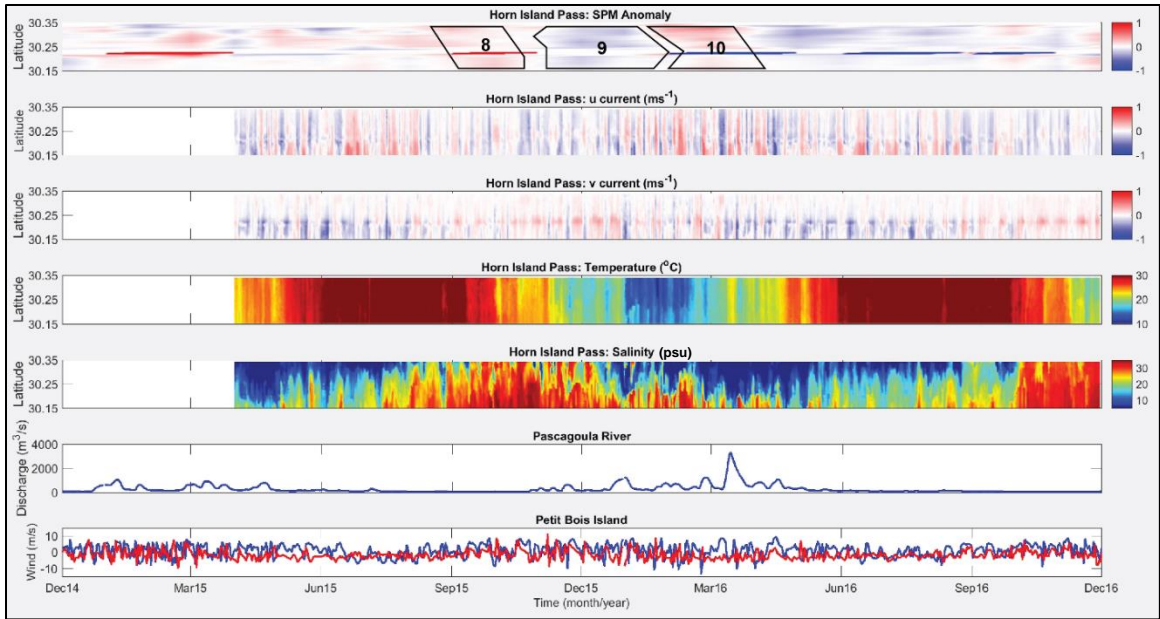


Figure 4.17 SPM anomaly at Horn Island Pass

Synthesis model alongshore current, synthesis model across shore current, synthesis model temperature, synthesis model salinity, in situ discharge at Pascagoula River and in situ alongshore and across shore wind at Petit Bois Island. Features 8, 9 and 10 are highlighted in the figure.

Sustained southeasterly winds with a velocity of approximately 5.0 ms^{-1} was observed at Horn Island Pass at the end of October. The northeastward current advected the high salinity (30 psu), cold water mass (17 to $22 \text{ }^{\circ}\text{C}$) shoreward. The northward movement of the water mass into the Sound resulted in a negative SPMa (feature 9) along the pass for a six-week period. The Bight waters associated with feature 9 replaced the Sound waters associated with feature 8. Westward ocean currents moved fresh water from Mobile Bay towards Horn Island Pass shortly after feature 9 exited Horn Island Pass. The minimum salinity and temperature of the water mass was 10 psu and $10 \text{ }^{\circ}\text{C}$. The cold fresh water moved southward from the Sound towards the Bight in February

2016 and transported a positive SPMa (feature 10). The positive SPMa was observed at Horn Island Pass from February to March 2016.

4.4.2.4 Dog Key Pass

A positive SPMa (feature 11) was observed in summer 2015 at Dog Key Pass (Figure 4.18). Westerly winds at the end of July and the beginning of August transported the positive SPMa feature southward. This feature was associated with a high temperature (30 °C), large salinity range (22 to 30) and propagated from the Sound into the Bight. The positive anomaly moved from 30.35 to 30.15 °N in two months (August and September), with a short period (3 to 5 days) at the end of August when the anomaly was significantly reduced. The reduced SPMa corresponded with a change in the wind direction from westerly to easterly.

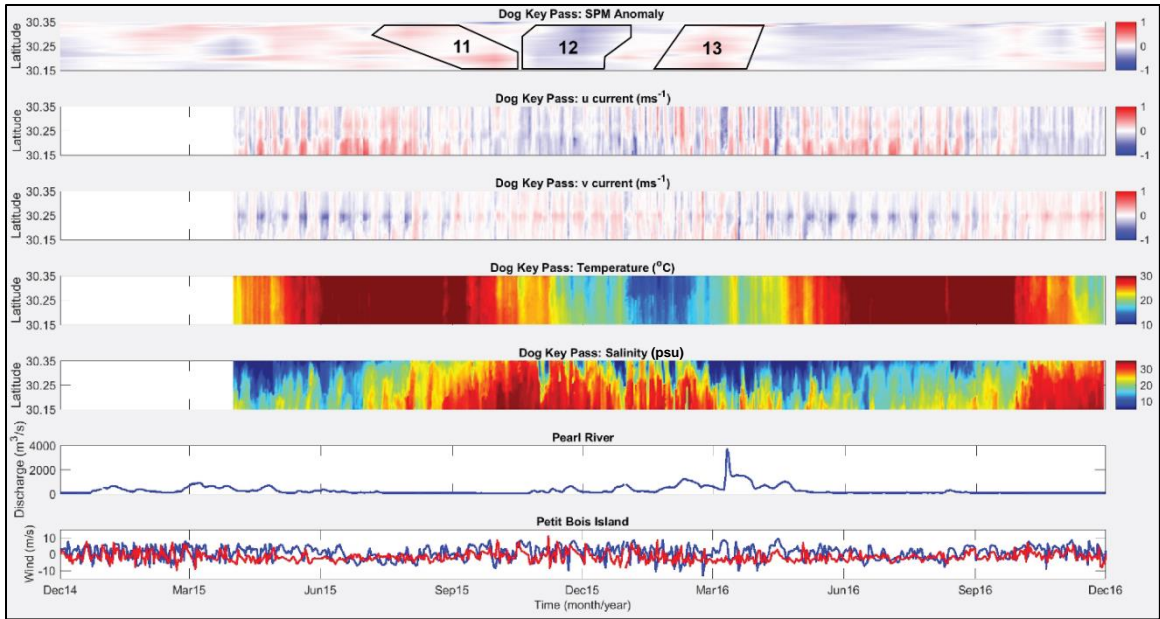


Figure 4.18 SPM anomaly at Dog Key Pass

Synthesis model alongshore current, synthesis model across shore current, synthesis model temperature, synthesis model salinity, in situ discharge at Pascagoula River and in situ alongshore and across shore wind at Petit Bois Island. Features 8, 9 and 10 are highlighted in the figure.

A negative SPMa (feature 12) propagated northward from MS Bight towards the Sound in fall 2015. A northeasterly wind was observed for a total of approximately 15 days in October and November at the Pass. The resultant alongshore current was westward and the across shore current was northward. The northwestward current advected a variable salinity (15 to 30), low temperature (14 to 20 °C) water mass shoreward in November and December. Feature 12 was followed by the development of a positive SPMa at Dog Key Pass. The positive SPMa (feature 13) was associated with the estuarine discharge through Pass aux Herons in February 2016. Feature 13 moved southward and developed at approximately the same time as feature 10 (Horn Island

Pass). The salinity of the fresh water exiting Dog Key Pass was 10 to 15 psu and the temperature ranged between 10 to 20 °C.

4.4.2.5 Ship Island Pass

A positive SPMa (feature 14) and negative SPMa (feature 15) were observed at Ship Island Pass in summer and fall 2015 (Figure 4.19). Westerly alongshore wind propagated the positive SPMa southward, and entrained high temperature (30 °C) and low salinity (22 to 24 psu) water from the Sound into the Bight. Feature 14 was located at the Pass from August to October 2015. A change in the alongshore wind to easterly at the end of October and the beginning of November 2015 moved a negative SPMa (feature 15) northward in November 2015. The temperature and salinity of the water mass transported northward into the Sound was 15 to 20 °C and 30 psu.

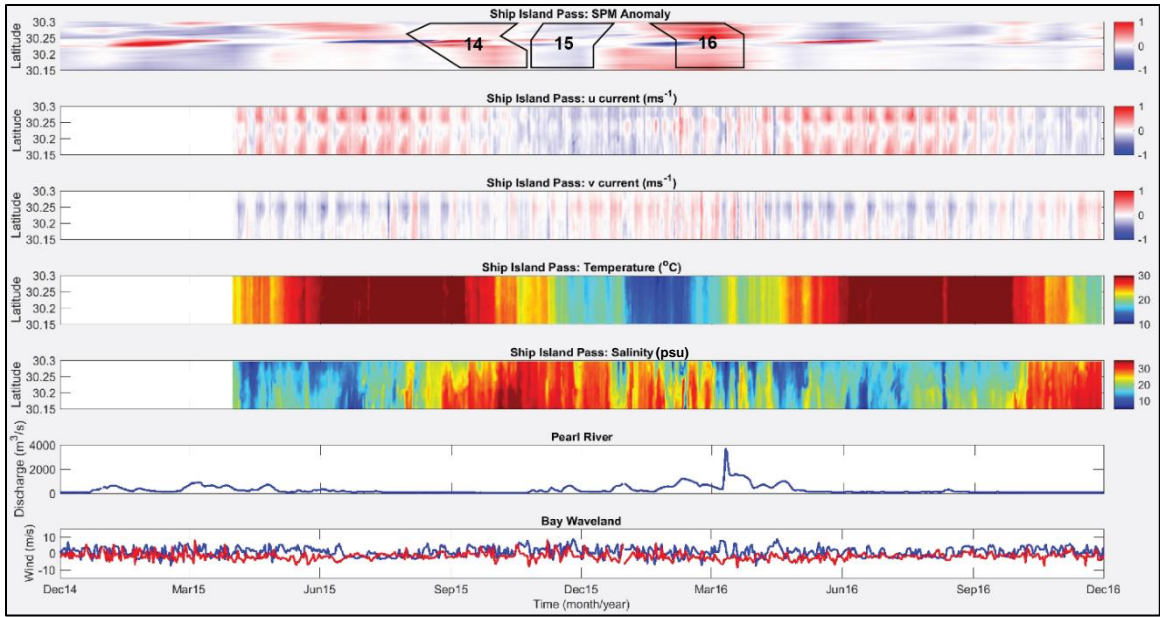


Figure 4.19 SPM anomaly at Ship Island Pass

Synthesis model alongshore current, synthesis model across shore current, synthesis model temperature, synthesis model salinity, in situ discharge at Pascagoula River and in situ alongshore and across shore wind at Petit Bois Island. Features 8, 9 and 10 are highlighted in the figure.

The major direction of the wind observed in February 2016 was southeasterly. The wind generated a northeastward ocean current and propagated a positive SPMa (feature 16) towards the Sound. The salinity and temperature of the water mass ranged from 22 to 30 psu and 10 to 20 °C. The current transported the positive anomaly from the Sound to the Bight over a four-week period.

4.4.2.6 MS Sound

A sequence of positive (features 5, 8, 11 and 14), negative (features 6,9,12 and 15) and positive (features 7, 10, 13 and 16) anomalies were observed at the tidal passes in MS Sound in summer 2015, fall 2015 and winter 2015. The positive anomaly observed

at Petit Bois Pass (feature 5) and Dog Key Pass (feature 11) occurred in July 2015 and propagated southward into the Bight. The corresponding positive anomalies at Horn Island Pass (feature 8) and Ship Island Pass (feature 14) occurred in August 2015 and moved offshore.

The negative anomalies in the Sound occurred simultaneously at all the passes (Petit Bois, Horn Island, Dog Key and Ship Island) in November 2015. The negative anomalies at all the passes propagated northward and had comparable temperature (15 to 22 °C). The minimum salinity of the negative anomalies at Petit Bois, Horn Island, Dog Key and Ship Island Passes were 15, 10, 10 and 22. The anomalies at the tidal passes transitioned from negative to positive (features 7, 10, 13 and 16) in February 2016. The positive anomalies moved southward, and the ocean currents advected lower salinity (10 to 22), lower temperature (10 to 22 °C) water masses into the Bight.

4.5 Discussion

4.5.1 Characterization of Suspended Sediments in MS Sound during winter, spring and summer using in situ CTD, SPM and LISST data

4.5.1.1 Summer 2015

This section discusses the changes in the particle sizes observed at the MS Sound stations during the monthly cruises. Winds at Bay Waveland were southwesterly on 18 and 19 August, corresponding to one day before and the day of the summer 2015 cruise (Figure 4.20). Particle sizes in the range of very fine sand (63 to 125 μm) at the center of

Camille Cut and West Ship Island could be due to sediment transported from the Bight by northward propagating waves or westward alongshore transport from Dog Key Pass during northwesterly winds (Ekman) on 17 August 2015 (Walker et al., 1996; Eisemann et al., 2018). The other two stations at Camille Cut consisted of particle sizes corresponding to the background surficial sediment type (silt) in the Cut (Figure 4.5).

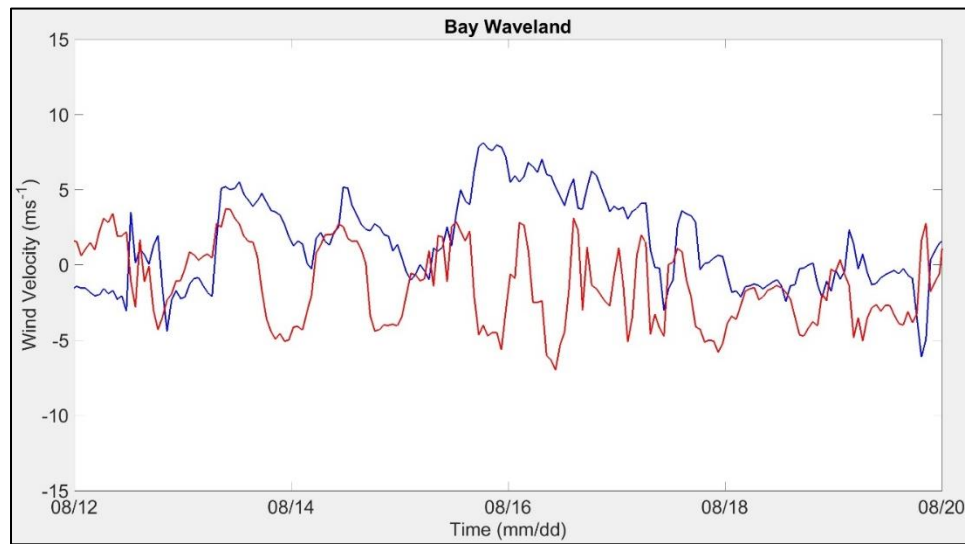


Figure 4.20 In situ alongshore (blue) (positive east) and across shore (red) (positive north) wind velocity at Bay Waveland (MS) one week prior to the 19 August 2015 cruise at Ship Island

4.5.1.2 Winter 2015

Southwesterly winds at Bay Waveland station for a period of 45 hours between 22 and 24 January resulted in southeastward ocean currents via Ekman transport (Dzwonkowski et al., 2014) (Figures 4.21 and 4.22). The constricted channel between the headland at Heron Bay Point (MS) and Grand Island (LA) intensified ocean currents near STJP due to the conservation of water mass. The mass of water entering west of the

channel was equal to the mass of water exiting east of the channel, and resulted in increased velocity of the water mass as it flowed through the channel (Knauss, 1997). Bed shear stress (directly proportional to the square of the velocity) increased as the velocity of the water mass increased, and resuspended particulate matter on the seabed at STJP on 24 January (Fredsoe & Deigaard, 1992). This was evident in the high bottom SPM concentration observed at STJP. Settling of the particulate matter at STJP limited the surface SPM concentration. Surface and bottom SPM concentrations at PRIV were similar to the other stations (except STJP), which suggests the high bottom SPM concentration at STJP was not due to input from Lake Borgne (Flocks et al., 2009). Bottom SPM concentration at PRIV would also be high if Lake Borgne was a major source of particulate matter input to west MS Sound.

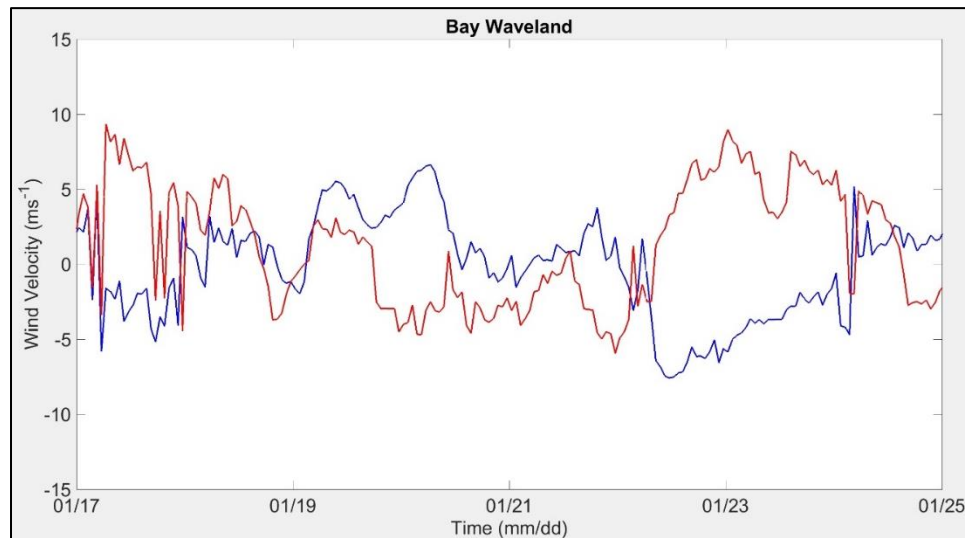


Figure 4.21 In situ alongshore (blue) (positive east) and across shore (red) (positive north) wind velocity at Bay Waveland one week prior to the 24 January 2016 cruise in MS Sound

Southwesterly winds affected the western Sound between 22-24 January for a total of 45 hours.

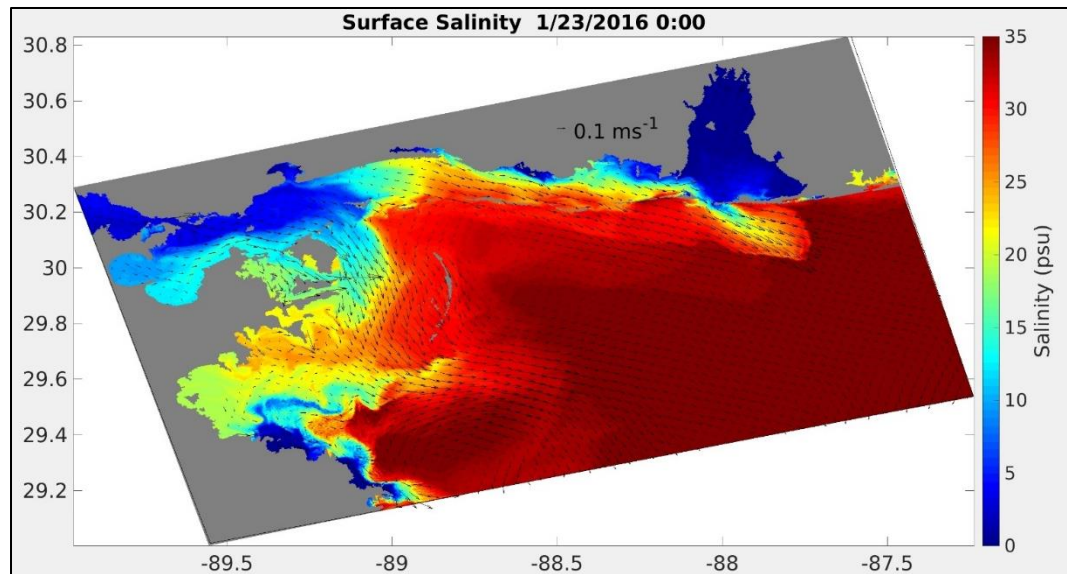


Figure 4.22 Synthesis model output of surface ocean current superimposed on surface salinity on 23 January 2016

The ocean current is southeastward in the Sound.

Non wind-driven northwestward ocean currents advected larger particle sizes from the Bight towards the Sound on 31 January (Figures 4.5 and 4.23). Larger current velocities are required to transport the larger particle sizes, therefore, as the current speed reduced, the larger particle sizes settled out of suspension before the smaller particle sizes (Stokes, 1850). Reduced current velocities resulted in the larger particle sizes present at stations closer to the Bight (FLET, PMAR and TELR) and smaller particle sizes deposited at stations further north (GDMR, PCTR, PDMR and STJP). Higher salinity Bight waters advected below the fresh water surface plume were observed in the CTD measurements at PMAR, TELR, FLET and GDMR (Figure 4.8).

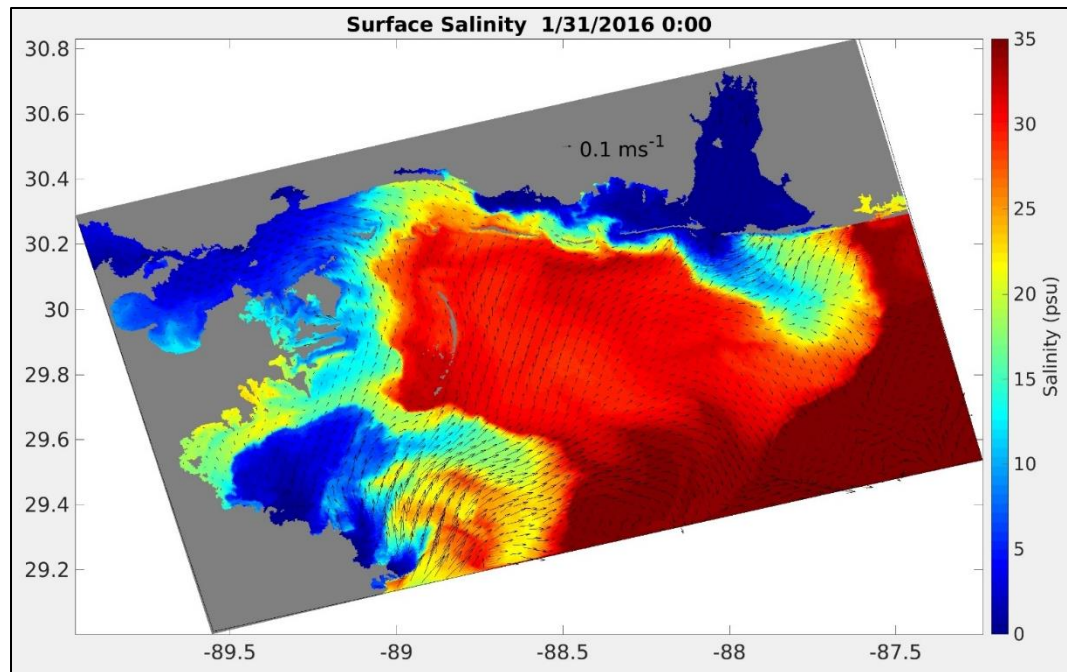


Figure 4.23 Synthesis model output of surface ocean current superimposed on surface salinity on 31 January 2016

The ocean current is southeastward in the Sound.

Weak northwestward ocean currents on 12 February transported Bight waters through the passes into the Sound, and transported SPM similar to 31 January (Figure 4.24). Maximum salinity of the bottom water in the Sound was higher than 31 January due to the further intrusion of the Bight water. Particulate matter input from the Bight into the Sound in January and February, and increased river discharge from the Pearl River and Pascagoula River (Figures 4.25 and 4.26) was evident in higher surface SPM concentration at (PRIV, STJP and TELR) and higher bottom SPM concentration at the west and central stations (GDMR, PDMR and PCTR).

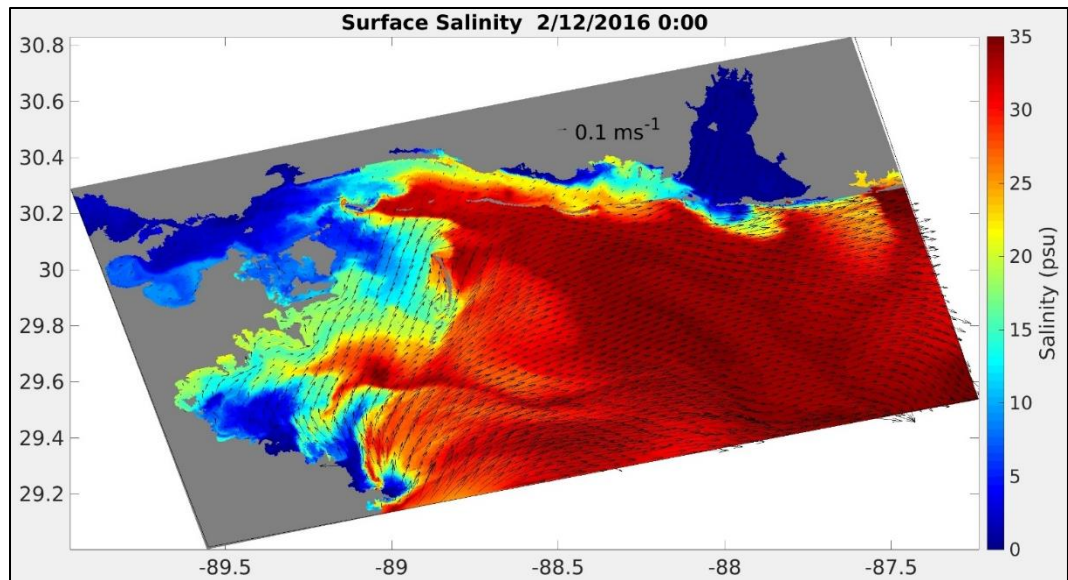


Figure 4.24 Synthesis model output of surface ocean current superimposed on surface salinity on 12 February 2016

The ocean current is northwestward in the Bight.

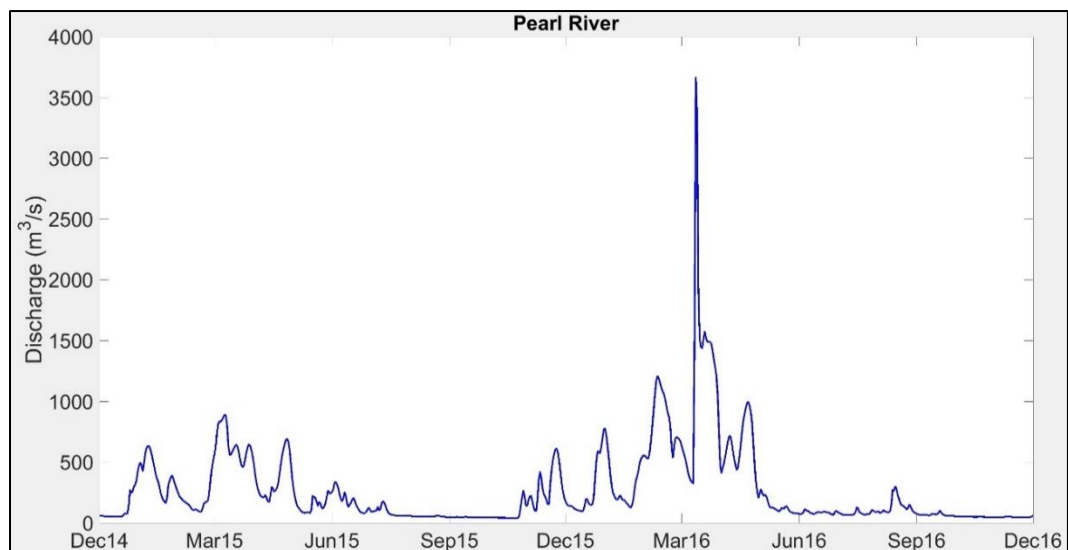


Figure 4.25 In situ time series of daily river discharge at Pearl River

Increased river discharge occurred in January and February 2016.

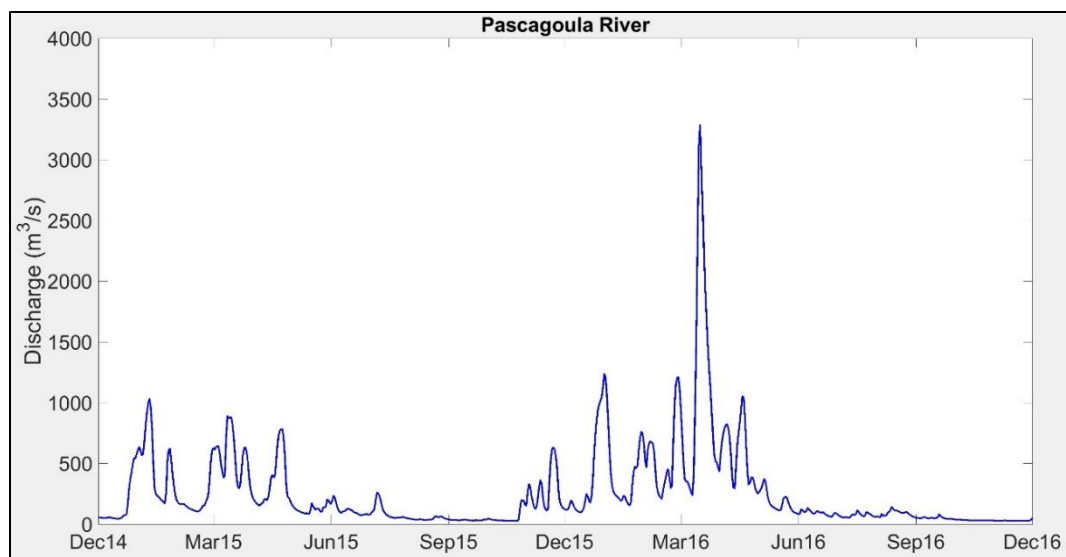


Figure 4.26 In situ time series of daily river discharge at Pascagoula River

Increased river discharge occurred at the Pascagoula River in January and February 2016

4.5.1.3 Spring 2016

Southeasterly winds from 15 to 21 April mixed the water column in MS Sound and resuspended particulate matter on the seabed (Figure 4.27). The depth of the mixed layer increased from 1.0 m on 12 February to 2.0-3.0 m on 22 April (Figure 4.10). SPM in the surface water settles within the mixed layer due to the density gradient at the halocline resisting the exchange of particulate matter in the surface and bottom water (Knauss, 1997). Surface SPM concentration was higher on 12 February than 22 April because surface SPM represented the concentration measured in the first meter of the water column. An increase in the mixed layer depth resulted in a lower surface SPM concentration within the first meter at the DMR stations on 22 April. Larger particle sizes settled faster than smaller particle sizes, and resulted in the particle size range of 40 to 50 μm present at the majority of the stations (Stokes, 1850).

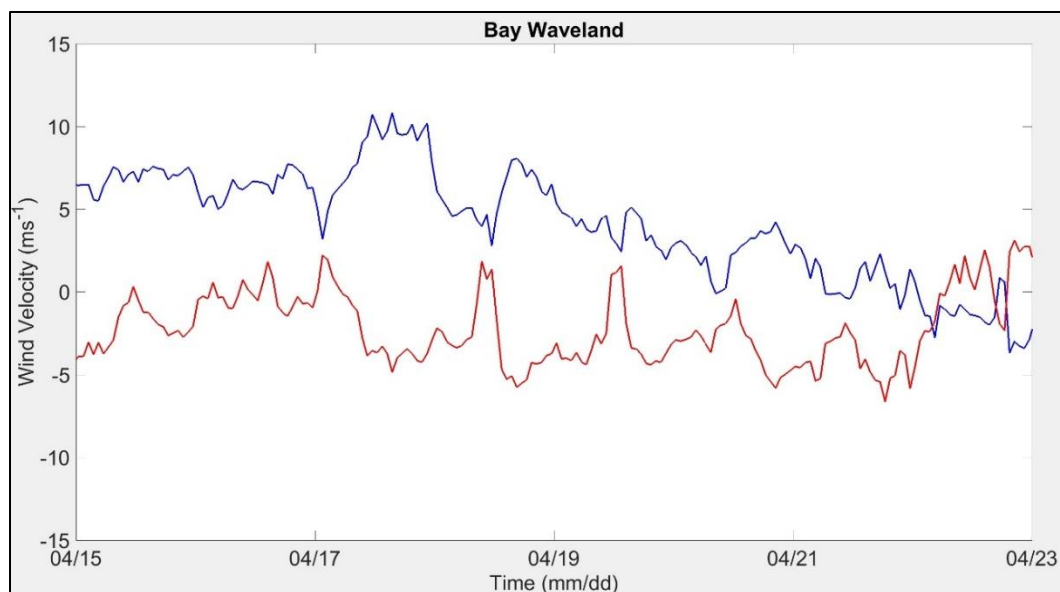


Figure 4.27 In situ alongshore (blue) (positive east) and across shore (red) (positive north) wind velocity at Bay Waveland one week prior to the 22 April 2016 cruise in MS Sound

The predominant wind direction was southeasterly.

Wind velocity at Bay Waveland was variable the week of 17 to 24 May, changing direction between southeasterly, northeasterly and northwesterly (Figure 4.28). Wind activity in spring 2016 completely mixed the water column at PRIV, STJP, PCTR, TELR, PMAR and FLET. The mixed layer decreased to 1.0 m at PDMR and GDMR. Spring river discharge peaked at Pearl River ($\sim 3,500 \text{ m}^3\text{s}^{-1}$) and Pascagoula River ($\sim 3,500 \text{ m}^3\text{s}^{-1}$) in March and decreased to 300 and 400 m^3s^{-1} respectively in May (Figures 4.25 and 4.26). Reduced river discharge in April and May resulted in similar surface SPM concentrations in MS Sound during both spring cruises.

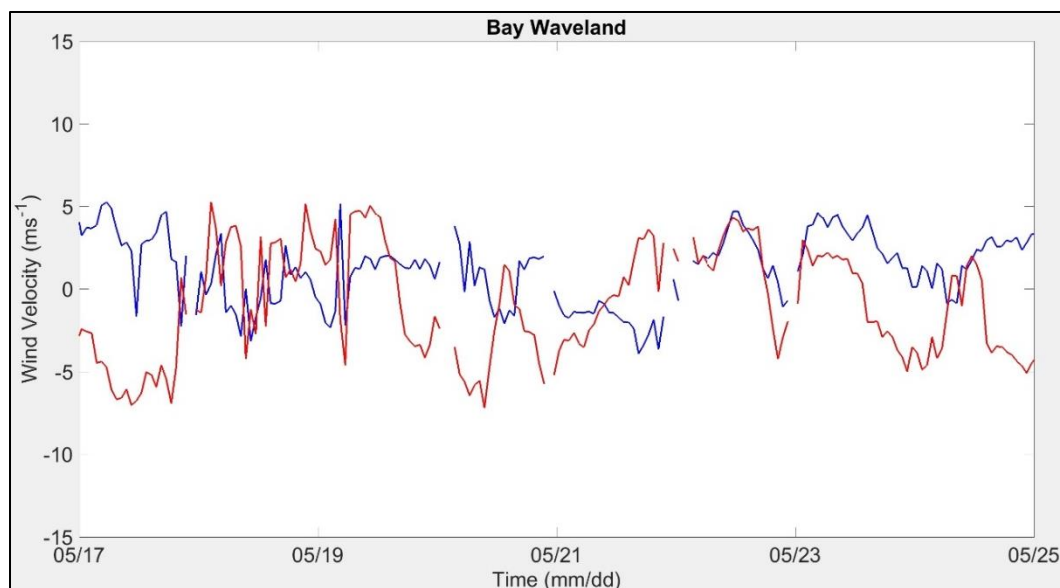


Figure 4.28 In situ alongshore (blue) (positive east) and across shore (red) (positive north) wind velocity at Bay Waveland one week prior to the 24 May 2016 cruise in MS Sound

The wind direction is variable and switches between southeasterly, northeasterly and northwesterly.

4.5.1.4 Summer 2016

River discharge at Pearl River and Pascagoula River were $120 \text{ m}^3\text{s}^{-1}$ and $70 \text{ m}^3\text{s}^{-1}$ in June 2016 (Figures 4.25 and 4.26). As the streamflow velocity increases, particulate matter will move if the driving force exerted on the particle size exceeds the stabilizing force (critical flow velocity) (Fredsoe & Deigaard, 1992). Reduced river discharge and flow speed resulted in a smaller volume of particulate matter transported along the Pearl and Pascagoula Rivers as bed load and in suspension. Reduced river stream flow caused less particulate matter to deposit in the Sound and resulted in smaller surface and bottom SPM concentrations at the stations (Kineke et al., 2006). Eastward current velocity increased in the channel between Heron Bay Point (MS) and Grand Island (LA), and resuspended particulate matter at STJP, similar to 24 January (Figures 4.12 and 4.29).

Enhanced ocean currents increased the surface SPM concentration to 72 mgL^{-1} at STJP. High bottom SPM concentration was not observed at PRIV, suggesting the bottom SPM at STJP was not due to sediment input from Lake Borgne.

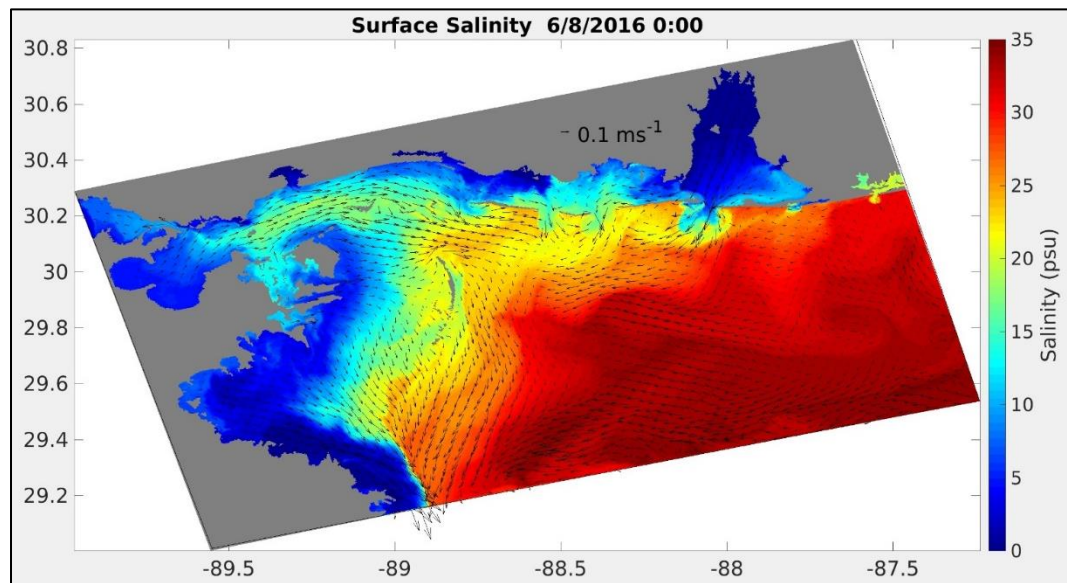


Figure 4.29 Synthesis model output of surface ocean current superimposed on surface salinity on 8 June 2016

Eastward surface ocean current in west MS Sound resuspends sediments at station STJP.

Winds completely mixed the water column at all the stations except GDMR. Eastward currents from 28 June to 5 July transported particulate matter from the western to eastern Sound (Figure 4.30). Larger particle sizes settled out first from the ocean current and finer particle sizes were transported further east to PDMR. This increased the mean particle size in west MS Sound and the DMR stations. Resuspension and transport of particulate matter by the eastward currents contributed to the high surface and bottom SPM concentrations at all the stations. Smaller particle sizes remained in suspension for

a longer time than the larger particle sizes as it advected east and had a greater impact on the SPM concentration than larger particle sizes.

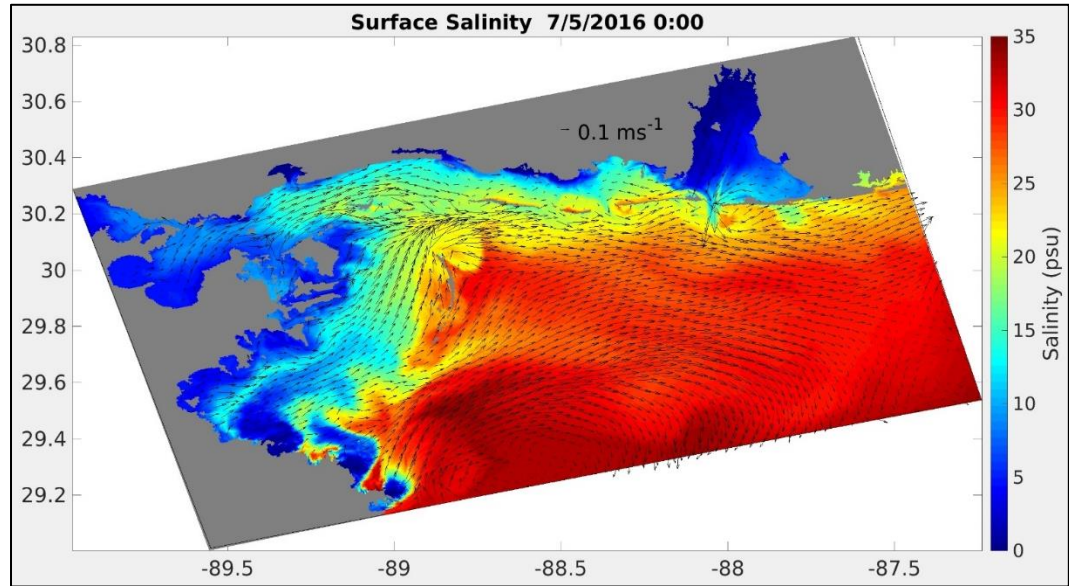


Figure 4.30 Synthesis model output of surface ocean current superimposed on surface salinity on 5 July 2016

Eastward surface ocean current in west MS Sound transports sediments westward.

Eastward ocean currents in August transported particulate matter from the western to eastern Sound similar to the July cruise. Limited particulate matter input from the rivers and eastward transport increased the particle size by 10 to 70 μm at 80% of the stations. Advection of smaller particle sizes (40 to 50 μm) in July resulted in higher surface and bottom SPM concentrations compared to the advection of mainly large particle sizes (greater than 70 μm) in August. This was because larger particle sizes settles out of suspension faster than smaller particle sizes (Stokes, 1850).

4.5.2 Characterization of Suspended Particulate Matter at the passes and MS Bight during winter, spring and summer using a remote sensing algorithm

4.5.2.1 Main Pass

Alabama and Tombigbee River experienced a peak discharge of $4,600 \text{ m}^3\text{s}^{-1}$ at the start of March 2015 (Figure 4.15). A baroclinic pressure gradient developed in the surface water at Mobile Bay due to the horizontal density gradient between the fresh water discharge (salinity of 12 psu) and high salinity (30 psu) offshore water (Dzwonkowski & Park, 2012). The pressure gradient resulted in the southern transport of the freshwater and a positive SPMa (feature 1) at the beginning of March. The wind changed direction from northeasterly to southeasterly and propagated a high salinity (31 psu), high temperature ($30 \text{ }^\circ\text{C}$) water mass north via Ekman transport (Dzwonkowski et al., 2014). The high salinity water mass transported a positive SPMa (feature 2) at the end of April. Feature 2 moved further north from $30.15 \text{ }^\circ\text{N}$ to $30.35 \text{ }^\circ\text{N}$ over a six-week period.

Non-wind driven southwest ocean currents propagated a negative SPMa (feature 3) towards the Bight at the end of August 2015. The salinity and temperature of the water mass associated with feature 3 was 12 psu and $31 \text{ }^\circ\text{C}$, suggesting the water originated from northern Mobile Bay. The fresh water mass was not associated with the Alabama/Tombigbee outflow since the river discharge was approximately $350 \text{ m}^3\text{s}^{-1}$. Feature 3 moved south in September 2015, until the wind rotated clockwise from northeasterly to southeasterly. Southeasterly winds advected Bight waters ($24 \text{ }^\circ\text{C}$ and salinity of 31 psu) northward via Ekman transport (Dzwonkowski et al., 2014). The

colder saline water mass prevented feature 3 from propagating further offshore at the end of September.

4.5.2.2 Petit Bois Pass

Alabama/Tombigbee peak spring river discharge of $5,600 \text{ m}^3\text{s}^{-1}$ occurred at the end of April 2015 (Figure 4.16). It takes 5-9 days for the water recorded at the Alabama and Tombigbee river gauges to deposit into Mobile Bay (Schroeder, 1979), and approximately 15 % of the estuarine discharge from Mobile Bay enters MS Sound via Pass aux Herons (Ryan, 1969), situated at a latitude of 30.3°N . Westward along shore ocean current at Main Pass and Petit Bois Pass transported surface water from Mobile Bay to MS Sound through Pass aux Herons at the beginning of May. Temperature and salinity of the water mass at Main Pass and Petit Bois Pass (30.3°N) at the start of May was 22°C and 10 psu, supporting the inference that fresh water was transported west from Mobile Bay towards Petit Bois Pass. The salinity of the surface water at the southern extent of Petit Bois Pass was 30 psu, setting up a salinity gradient between the estuarine discharge and the Bight. The baroclinic pressure gradient due to the across shore salinity gradient at Petit Bois Pass transported a negative SPMa (feature 4) southward through Petit Bois Pass. Feature 4 propagated south for approximately 1 month until a southeasterly wind advected (Ekman transport) offshore Bight waters northward in mid-June and stopped the feature from propagating further south (Dzwonkowski et al., 2014).

The alongshore wind at Katrina Cut was westerly for a total of 3 weeks in July and 1 week in August 2015. The westerly alongshore wind resulted in southward Ekman transport towards the Bight (Dzwonkowski et al., 2014). The westerly winds transported

a positive SPMa (feature 5) from MS Sound into the Bight over a 9-week period. A northward propagating negative SPMa (feature 6) followed feature 5 in November 2015. Southeasterly winds advected cold (24 °C), high salinity (30 psu) waters, and the negative SPMa northeastward from the Bight towards the Sound via Ekman transport for approximately two months (Dzwonkowski et al., 2014).

The maximum winter river discharge of 8,400 m³s⁻¹ (Alabama/Tombigbee) was observed at the beginning of January 2016. A water mass with a salinity of 10 psu and a temperature of 10 °C was observed at a latitude of approximately 30.3 °N at Main Pass in mid-January. Westward ocean currents transported a water mass with a salinity of 10 and a temperature of 10 °C through Pass aux Herons (30.3 °N) on 3 February 2016 (Figure 4.31). The water mass south of 30.25 °N at Petit Bois Pass had a salinity range of 24 to 30 psu compared to the salinity of 10 psu at 30.3 °N. The across shore salinity gradient set up a baroclinic pressure gradient, and the resultant southward current transported the fresh estuarine water and a positive SPMa (feature 7) towards the Bight (Dzwonkowski & Park, 2012). This was evident by the fresh water replacing the high salinity water south of 30.25 °N by the end of February 2016.

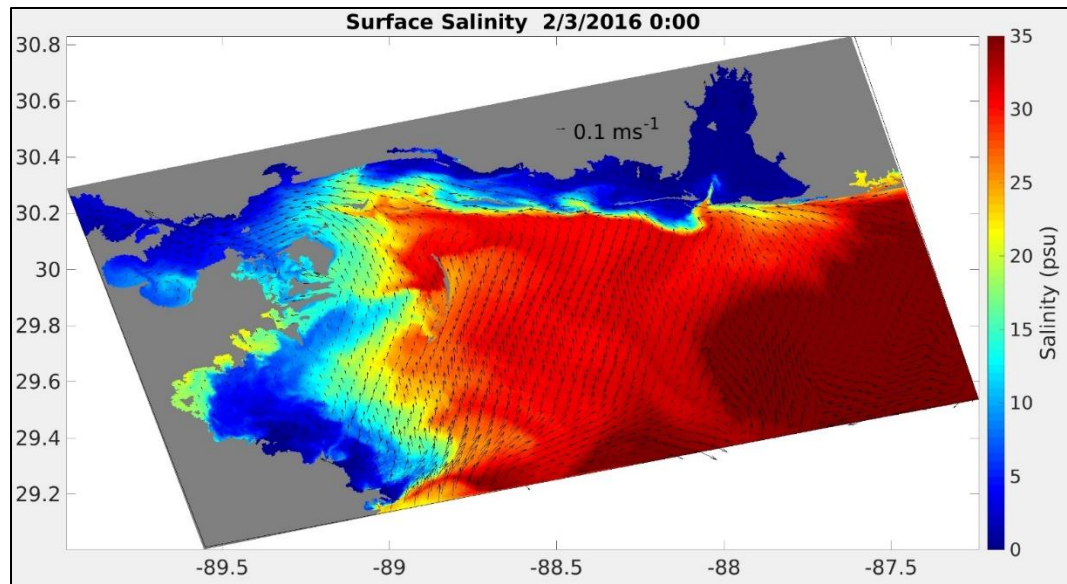


Figure 4.31 Synthesis model output of surface ocean current superimposed on surface salinity on 3 February 2016

Westward propagation of estuarine discharge from Pass aux Herons towards Horn Island Pass.

4.5.2.3 Horn Island Pass

The alongshore wind direction was westerly for most of July and the beginning of August 2015 at the Petit Bois station (Figure 4.17). The Coriolis force (towards the right) associated with the westerly wind advected the surface water southward and resulted in water flowing from MS Sound to the Bight. The advected water mass had a salinity range of 10 to 29 psu and a temperature range of 29 to 30 °C. Westerly winds propagated a positive SPMa (feature 8) southward from mid-July to the end of September.

The alongshore and across shore wind directions switched to easterly and southerly at the end of October 2015. Southeasterly wind advected waters northeastward from the Bight via Ekman transport (Dzwonkowski et al., 2014). Bight waters had a salinity of approximately 30 and a temperature range of 17 to 22 °C. Bight waters

replaced the warmer higher salinity Sound waters in mid-November and December 2015. The northward propagation of the Bight waters transported the negative SP_{Ma} (feature 9) shoreward.

The estuarine discharge transported through Pass aux Herons at the start of February 2016, propagated further west towards Horn Island Pass (Figure 4.31). The estuarine water maintained the salinity and temperature of 10 psu and 10 °C near Horn Island Pass. The water south of Horn Island Pass had a salinity range of 22 to 30 psu and generated an across shore salinity gradient of at least 12 psu. The baroclinic pressure gradient (due to salinity gradient) transported the estuarine water and a positive SP_{Ma} (feature 10) southward through the pass into MS Bight over an 8-week period, and the fresh colder water propagated to the latitude of 30.22 °N by the end of March 2016 (Dzwonkowski & Park, 2012).

4.5.2.4 Dog Key Pass

A positive SP_{Ma} (feature 11) propagated offshore from August to September 2015 (Figure 4.18). Persistent alongshore westerly winds in the final week of July 2015 initiated the southward transport. The alongshore wind advected the surface water southward (Ekman transport) into the Bight (Dzwonkowski et al., 2014). The alongshore wind changed direction to easterly at the start of August for a few days, reversing the Ekman transport to northward and reducing the magnitude of the positive SP_{Ma} at the pass (Dzwonkowski et al., 2014). The return of the westerly winds in mid-August increased the positive SP_{Ma} and continued to transport the feature further southward until the end of September.

The wind at Dog Key Pass was northeasterly for approximately 10 days in October and 5 days in November 2015. The northeasterly winds generated northwestward ocean currents in the tidal pass via Ekman transport and propagated a negative SPMa (feature 12) shoreward for two months (Dzwonkowski et al., 2014). The temperature of the water mass was approximately 14 to 20 °C and the salinity ranged from 15 to 30 psu. The negative anomaly transported Bight waters as far north as 30.35 °N within 1 month.

The estuarine discharge from Mobile Bay through Pass aux Herons in February took a longer time (compared to Petit Bois and Horn Island) to advect further west to Dog Key Pass. A water mass with a salinity of 10 psu and a temperature of 10 °C was observed in the second week of February at Dog Key Pass although the discharge exited Mobile Bay on 3 February (Figure 4.31). The water at the south of the tidal pass had a salinity range of 22 to 30 psu and set up an across shore salinity gradient. The baroclinic pressure gradient due to the across shore salinity gradient propagated the estuarine fresh water and a positive SPMa (feature 13) south into the Bight and flushed the high salinity water at the southern end of the tidal pass (Dzwonkowski & Park, 2012).

4.5.2.5 Ship Island Pass

The alongshore wind was westerly at Bay Waveland during the last week in July and approximately 4 days at the start of August 2015 (Figure 4.19). Persistent westerly alongshore wind pushed the Sound water into the Bight via Ekman transport and propagated a positive SPMa (feature 14) (Dzwonkowski et al., 2014). Feature 14 was followed by a negative SPMa (feature 15) transported north in November 2015. Easterly

alongshore wind during the last week of October and first week of November transported the surface water northward via Ekman transport. The northward across shore current transported high salinity (22 to 30 psu), cold (15 to 24 °C) water shoreward.

The alongshore and across shore wind at Ship Island was primarily easterly and southerly in February 2016. Surface ocean current was directed northeastward via Ekman transport and transported a positive SPMa (feature 16) northward from the Bight (Dzwonkowski et al., 2014). The high salinity surface water ranged from 22 to 30 psu and the temperature ranged from 10 to 20 °C. The feature propagated from approximately mid-February to mid-March before it dissipated.

4.5.2.6 Main Pass: summer 2015 and summer 2016

SPMa in summer 2015 was mostly positive and the SPMa in summer 2016 was negative at Main Pass. In situ, remote sensing and synthesis model (surface ocean current, surface temperature and surface salinity) data provided insight into the possible reasons for the anomaly difference in summer 2015 and summer 2016. Mean river discharge is a proxy for particulate matter discharge; with Mobile Bay receiving 4.30×10^9 kg of suspended solids each year (Ryan, 1969).

Mean river discharge in winter 2014 was not computed because the river discharge was not available for December 2014 and the first two weeks in January 2015. Spring 2015 discharge was 3 % lower than the five-year (2012-2016) mean and summer 2015 was 19 % lower than the five-year mean. In comparison, winter 2015 discharge was 19 % higher than the five-year mean, spring 2016 was 4 % lower than the five-year mean, and summer 2016 was 49 % lower than the five-year mean.

The peak river discharge of $5,500 \text{ m}^3\text{s}^{-1}$ in winter 2014/spring 2015 occurred in April 2015, and the peak discharge of $8,300 \text{ m}^3\text{s}^{-1}$ in winter 2015/spring 2016 occurred in January 2016. Maximum summer river discharges were similar and occurred around the same time in both years, June 2015 ($3,000 \text{ m}^3\text{s}^{-1}$) and May 2016 ($2,500 \text{ m}^3\text{s}^{-1}$). The early peak river discharge in January 2016 was followed by a decline in the river discharge in summer 2016 (compared to the five-year mean discharge), and contributed to the negative SPMa observed in summer 2016. The time of the year when the peak discharge occurred had a greater effect on the SPMa in summer compared to the volume of the peak river discharge during spring/winter. This is highlighted by the fact that the spring discharge in 2015 and 2016 were similar, and both summer 2015 and summer 2016 discharges were at least 15 % less than the five-year mean.

4.5.2.7 Horn Island Pass, Dog Key Pass and Ship Island Pass: summer 2015 and summer 2016

There was a notable difference in the SPMa at Horn Island Pass, Dog Key Pass and Ship Island Pass during summer 2015 and summer 2016. Positive SPMa in summer 2015 contrasted with the predominantly negative anomalies at the passes in 2016. Winds were westerly 67 % of the time at Dog Key Pass/Horn Island Pass (Petit Bois Island weather station) and 64 % of the time at Ship Island Pass, and had mean velocities of 4.7 ms^{-1} and 3.0 ms^{-1} in summer 2015. Westerly winds occurred 57% and 56% of the time at Dog Key Pass/ Horn Island Pass and Ship Island Pass, and had mean velocities of 4.5 ms^{-1} and 2.8 ms^{-1} in summer 2016.

Westerly winds advected surface water from the Sound into the Bight through the tidal passes and resulted in upwelling of colder, high salinity water along the southern coastline of the three barrier islands, and the resuspension of particulate matter deposited by the rivers in spring. Easterly winds caused downwelling along the coastline and the northward propagation of low sediment concentration, warm fresh Bight waters through the tidal passes (Dzwonkowski et al., 2014). Since the upwelling (downwelling) process plays a critical role in increasing (decreasing) particulate matter in the surface water, the higher frequency and magnitude of the westerly winds in summer 2015 contributed to the positive anomaly in 2015 and the negative anomaly in 2016.

4.6 Conclusion

4.6.1 Characterization of Suspended Sediments in MS Sound during winter, spring and summer using in situ CTD, SPM and LISST data

Eastward ocean current velocity increases in the western Sound near Saint Joe Pass due to the conservation of mass as it enters and exits the Pass. The enhanced velocity resuspends finer particles on the seabed and increases the SPM concentration. Increased SPM concentration was not observed at the mouth of the Pearl River during the resuspension events (winter 2015 and summer 2016) at Saint Joe Pass. The observations suggest Lake Borgne was not a major sediment source to MS Sound during winter 2015 and summer 2016. Northwestward ocean currents acted as a medium for the transport of finer particles from the Bight into the Sound in winter 2016.

Enhanced wind velocity in the spring mixes the water column and increases the depth of the mixed layer in MS Sound. Sediments in the surface water move towards the bottom of the mixed layer and reduces the SPM concentration at the surface. Eastward ocean currents in summer act as a sediment sink for finer particle sizes in the eastern MS Sound and transports the finer particles further east. This increases the median grain size in July and August in the western Sound by 10 to 70 μm .

4.6.2 Characterization of Suspended Particulate Matter at the passes and MS Bight during winter, spring and summer using a remote sensing algorithm

Alabama/Tombigbee Rivers are the major particulate matter sources for Mobile Bay with the maximum input in winter and spring. The period when the average peak winter/spring discharge occurs has a more significant effect on the SPM concentration in the summer than the volume of river discharge. Peak discharge during the spring season generates a positive SPMa in summer at the tidal passes, and a peak discharge in winter causes a negative SPMa in summer. Fresh water discharge from the rivers into the Sound and Mobile Bay sets up a horizontal density gradient at the surface. The associated baroclinic pressure gradient causes positive SPMa to flow from Mobile Bay/MS Sound into the Bight during winter and spring. Westward ocean currents in Mobile Bay promote the exchange of estuarine water from the Bay to MS Sound, and contributes to the development of the baroclinic pressure gradient in MS Sound.

Westerly upwelling winds and easterly downwelling winds have an effect on the SPMa at the tidal passes. Westerly winds advect surface water from the Sound to the Bight, and resuspends particulate matter (during upwelling) on the seabed. These

processes results in increased SPM concentration at the tidal passes. Conversely, easterly winds advects water from the Bight into the Sound and transports particulate matter from the surface to deeper depths during downwelling at the barrier island's coastline. The frequency of the westerly/easterly winds directly affects the presence/absence of a positive SPMa in the tidal passes during the summer.

CHAPTER V

5.1 Abstract

Cold front events occur frequently (5 to 7 days) in the northern Gulf of Mexico and enhance the resuspension and transport of particulate matter in late fall through spring. Five Acoustic Doppler Current Profilers (ADCPs) were deployed as part of the Consortium for oil spill exposure pathways in Coastal River-Dominated Ecosystems' (CONCORDE) field campaigns in the Mississippi Bight during spring 2016. A suspended particulate matter concentration time series was generated from the ADCP's echo intensity through calibration with profile measurements of in situ suspended particulate matter concentration, temperature, salinity and particle size data. Two cold front events on 1 and 10 April generated westward alongshelf and southward across shelf surface currents, and opposite flows below the surface water at two ADCP sites. Temperature and salinity from a synthesis model (developed for CONCORDE studies) and in situ line moorings combined with in situ wind and currents suggest the southward transport of fresh water from Mobile Bay during the post-cold front phase enhanced the particulate matter concentration south of Main Pass. Results from this study provide baseline data on suspended particulate matter transport in the northern Gulf of Mexico during a cold front event.

5.2 Introduction

Cold fronts occur every 3-7 days, from mid-October to April every year in the northern Gulf of Mexico (Wiseman et al., 1986). Prior to the cold front, southerly moist winds blow towards the advancing front. Cold fronts advancing obliquely towards the

coast are associated with southeasterly winds, and fronts progressing parallel to the coast generate southwesterly winds (Moeller et al., 1993). Southerly winds move towards the front and results in set up of water level along the coast and shoreward wave propagation during the pre-front phase (Roberts et al., 1989). The barometric pressure decreases as the front passes and produces squalls. The environmental conditions change dramatically as the front moves across the shoreline and the winds shift to northerly. The barometric pressure increases, and the temperature and humidity decreases as the front moves away from the affected area (Robert et al., 1989). Northerly winds reduce the water levels along the coast and produces offshore flow. The wind and waves associated with a frontal system resuspends and transports particulate matter onshore / offshore (Robert et al., 1989). The high frequency of cold fronts in this region affects the distribution of sediments present in the nearshore and on the continental shelf.

Tides also affect the particulate matter morphodynamics in the Mississippi Sound (MS Sound) and Bight (MS Bight). The astronomical tide along the northern Gulf of Mexico is diurnal. Tides are microtidal and have a mean tidal range of 0.37 m (Hardin et al., 1976). Tidal currents within the MS Sound are of the order of 0.15 ms^{-1} at the tidal passes. During the flood/ebb tidal cycle, bed shear stresses in the passes are sufficient to resuspend and transport the finer particulate matter through the passes, resulting in the exchange of particulate matter between MS Sound, Mobile Bay and MS Bight (Sheng, 1983).

In this study, four 614 kHz and one 1228 kHz ADCPs were deployed along the CONSortium for oil spill exposure in Coastal River Dominated Ecosystems (CONCORDE) transect in the MS Bight in spring 2016. Two cold fronts affected the

northern Gulf of Mexico on 1 and 10 April. A suspended particulate matter (SPM) concentration time series was generated from the ADCP's echo intensity using in situ SPM concentration, temperature, salinity and Laser In-Situ Scattering and Transmissometry (LISST) particle size. The effects of the wind forcing on the particulate matter concentration during the cold front events are assessed with CONCORDE synthesis model's temperature, salinity, wind, in situ temperature, salinity, wind, river discharge and tides.

5.3 Data and Methods

5.3.1 Data

5.3.1.1 Cruise and Sampling

Small boat cruises were conducted in spring 2016 along a transect located at Main Pass and five mooring stations in MS Bight (Figure 5.1). Particle size, salinity and temperature profiles were measured with a LISST and Sea-Bird conductivity-temperature-depth (CTD) sensors (Wiggert et al., 2018b). Discrete surface and bottom (approximately 1 m from the seabed) water samples were collected using a 5-L Niskin bottle to measure the concentration of SPM in the laboratory.

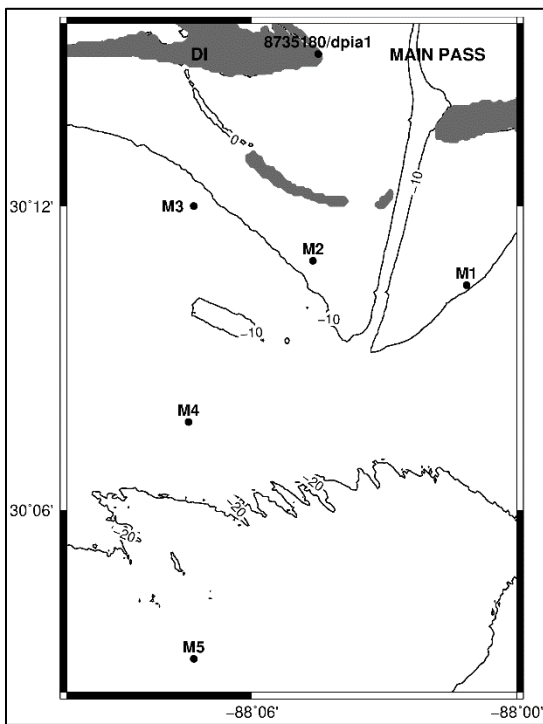
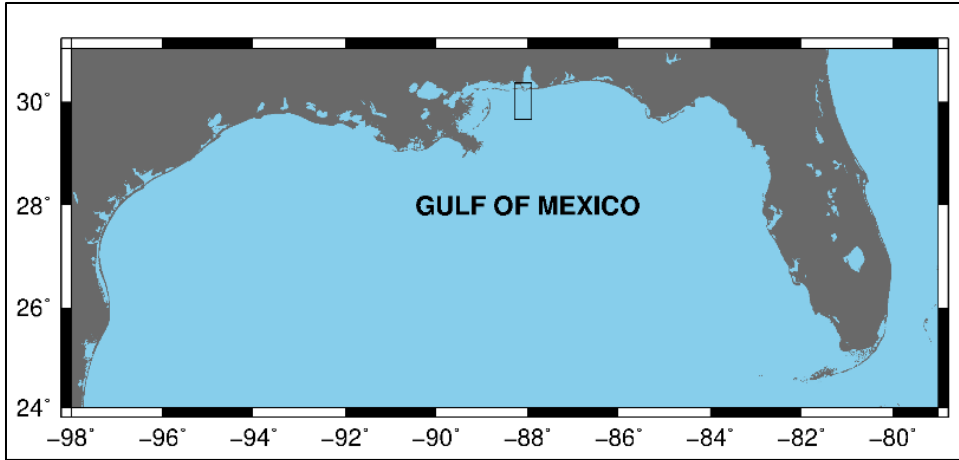


Figure 5.1 Location map of the mooring stations (M1, M2, M3, M4 and M5) located in Mississippi Bight

Data from NOAA National Data Buoy Center tidal (8735180) and meteorological (dpi1) stations located in Dauphin Island (DI) were used in this study.

5.3.1.2 ADCP and Line Moorings

Bottom moorings with pressure sensors and an upward-looking ADCP measured the water current south of Mobile Bay (M1-M5) to capture the fresh water flow in spring 2016 (Figure 5.1). The ADCP at M2 had a frequency of 1228.8 kHz and the other ADCPs had a frequency of 614.4 kHz (Tables 5.1 and 5.2). The Bio-Optical Physical Pop-up Environmental Reconnaissance System (BOPPER) measured the optical properties at M2. Line moorings with sensors measuring pressure, temperature and salinity were deployed at stations M4-M6 (Greer et al., 2018).

Table 5.1 Twelve hundred kHz ADCP (M2) settings.

Parameter	Value
Frequency (kHz)	1228.8
Bin Size (m)	0.25
Pulse Length (m)	0.36
Transmit Power (dB)	12.6

Table 5.2 Six hundred kHz ADCP (M1, M3, M4 and M5) setting

Parameter	Value
Frequency (kHz)	614.4
Bin Size (m)	0.25
Pulse Length (m)	0.72
Transmit Power (dB)	15.4

5.3.1.3 Historical in situ and CONCORDE Synthesis Model Data

Wind data was obtained from National Oceanic and Atmospheric Administration (NOAA) National Data Buoy Center's station dplc and tidal data was extracted from NOAA National Ocean Service station 8735180. Both stations are located on Dauphin Island at 30.25° N and 88.08° W (Figure 5.1). Mean Lower Low Water (MLLW) is the vertical datum of the tidal height. Temperature profiles, salinity profiles and wind velocity were obtained from CONCORDE's synthesis model to analyze the wind stress and advection of high salinity oceanic waters at the mooring stations.

5.3.2 Methods

5.3.2.1 In situ Suspended Particulate Matter Concentration

In situ SPM concentration was measured in the surface and bottom water at the ADCP stations (Figure 5.1). A Whatman 1.5 µm pore size GF/F filter was placed on a filter holder and washed with three successive 20 mL volumes of Nanopure water. The filters were oven dried at 103-105 °C for at least 90 minutes and weighed periodically until the weight change was less than 4 % of the previous weight. The filter was placed on a filter holder and the seawater sample (1-2 L) was filtered. The filter was then rinsed with three 20 mL volumes of Nanopure water and a vacuum was applied to remove traces of water. The filter was removed from the base and dried in an oven at 103-105 °C. The filter was weighed periodically, and dried until the weight change was less than 4 % of the previous weight (United States EPA, 1982). The SPM concentration was computed using the following equation:

$$SPM_{WS} = \frac{(FPR-FP)}{V_S} \quad \text{[Equation 5.1]}$$

where FPR is the combined weight of the filter, petri dish and residue, FP is the combined weight of the filter and petri dish and V_S is the volume of seawater sample filtered.

5.3.2.2 LISST and CTD Data Processing

The ADCP's backscatter echo intensity was calibrated to estimate SPM concentration using LISST and CTD profile data. Matlab scripts were created to convert the light diffraction angles measured by the LISST to particle sizes. LISST data was converted to mean grain size, median grain size and volume concentration (Sequoia, 2013). CTD data was processed with Sea-Bird Scientific software to generate salinity and temperature depth profiles.

5.3.2.3 Suspended Particulate Matter Concentration derived from ADCP

Backscatter

The sound absorption coefficient of water (equation 5.2) was computed (Francois & Garrison, 1982a; Francois & Garrison, 1982b) at the depths corresponding to the surface and bottom water samples, using the in situ salinity, temperature and depth measured by the CTD. The attenuation coefficient of sound in water was computed at the discrete ADCP (M2, M4 and M5) depth bins using the temperature and salinity measured by the BOPPER (M2) and line moorings (M4 and M5).

$$A_1 = \frac{8.86}{c} \times 10^{(0.78 \times pH - 5)} \quad \text{[Equation 5.2a]}$$

$$P_1 = 1 \quad [\text{Equation 5.2b}]$$

$$f_1 = 2.8 \times \sqrt{\frac{S}{35}} \times 10^{(4-(1245 \div (T+273)))} \quad [\text{Equation 5.2c}]$$

$$c = 1412 + 3.21 \times T + 1.19 \times S + 0.0167 \times z \quad [\text{Equation 5.2d}]$$

$$A_2 = 21.44 \times \frac{S}{c} \times (1 + 0.025 \times T) \quad [\text{Equation 5.2e}]$$

$$P_2 = 1 - 1.37 \times 10^{-4} \times z + 6.2 \times 10^{-9} \times z^2 \quad [\text{Equation 5.2f}]$$

$$f_2 = \frac{8.17 \times 10^{(8-(1990 \div (T+273)))}}{1+0.0018 \times (S-35)} \quad [\text{Equation 5.2g}]$$

$$P_3 = 1 - 3.83 \times 10^{-5} \times z + 4.9 \times 10^{-10} \times z^2 \quad [\text{Equation 5.2h}]$$

$$T < 20 \text{ }^\circ\text{C}$$

$$A_3 = 4.937 \times 10^{-4} - 2.59 \times 10^{-5} \times T + 9.11 \times 10^{-7} \times T^2 - 1.5 \times 10^{-8} \times T^3$$

$$T > 20 \text{ }^\circ\text{C}$$

$$A_3 = 3.964 \times 10^{-4} - 1.146 \times 10^{-5} \times T + 1.45 \times 10^{-7} \times T^2 - 6.5 \times 10^{-10} \times T^3$$

$$[\text{Equation 5.2i}]$$

$$A_W = A_1 P_1 \frac{f_1 \times f^2}{f_1^2 + f^2} + A_2 P_2 \frac{f_2 \times f^2}{f_2^2 + f^2} + A_3 P_3 \quad [\text{Equation 5.2j}]$$

where A_w is the attenuation of sound in water, z is the depth, S is the salinity, T is the temperature, c is sound velocity and f is the frequency.

The contribution of particulate matter to the sound attenuation coefficient is the sum of attenuation due to viscous absorption (ζ_v) and scattering (ζ_s). Viscous absorption is a result of the difference between the particle density and the fluid density. The density difference generates inertial forces, resulting in a velocity gradient between the fluid and the particle. The equations for the attenuation of sound due to viscous absorption (Urlick, 1948), scattering (Richards et al., 1996) and the attenuation due to particles at a distance R from a sensor (Thorne & Hanes, 2002) are listed in equation 5.3.

$$\zeta_v = (10 \times \log e^2) \times \left(\frac{\varepsilon \times k \times (\sigma - 1)^2}{2} \times \frac{s}{s^2 + (\sigma + \delta)^2} \right) \quad [\text{Equation 5.3a}]$$

$$s = \frac{9}{4 \times \beta \times \langle a_S \rangle} \times \left(1 + \frac{1}{\beta \times \langle a_S \rangle} \right) \quad [\text{Equation 5.3b}]$$

$$\delta = \frac{1}{2} \times \left(1 + \frac{9}{2 \times \beta \times \langle a_S \rangle} \right) \quad [\text{Equation 5.3c}]$$

$$\sigma = \frac{\rho_S}{\rho_0} \quad [\text{Equation 5.3d}]$$

$$\beta = \left(\frac{\omega}{2 \times \nu} \right)^{1/2} \quad [\text{Equation 5.3e}]$$

$$\zeta_s = (10 \times \log e^2) \times \left(\frac{\varepsilon \times k^4 \times \langle a_S \rangle^3}{\rho_S \times (1 + k^2 \times \langle a_S \rangle^2 + 0.24 \times k^2 \times \langle a_S \rangle^4)} \right) \quad [\text{Equation 5.3f}]$$

$$A_S = \alpha_S \times SSC_{WS} \quad [\text{Equation 5.3g}]$$

where A_S is the sound attenuation due to particulate matter, α_S is particulate matter attenuation coefficient, β is the depth of the oscillatory boundary layer, ε is the volume concentration of scatterers, k is the acoustic number, σ is the ratio of the densities of the solid and fluid phases, $\langle a_S \rangle$ is the mean particle radius, ρ_S is the density of particulate matter, ρ_0 is the density of water, ν is the kinematic viscosity of water and ω is the angular velocity.

The computed sound absorption coefficient of water and the contribution of particulate matter to the sound attenuation coefficient were included in the sonar equation. The sonar equation (equation 5.4) was used to calibrate the ADCP and derive the estimated SPM concentration from the ADCP's backscatter (Deines, 1999; Kim et al., 2004).

$$10 \times \log_{10}(SPM_{WS}) = C + 10 \times \log_{10}(R^2) + 2 \times (A_W + A_S) \times R - L_{DBM} - P_{DBW} + K_c \times (E - E_r)$$

$$[\text{Equation 5.4a}]$$

$$SPM_v = 10 \times \log(SPM_{WS}) - 10 \times \log_{10}(R^2) - 2 \times (\alpha + A_S) \times R + L_{DBM} + P_{DBW}$$

[Equation 5.4b]

$$SPM_v = K_C \times (E - E_R) + C$$

[Equation 5.4c]

where C is a constant that incorporates several ADCP parameters (e.g. sonar efficiency and noise power), R is the range to the scattering particles, L_{DBM} is $10\log_{10}$ (transmit pulse length), P_{DBW} is $10\log_{10}$ (transmit power), K_C is received signal strength indicator, E is echo strength, E_R is the reference echo strength measured by Deines (1999), SPM_{WS} is in situ SPM concentration.

C and K_C were calculated by linear regression of the relative backscatter intensity ($E-E_R$) and SPM_v at the 614 kHz ADCPs (M1, M3, M4 and M5) (Deines, 1999). Kim et al. (2004) computed a K_C value of $0.43 \text{ dB count}^{-1}$ for a 1200 kHz RDI ADCP, similar to the range ($0.35 - 0.55 \text{ dB count}^{-1}$) computed by Deines et al. (1999) for the same ADCP model and frequency. Kim et al. (2004) showed the ADCP parameters were similar for ADCPs with the same manufacturer and frequency.

SPM concentration was derived from the ADCP backscatter intensity, ADCP parameters and water attenuation (equation 5.5). The ADCP's parameters (C and K_C) were not computed at M2 (1228 kHz) because only two pairs of surface and bottom water samples were collected at the station (Figure 5.2) (Wiggert et al., 2018c). SPM concentration was not derived at M1 and M3 because temperature and salinity time series were not available at these two stations, therefore, the attenuation coefficient of water required in the sonar equation could not be estimated. SPM concentration values derived from the ADCP's echo intensity with a concentration exceeding 20 mgL^{-1} were converted

to missing data in the time series at M4 and M5, since the maximum in situ SPM concentration observed at both stations was 20 mgL⁻¹ (Landers et al., 2016).

$$SPM = 10^{(C+20\log_{10}(R)+2\times(A_W+A_S)\times R-L_{DBM}-P_{DBW}+K_C\times(E-E_R))\div 10} \quad [\text{Equation 5.5}]$$

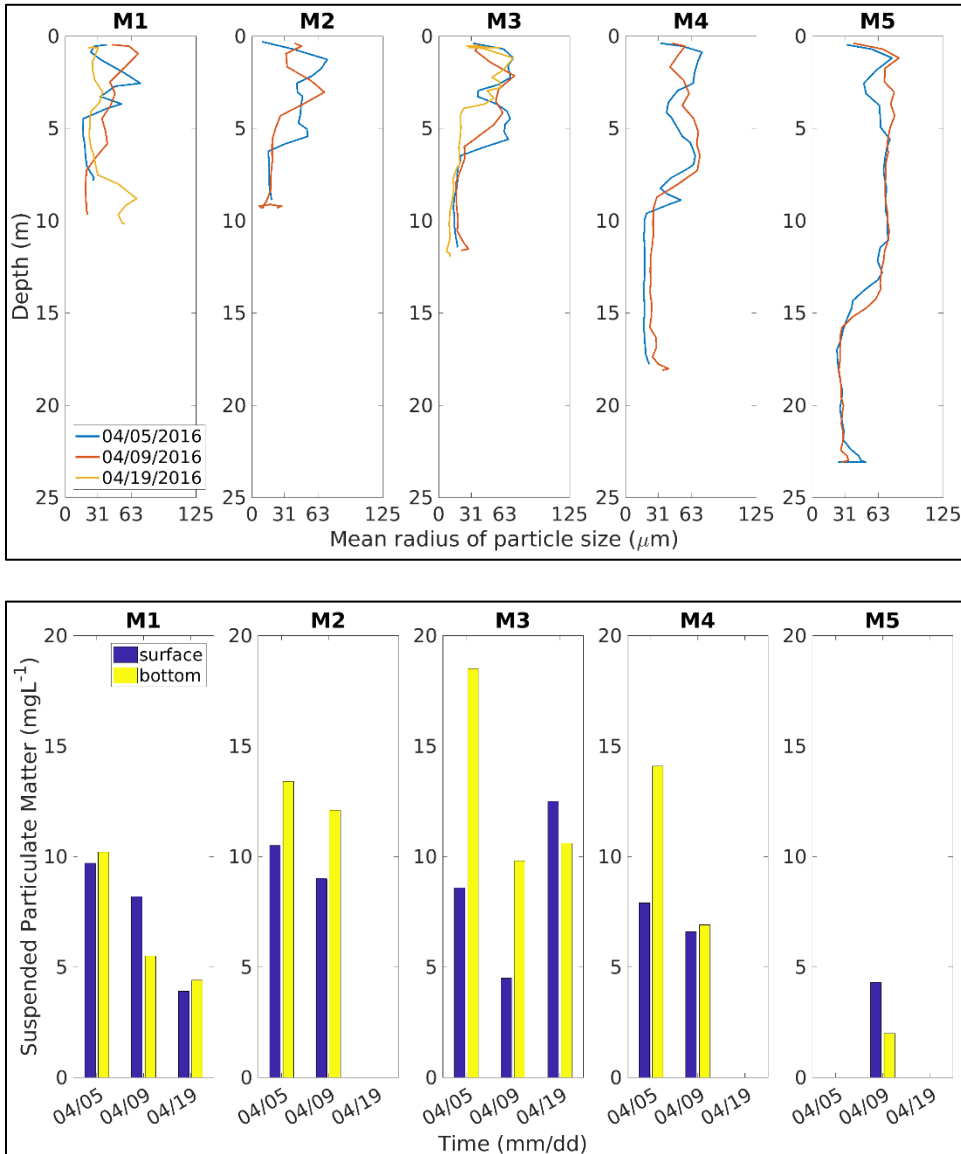


Figure 5.2 LISST mean particle size and in situ suspended particulate matter (SPM) measurements at the ADCP stations in April 2016

5.3.2.4 Calibration of ADCP Echo Intensity to Estimate Suspended Sediment Concentration

SPM_v was calculated in equation 5.4b using the in situ SPM concentration and the ADCP parameters. The values of K_C and C were computed from the linear regression analysis of SPM_v and $(E-E_R)$ (equation 5.4c). The best-fit values for K_C and C were 0.37 and -22.95 dB (Figure 5.3). The R^2 value of the linear regression fit was 0.43, indicating the regression model explains 43% of the variability present in SPM_v (Sullivan, 2008). SPM concentration time series were generated at M4 and M5 by substituting the echo intensity, C and K_C parameters into equation 5.5 (Figures 5.4 and 5.5).

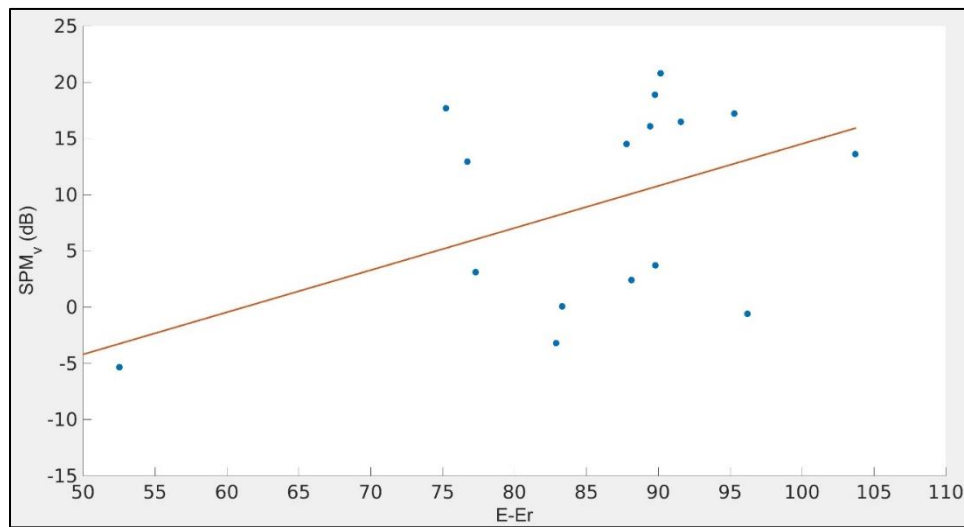


Figure 5.3 Linear regression analysis of SPM_v and $(E-E_r)$ for the 614.4 kHz ADCPs

The red line represents the linear regression solution.

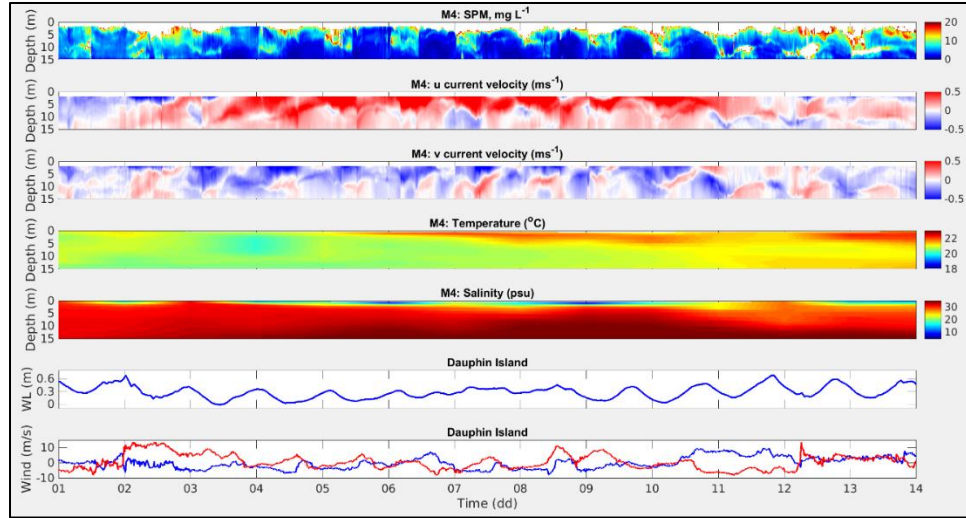


Figure 5.4 M4 April 2016 time series

Suspended particulate matter concentration derived from the ADCP's echo intensity (i) ADCP alongshore current velocity (ii) ADCP across shore current velocity (iii) CONCORDE's synthesis model temperature (iv) CONCORDE's synthesis model salinity (v) tidal height with respect to Mean Lower Low Water at NOAA Dauphin Island station, 8735180 (vi) alongshore wind (blue) and across shore wind (red) at NOAA Dauphin Island station, dpia1c (vii).

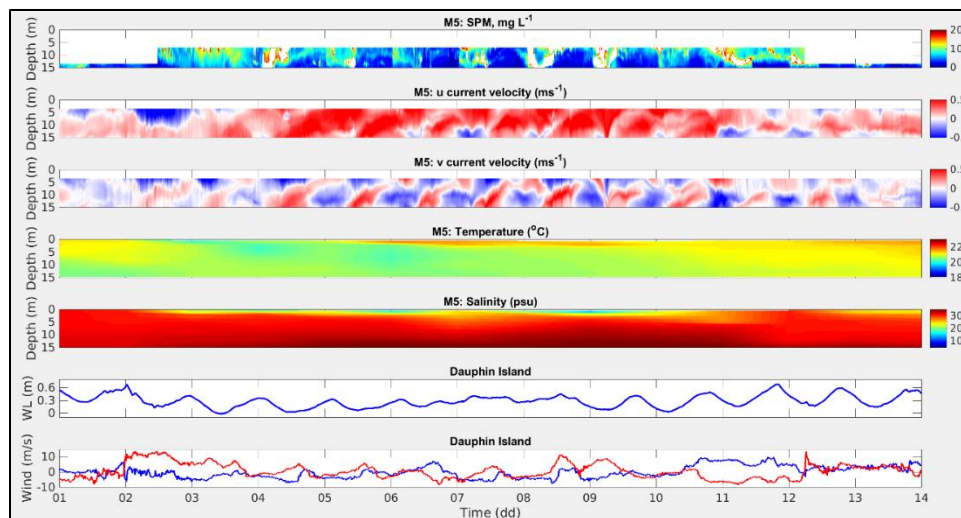


Figure 5.5 M5 April 2016 time series

Suspended particulate matter concentration derived from the ADCP's echo intensity (i) ADCP alongshore current velocity (ii) ADCP across shore current velocity (iii) CONCORDE's synthesis model temperature (iv) CONCORDE's synthesis model salinity (v) tidal height with respect to Mean Lower Low Water at NOAA Dauphin Island station, 8735180 (vi) alongshore wind (blue) and across shore wind (red) at NOAA Dauphin Island station, dpia1c (vii).

The low R^2 value (0.43) of the SPM regression model highlights some of the limitations in the data collection. Mobile Bay fresh water outflow south of Main Pass during CONCORDE's spring cruise resulted in a stratified water column consisting of a fresh water surface plume and higher salinity bottom water (Greer et al., 2018). Density gradients at the interface of the surface and bottom waters increase the acoustic scattering strength (Goodman, 1990). The ADCP records an increase in the backscatter at the interface although there is no change in the size or concentration of the particulate matter (Ross & Lueck, 2003). Another limitation is the use of a single frequency (614.4 kHz) sonar to estimate SPM concentration. A single frequency sonar cannot distinguish between changes in concentration level and changes in particle size. If mass concentration remained constant during sampling and particle size changed, the change was incorrectly recorded as a change in the mass concentration (Gartner, 2004). This affected the backscatter intensity recorded by the ADCP.

5.3.2.5 Acoustic Sensitivity to Particle Size

The acoustic sensitivity of an ADCP is directly proportional to the form factor, which is related to the scattering properties of the ensonified particle. The peak of acoustic sensitivity occurs when the circumference of the particle is close to the acoustic wavelength, assuming a spherical shape (equation 5.6).

$$k \times a \approx 1 \quad \text{[Equation 5.6a]}$$

$$k = \frac{2 \times \pi \times f}{c} \quad \text{[Equation 5.6b]}$$

where a is the particle radius.

The ADCP's sonar can detect particles provided ' $k \times a$ ' is greater than 0.05, given there is no significant concentration of particles with ' $k \times a$ ' approximately equal to 1 (Lohrmann, 2001). The ' $k \times a$ ' value of 1 at a frequency of 614.4 kHz corresponds to a particle diameter of 777 μm and a value of 0.05 corresponds to 38 μm (Lynch et al, 1994; Thorne & Hanes, 2002; Thorne et al., 1993; Vincent 2007). This range of particle sizes (38 to 777 μm) represents the resolution of the particulate matter measured at M4 and M5 near the Mobile Bay outflow.

5.4 Results

5.4.1 Wind at Station DPIA1: 1 April to 14 April

A cold front affected the northern Gulf of Mexico on 30 March, followed by calm wind conditions before a second cold front affected the region. The first cold front event affected MS Sound and Bight beginning on 30 March and ending on 3 April 2016. ADCP measurements started on 1 April during the post front phase of the event. The wind switched direction from southerly to northerly on 1 April until 3 April, with a maximum velocity of 13 ms^{-1} and minimum velocity of 1 ms^{-1} . Maximum winds occurred on 2 April and minimum wind velocity occurred on 3 April as the cold front moved away from the region.

A regular wind pattern characterized the first 12 hours of each day during calm wind conditions between 4 and 8 April. The wind direction at the start of each day was southwesterly and rotated clockwise to westerly followed by a northerly direction (northwesterly or northerly). The wind continued to shift clockwise to northeasterly or

anticlockwise to northwesterly, and the velocity range was 1 to 9 ms⁻¹. The northwesterly wind velocity decreased and the wind shifted between a northerly and northwesterly direction on 9 April. At the beginning of 10 April, the wind velocity decreased and switched to southerly, followed by southwesterly. The wind velocity increased, rotated clockwise to westerly and continued to increase and rotate clockwise to northeasterly.

A second cold front affected MS Sound and Bight at the end of 10 April. The prefrontal southeasterly winds increased from 6 to 11 ms⁻¹. The wind velocity was variable as the wind rotated clockwise to westerly on 12 April. At 0600 on 12 April, the post front winds switched to northerly and increased from 6 to 8 ms⁻¹ within two hours. The wind velocity continued to rotate between northeasterly and northerly until the end of the cold front event at 2000 on 13 April. Changes in model temperature, model salinity, in situ currents and derived SPM concentration at M4 and M5 during each phase of the two-week period are described in the next section.

5.4.2 M4: In situ Alongshore and Across shore Velocity, Model Temperature and Salinity and Derived SPM Concentration

5.4.2.1 1 April to 3 April: Post Cold Front

5.4.2.1.1 In situ Alongshore and Across shore Velocity

This section describes changes in model temperature, model salinity, in situ ocean current and SPM concentration at M4 during the first cold front. On 1 April, in situ alongshore velocity in the surface water was westward and had a velocity of -0.2 ms⁻¹,

and bottom water was eastward with a velocity of 0.1 ms^{-1} (Figure 5.4). The across shore velocity in the surface plume was southward with a velocity of -0.2 ms^{-1} and the bottom water had a northward velocity of 0.1 ms^{-1} . The surface plume was northward (0.1 ms^{-1}) and the bottom water was southward (-0.1 ms^{-1}) from 1000 to 1200 Coordinated Universal Time (UTC). The across shore velocity of the surface plume (-0.1 ms^{-1}) and bottom water (-0.2 ms^{-1}) were southward from 1200 to 2400.

The surface plume alongshore velocity increased to -0.3 ms^{-1} on 2 April, and subsequently changed direction to eastward (0.2 ms^{-1}) (Figure 5.4). The bottom water at a depth of 5 m moved westward with a velocity of -0.2 ms^{-1} . The across shore velocity of the surface plume increased to -0.3 ms^{-1} , and the bottom water changed direction to northward with a velocity of 0.2 ms^{-1} . The alongshore velocity of the bottom water increased to 0.2 ms^{-1} , and decreased to a velocity of 0.1 ms^{-1} on 3 April. The surface plume changed direction for a short time to westward with a velocity -0.2 ms^{-1} , before moving eastward with a velocity of 0.5 ms^{-1} . The across shore velocity of the surface plume increased to -0.4 ms^{-1} and the bottom water switched to southward (-0.3 ms^{-1}).

5.4.2.1.2 Model Temperature, Model Salinity and Derived SPM Concentration

Model temperature and salinity showed a thin fresh water plume on 2 April with a salinity of 15 psu at a depth of 1 m (Figure 5.4). High salinity (35 psu) bottom water was observed throughout the rest of the water column on that day. The temperature of the surface and bottom water masses were 21 and 20 °C. Maximum SPM concentration of 20 mgL^{-1} was observed in the bottom water (salinity of 25), and increased SPM concentration with a range of 5 to 10 mgL^{-1} was observed at other depths.

At the end of 2 April, the fresh water plume disappeared and the water was well mixed with a salinity of 35 psu at M4 (Figure 5.4). The temperature of the surface water decreased to 20 °C. Maximum SPM concentration (20 mgL^{-1}) was restricted to depths between 4 to 5 m, and the concentration was 5 to 15 mgL^{-1} at depths greater than 5 m. A fresh water plume and water mass with a salinity of 25 psu were observed at the site two hours later. This coincided with a decrease in the SPM concentration throughout the water column to less than 6 mgL^{-1} .

5.4.2.2 4 April to 8 April: Calm Wind Conditions

5.4.2.2.1 In situ Alongshore and Across shore Velocity

As the first cold front moved away from the area, wind conditions were mostly calm. In situ alongshore velocities of the surface plume (0.5 ms^{-1}) and bottom water (0.1 ms^{-1}) were eastward on 4 April (Figure 5.4). The across shore velocity of the surface plume and bottom water during the first 12 hours were southward and northward with velocities of -0.5 and 0.2 ms^{-1} . The velocity of the surface plume and bottom water decreased to -0.3 and 0.1 ms^{-1} from 1200 to 2400.

During the first 12 hours on 5 April, the alongshore velocity of the surface and bottom water remained unchanged (Figure 5.4). The across shore velocity at the surface was southward (-0.3 ms^{-1}) and the bottom water was northward (0.2 ms^{-1}). The alongshore velocity at the surface decreased to 0.3 ms^{-1} after 1200 on 5 April, and the across shore velocity throughout the water column switched to southward with a velocity of -0.1 ms^{-1} .

On 6 April, the alongshore velocity at the surface increased to 0.5 ms^{-1} . The velocity of the bottom water was eastward (0.1 ms^{-1}) from 0000 to 1200 UTC (Figure 5.4). The across shore velocity at all depths was southward with a velocity of -0.3 ms^{-1} . The alongshore velocity of the bottom water switched to westward (-0.1 ms^{-1}) and the across shore velocity of the bottom water decreased (-0.1 ms^{-1}).

The direction and magnitude of the alongshore velocity at the surface on 7 April remained unchanged (Figure 5.4). The across shore velocity of the surface plume increased (-0.5 ms^{-1}) and the bottom water velocity switched to northward (0.2 ms^{-1}). From 2000 to 2400 UTC, the velocity of the bottom water changed direction to eastward with a velocity of 0.1 ms^{-1} . The across shore velocity of the surface plume and bottom water decreased to -0.1 ms^{-1} and 0.1 ms^{-1} .

At the start of 8 April there was no change in the alongshore velocity, and the across shore velocity of the surface plume increased to -0.5 ms^{-1} (Figure 5.4). From 1200 to 1300 (UTC) the alongshore velocity of the surface plume changed to westward (-0.3 ms^{-1}), then switched to eastward with a velocity of 0.4 ms^{-1} . The velocity of the bottom water increased to 0.3 ms^{-1} , and later decreased to 0.1 ms^{-1} . The across shore velocity of the surface plume and bottom water switched direction to north (0.1 ms^{-1}) and south (-0.2 ms^{-1}) at the end of the day.

5.4.2.2.2 Model Temperature, Model Salinity and Derived SPM Concentration

Model temperature and salinity showed the fresh water plume deepened to 3 m on 5 April with a salinity of 10 psu (Figure 5.4). The temperature of the surface water increased to $22 \text{ }^{\circ}\text{C}$. Maximum SPM concentration initially occurred only at the surface

and extended to 10 m on 5 April. An elevated concentration of SPM was observed between depths of 5 to 12 m on 6 April. Salinity of the surface water increased to 20 psu and temperature remained constant on 6 April. SPM concentration had a regular pattern of high concentrations within the first 12 hours of the day and low concentrations during the second half of the day.

Salinity of the surface water decreased throughout the day on 7 April, and decreased to a minimum of 10 psu the following day. The temperature of the surface plume remained at 22 °C. The highest SPM concentration of 20 mg L⁻¹ was observed at 5 m, and a concentration of 12 mg L⁻¹ extended to 12 m. On 8 April, increased concentration of particulate matter was observed only at the depth of 5 m.

5.4.2.3 April 10 to April 13: Pre Cold Front to Post Cold Front

5.4.2.3.1 In situ Alongshore and Across shore Velocity

Another cold front followed calm wind conditions at M4. On 10 April in situ alongshore velocity of surface and bottom waters were eastward with velocities of 0.5 and 0.1 ms⁻¹ (Figure 5.4). The across shore velocity of surface and bottom waters were -0.3 ms⁻¹. The alongshore velocity of the surface water decreased to 0.1 ms⁻¹ and the bottom water remained constant (0.1 ms⁻¹) at the start of 11 April. The across shore velocity of the surface plume decreased to -0.1 ms⁻¹, and the bottom water changed direction to northward with a velocity of 0.2 ms⁻¹. From 2000 to 2200, the surface plume switched direction to westward with a velocity of -0.1 ms⁻¹, and returned to eastward during the last 2 hours of the day. The across shore velocity of the surface plume

changed direction to northward with a velocity of 0.2 ms^{-1} and the bottom water changed direction to southward with a velocity of -0.2 ms^{-1} .

At the beginning of 12 April, the surface and bottom waters had an alongshore velocity of -0.1 ms^{-1} (Figure 5.4). Across shore velocity of the entire water column was northward with a velocity of 0.3 ms^{-1} . From 1200 to 2400 (UTC), surface water had an alongshore velocity of -0.1 ms^{-1} and bottom water had a velocity of 0.1 ms^{-1} . The across shore velocity switched direction to southward with a velocity of -0.2 ms^{-1} .

Alongshore velocity of the surface plume increased to -0.2 ms^{-1} and bottom water remained unchanged on 13 April (Figure 5.4). The surface plume switched to eastward (0.2 ms^{-1}) and the bottom water changed direction to westward (-0.1 ms^{-1}) from 0200 to 2000 (UTC). The across shore velocity of the surface plume was southward with a velocity of -0.2 ms^{-1} and the bottom water was northward with a velocity of 0.2 ms^{-1} . The alongshore velocity of the surface and bottom water changed direction again to westward (-0.1 ms^{-1}) and eastward (0.1 ms^{-1}), and the across shore velocity of the entire water column was southward with a velocity of -0.2 ms^{-1} .

5.4.2.3.2 Model Temperature, Model Salinity and Derived SPM Concentration

Model salinity of surface and bottom waters were 20 and 35 psu at the start of 10 April (Figure 5.4). Surface water salinity increased to 25 psu and temperature decreased to $21.5 \text{ }^{\circ}\text{C}$ at the end of the day on 10 April. SPM concentration of 20 mgL^{-1} was observed between the depths of 5 to 12 m, and concentrations of 5 mgL^{-1} was present at 15 m, during the first 12 hours on 10 April. Surface water salinity increased further to 27 psu on 11 April. The sediment concentration increased and SPM concentration of 20

mgL⁻¹ was present at 5 and 15 m on 11 April. The salinity of the surface water decreased to 25 psu at 0300 UTC on 11 April.

A fresh water plume with a salinity and temperature of 20 psu and 22 °C was observed at 1 m on 11 April (Figure 5.4). The plume deepened to 3 m on 13 April at 0600 UTC. SPM concentration of 20 mgL⁻¹ was observed between 5 to 8 m and 14 to 15 m, and SPM concentration throughout the rest of the water column ranged between 5 to 15 mgL⁻¹. SPM concentration remained high on 13 April, and maximum concentrations occurred at 5 and 10 m.

5.4.3 M5: In situ Alongshore and Across shore Velocity, Model Temperature and Salinity and Derived SPM Concentration

5.4.3.1 2 April to 3 April: Post Cold Front

5.4.3.1.1 In situ Alongshore and Across shore Velocity

This section provides an overview of derived SPM concentration, model temperature, model salinity and in situ ocean currents at M5 during the first cold front. At the start of 2 April, in situ alongshore velocity throughout the water column was eastward with a velocity of 0.1 ms⁻¹, and the across shore velocity throughout the water column was northward with a velocity of 0.1 ms⁻¹ (Figure 5.5). The alongshore velocity of surface water switched to westward with a velocity of -0.5 ms⁻¹. The across shore velocity of the surface water changed direction to southward (-0.3 ms⁻¹), then switched to

northward with a velocity of 0.1 ms^{-1} . The velocity of the bottom water increased to 0.2 ms^{-1} , then switched to southward with a velocity of -0.1 ms^{-1} .

Surface water alongshore velocity changed direction to eastward with a velocity of 0.1 ms^{-1} on 3 April (Figure 5.5). The across shore velocity of surface and bottom waters switched to southward and northward, with velocities of -0.5 ms^{-1} and 0.1 ms^{-1} . The alongshore velocity of the surface and bottom water increased to 0.5 ms^{-1} , and the across shore velocity of the surface water changed direction to northward with a velocity of 0.1 ms^{-1} from 0400 to 2400 (UTC).

5.4.3.1.2 Model Temperature, Model Salinity and Derived SPM Concentration

Model salinity of surface water reduced from 35 to 25 psu, and model temperature decreased from 21 to $20.5 \text{ }^{\circ}\text{C}$ on 2 April (Figure 5.5). SPM concentration of 20 mgL^{-1} was observed between the depths of 5 to 10 m. Salinity of the surface water decreased further to 25 psu on 3 April and the temperature remained constant. The maximum depth with elevated SPM concentration increased over the 2-day period from 10 to 20 m and resulted in a higher concentration of SPM on 3 April compared to 2 April.

5.4.3.2 4 April to 8 April: Calm Wind Conditions

5.4.3.2.1 In situ Alongshore and Across shore Velocity

The water column properties and meteorological conditions at M5 changed as the first cold front moved away from the coastline. In situ alongshore velocity throughout the water column decreased to 0.2 ms^{-1} (eastward) from 0000 to 1000 UTC on 4 April

(Figure 5.5). The across shore velocity of the surface and bottom water was southward with a velocity of -0.1 ms^{-1} . The alongshore velocity of the surface water switched to westward with a velocity of -0.1 ms^{-1} , followed by eastward with a velocity of 0.5 ms^{-1} . The across shore velocity of the surface water increased to -0.2 ms^{-1} , then changed direction to northward with a velocity of 0.2 ms^{-1} . The velocity of the bottom water switched to northward with a velocity of 0.5 ms^{-1} and decreased to 0.1 ms^{-1} .

The alongshore velocity in the bottom water decreased to 0.1 ms^{-1} on 5 April. The velocity of the surface water switched to northward with a velocity of 0.5 ms^{-1} and the velocity of the bottom water increased to 0.5 ms^{-1} (Figure 5.5). The across shore velocity of the surface water decreased to 0.1 ms^{-1} from 2000 to 2400. The alongshore velocity of the bottom water switched three times between eastward and westward with velocities of 0.1 and -0.1 ms^{-1} on 6 April. The across shore velocity of the surface water increased to 0.2 ms^{-1} and the bottom water switched to southward with a velocity of -0.5 ms^{-1} . The velocity of the surface water changed direction from northward to southward on three occasions with a range of -0.5 to 0.5 ms^{-1} .

The alongshore velocity in the bottom water increased to -0.5 ms^{-1} , then switched to eastward with a velocity of 0.1 ms^{-1} on 7 April (Figure 5.5). The across shore velocity of the surface and bottom water changed direction to southward and northward with velocities of -0.2 ms^{-1} and 0.5 ms^{-1} . The velocity of the surface water then switched to northward with a velocity of 0.5 ms^{-1} , and the bottom water switched to southward with a velocity of -0.2 ms^{-1} .

The alongshore velocity of the bottom water changed direction to westward with a velocity of -0.1 ms^{-1} from 0000 to 1000 on 8 April (Figure 5.5). The across shore velocity of the surface and bottom water decreased to 0.1 ms^{-1} and -0.1 ms^{-1} . The velocity of the surface water then changed direction to southward (-0.2 ms^{-1}) and increased (magnitude) to -0.3 ms^{-1} . The bottom water also changed direction to northward with a velocity of 0.2 ms^{-1} and decreased to 0.1 ms^{-1} .

5.4.3.2.2 Model Temperature, Model Salinity and Derived SPM Concentration

Model salinity and temperature of the surface water was 20 psu and $20.4 \text{ }^{\circ}\text{C}$ at depth of 1 m on 4 April (Figure 5.5). SPM concentration of 20 mgL^{-1} was observed between the depths of 10 to 15 m on 4 April. The particulate matter concentration decreased on 5 April, and maximum SPM concentration of 20 mgL^{-1} occurred at depths of 5 and 15 m.

The depth of the surface water increased to 2 m and the temperature increased to $22.5 \text{ }^{\circ}\text{C}$ on 6 April (Figure 5.5). The salinity of the surface water increased to 25 psu for approximately 8 hours and decreased to 15 psu the following day. Low SPM concentration observed on 6 April was followed by increased maximum concentration of 20 mgL^{-1} at 5 and 10 m on 7 April. The particulate matter concentration throughout the water column remained constant on 8 April.

5.4.3.3 April 10 to April 13: Pre Cold Front to Post Cold Front

5.4.3.3.1 In situ Alongshore and Across shore Velocity

This section outlines the effects of the pre and post-cold front periods on the currents, temperature, salinity and SPM concentration at M5. In situ alongshore velocity of the surface and bottom water were eastward and westward with velocities of 0.5 ms^{-1} and -0.1 ms^{-1} on 10 April from 0000 to 0200 (UTC) (Figure 5.5). The velocity throughout the water column was eastward with a velocity of 0.1 ms^{-1} from 0200 to 1200. The across shore velocity of the surface water was southward with a velocity of -0.1 ms^{-1} and the bottom water was northward with a velocity of 0.1 ms^{-1} . The direction of the surface and bottom water changed to northward with a velocity of 0.1 ms^{-1} and southward with a velocity of -0.1 ms^{-1} , and increased a few hours later to 0.5 ms^{-1} (surface) and -0.5 ms^{-1} (bottom). The alongshore velocity of the surface plume increased to 0.5 ms^{-1} , and the velocity of the bottom water switched to westward with a velocity of -0.1 ms^{-1} .

The alongshore velocity of the surface water decreased to 0.1 ms^{-1} and later switched to westward with a velocity of -0.1 ms^{-1} on 11 April (Figure 5.5). The across shore velocity of the surface water decreased to 0.3 ms^{-1} . The surface water decreased to a velocity of 0 ms^{-1} and the bottom water switched to northward with a velocity of 0.1 ms^{-1} from 0300 to 1500. The velocity of the surface and bottom water switched direction to northward with a velocity of 0.1 ms^{-1} and southward with a velocity of -0.4 ms^{-1} .

The alongshore velocity of the surface water changed direction to eastward with a velocity of 0.1 ms^{-1} from 0000 to 1200 on 12 April (Figure 5.5). The across shore velocity of the bottom water decreased to -0.2 ms^{-1} . The velocity of the surface water

switched to southward with a velocity of -0.1 ms^{-1} , and the velocity of the bottom water increased to -0.3 ms^{-1} . The alongshore velocity of the entire water column switched to eastward with a velocity of 0.3 ms^{-1} . The velocity of the bottom water changed direction to westward with a velocity of -0.1 ms^{-1} from 2000 to 2400. The across shore velocity of the surface water also switched to northward with a velocity of 0.3 ms^{-1} and the velocity of the bottom water increased to 0.4 ms^{-1} .

5.4.3.3.2 Model Temperature, Model Salinity and Derived SPM Concentration

Model salinity and temperature of the surface water was 25 psu and $20.5 \text{ }^{\circ}\text{C}$ on 10 April (Figure 5.5). Maximum SPM concentration of 20 mgL^{-1} occurred at a depth of 5 m and decreased with increasing depth to a minimum value of 5 mgL^{-1} . Salinity and temperature of the surface water increased to 35 psu and $21 \text{ }^{\circ}\text{C}$ over the next 48 hours. Maximum SPM concentration (20 mgL^{-1}) was present between the depths of 5 to 10 m and SPM concentration of 5 to 15 mgL^{-1} occurred throughout the water column on 11 April. The particulate matter concentration on 12 April was similar to the previous day.

5.4.4 Effect of Tides and Wind Stress on Suspended Particulate Matter Concentration

This section examines the effects of wind stress on the SPM concentration at the ADCP stations. To study the effects of wind stress on the SPM concentration, maximum tidal range was used as a constant variable since tides are the primary forcing at Main Pass (Hummell, 1990). A day with maximum tidal range and minimum wind stress was identified (2 April), and a day with maximum tidal range and maximum wind stress was

identified (13 April) (Ha & Park, 2012) (Figures 5.6 and 5.7). M4 and M5 experienced the third highest tidal range and maximum wind stress on 2 April. The sixth highest tidal range and second lowest wind stress occurred on 13 April. Derived SPM concentration, in situ current, in situ temperature (line mooring at 12 and 15 m), in situ tides, in situ wind and in situ river discharge were analyzed to understand the effects of the wind stress on SPM concentration. Only M4 was analyzed for the effects of the wind stress since M5 had missing data between 5 and 13 m on 2 and 13 April.

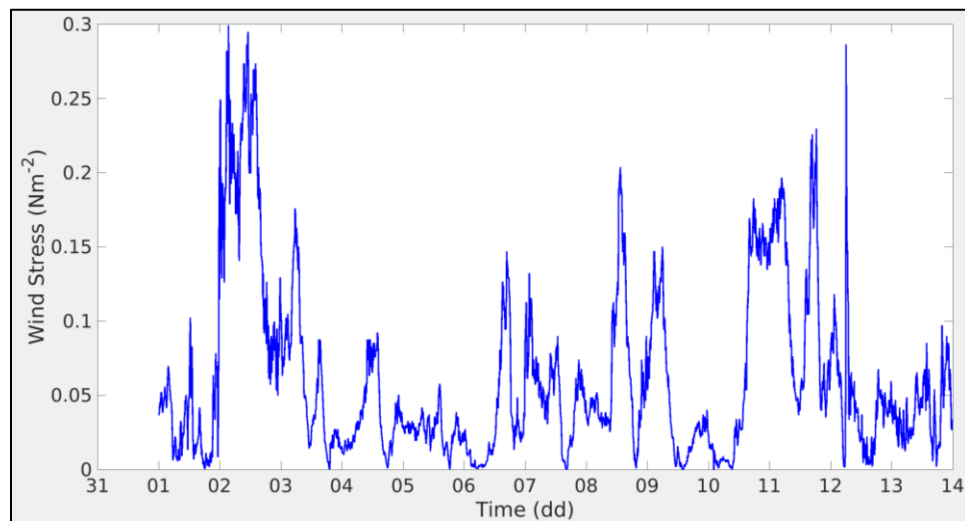


Figure 5.6 Wind stress at NOAA Dauphin Island station, dpia1

Maximum wind stress occurred on 2 April and the second lowest wind stress occurred on 13 April.

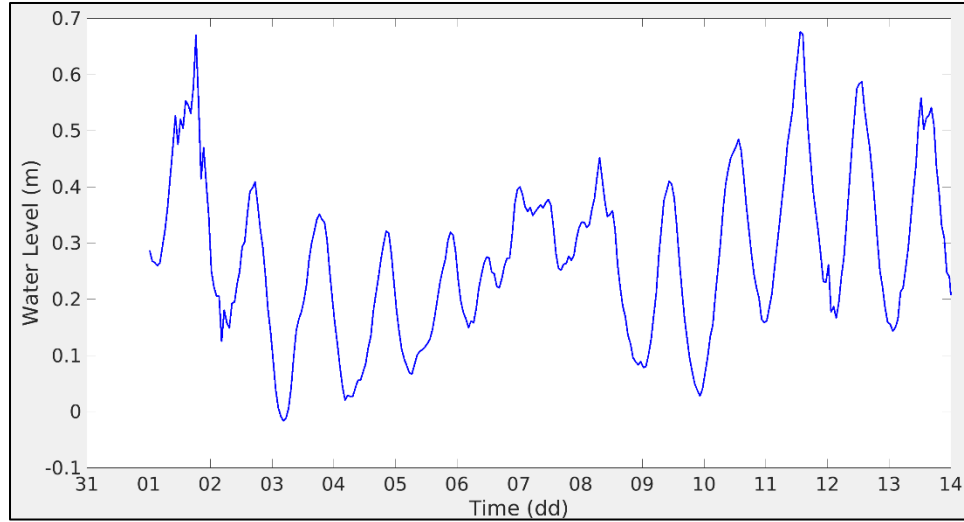


Figure 5.7 Hourly averaged tidal heights at Dauphin Island station 8735180 during the ADCP deployment

The third highest tidal range occurred on 2 April and the sixth highest tidal range occurred on 13 April.

As the wind blows across the surface of the ocean, energy transfers from the wind to the surface. The wind moves the water column to the right in the northern hemisphere due to the Coriolis force by Ekman transport. Convergent water masses result in downwelling and divergent water masses results in upwelling (Knauss, 1997). Ekman pumping transports SPM from the surface to a deeper depth (downwelling) or vice versa (upwelling). Model winds were utilized in this section to compute Ekman pumping (equation 5.7) between stations M4 and M5 because no in situ winds were measured at M4 and M5 (Glover et al., 2011).

$$w_E = -1 \times \left(\frac{d\tau_y}{d\phi} - \frac{d\tau_x}{d\lambda} \right) \quad [\text{Equation 5.7}]$$

where τ_y is the meridional wind stress, τ_x is the zonal wind stress, ϕ is the longitude and λ is the latitude. The sign convention is positive down.

Brunt Vaisala frequency was also computed at M4 between 12 and 15 m (equation 5.8). Brunt Vaisala frequency is directly proportional to the density gradient, and used to indicate the stability of a water mass (Knauss, 1997). The larger the Brunt Vaisala frequency, the more stable the water column, limiting mixing of sediments between the surface and bottom water.

$$N^2 = \frac{-1 \times g}{\rho_w} \times \frac{d\rho_w}{dz} \quad \text{[Equation 5.8]}$$

where g is the gravitational acceleration, ρ_w is the density of water and z is the depth.

5.4.4.2 SPM Concentration at M4 during Maximum Tidal Range and Maximum Wind Stress

Maximum in situ wind stress (0.28 Nm^{-2}) and the third largest tidal range (0.42 m) occurred on 2 April 2016 at M4 (Figures 5.6 and 5.7). At the start of 2 April, the winds switched from downwelling favorable southeasterly to upwelling favorable northwesterly (Figure 5.4). Ekman transport was evident in the southwestward propagating surface water and northeastward (opposite) propagating bottom water (Figure 5.8). SPM concentration throughout the water column was 7 mgL^{-1} , and increased a few hours later to 20 mgL^{-1} at 6 m and 14 m. Northward propagating Bight water increased the bottom water in situ salinity at 12 and 15 m from 32 to 34 psu and 33 to 35 psu. Bottom water between depths of 12 and 15 m remained well mixed due to the small difference in salinity and Brunt Vaisala ($3 \times 10^{-2} \text{ s}^{-2}$) (Figure 5.10). Northward advection of Bight water reduced the SPM concentration in the bottom water to the background value (3 mgL^{-1}) one hour before low tide. This was followed by an increase in SPM concentration to 7 mgL^{-1} throughout the water column at low tide.

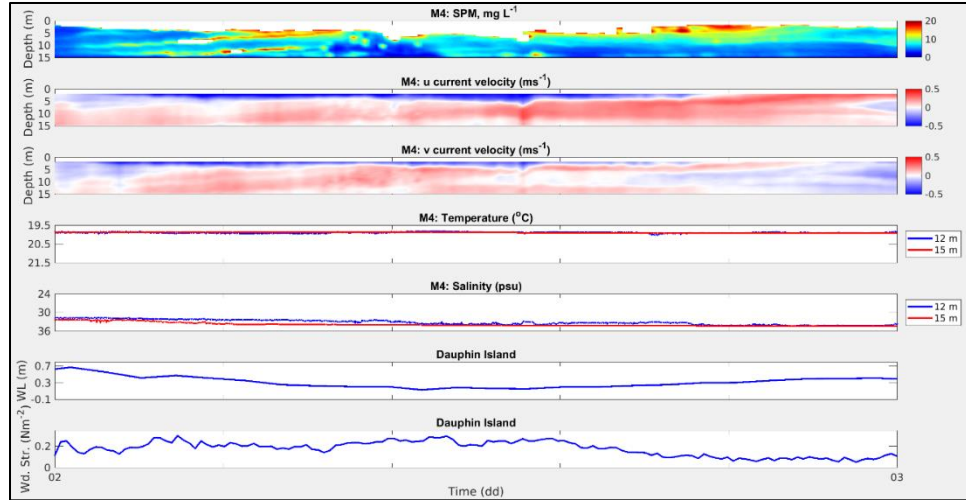


Figure 5.8 M4 April 2016 time series on 2 April

Suspended particulate matter concentration derived from the ADCP's echo intensity (i) ADCP alongshore current velocity (ii) ADCP across shore current velocity (iii) in situ temperature at a depths of 12 m and 15 m (iv) in situ salinity at depths of 12 m and 15 m (v) tidal height with respect to Mean Lower Low Water at NOAA Dauphin Island station, 8735180 (vi) wind stress at NOAA Dauphin Island station, dpia1c (vii).

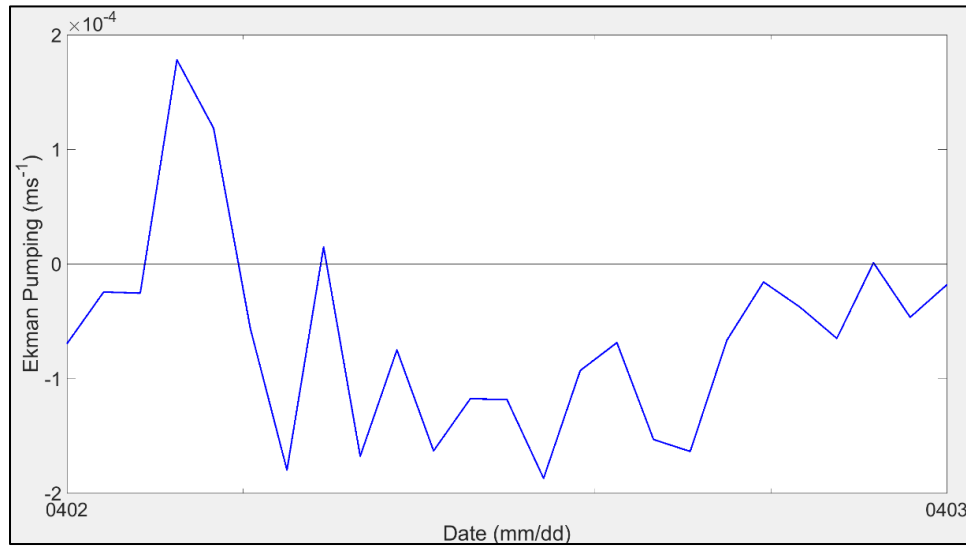


Figure 5.9 Ekman pumping rate between M4 and M5 on 2 April during the third highest tidal range and maximum wind stress

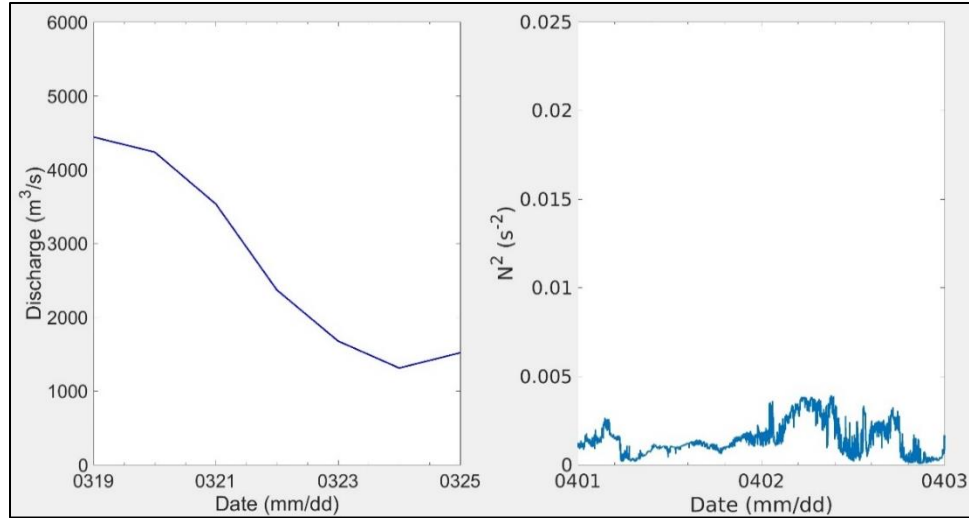


Figure 5.10 River discharge at Tombigbee/Alabama River gauges 7-14 days before 2 April (i) Brunt Vaisala frequency at M4 on 2 April. (ii).

In situ currents showed bottom water moved northward (0.5 ms^{-1}) and eastward (0.4 ms^{-1}) opposite the surface water during flood tide (Figure 5.8). Northward transport of Bight water increased in situ salinity at 12 m to 35 psu, and reduced the SPM concentration between 10 and 15 m to 3 mgL^{-1} . Northwesterly in situ surface winds maintained upwelling conditions during the rising tide and the rate of Ekman pumping decreased (-1.42 to $-0.42 \times 10^{-4} \text{ ms}^{-1}$) as the wind stress decreased (0.25 to 0.08 Nm^{-2}). Decreased wind stress did not affect the maximum SPM concentration (20 mgL^{-1}) observed in the surface water at a depth of 5 m.

5.4.4.3 SPM Concentration at M4 during Maximum Tidal Range and Minimum Wind Stress

M4 experienced the sixth highest tidal range (0.38 m) and second lowest wind stress (0.09 Nm^{-2}) on 13 April (Figures 5.6 and 5.7). Low wind stress resulted in reduced Ekman pumping of $1.28 \times 10^{-4} \text{ ms}^{-1}$ during ebb tide (Figures 5.11 and 5.12). The alongshore current in the surface and bottom water was southward and northward, and the across shore current was southward throughout the water column. High temperature ($21 \text{ }^\circ\text{C}$), fresh (27 psu) water advected southward across the station. The fresh water increased SPM concentration throughout the water column and resulted in maximum SPM concentration between 5 and 10 m. The water column was well stratified due to the advection of warm fresh water, as observed in the increase in Brunt Vaisala to 0.02 s^{-2} (Figure 5.13).

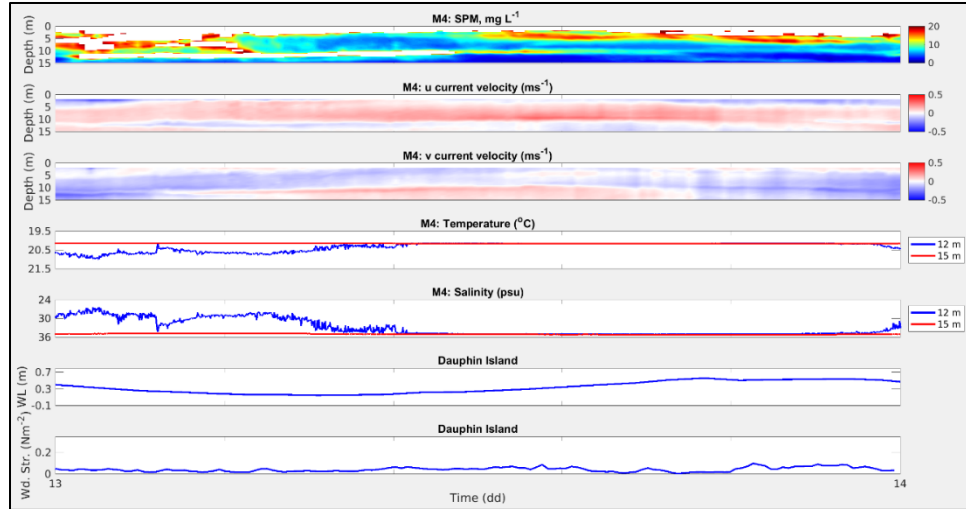


Figure 5.11 M4 April 2016 time series on 13 April

Suspended particulate matter concentration derived from the ADCP's echo intensity (i) ADCP alongshore current velocity (ii) ADCP across shore current velocity (iii) in situ temperature at a depths of 12 m and 15 m (iv) in situ salinity at depths of 12 m and 15 m (v) tidal height with respect to Mean Lower Low Water at NOAA Dauphin Island station, 8735180 (vi) wind stress at NOAA Dauphin Island station, dpia1c (vii).

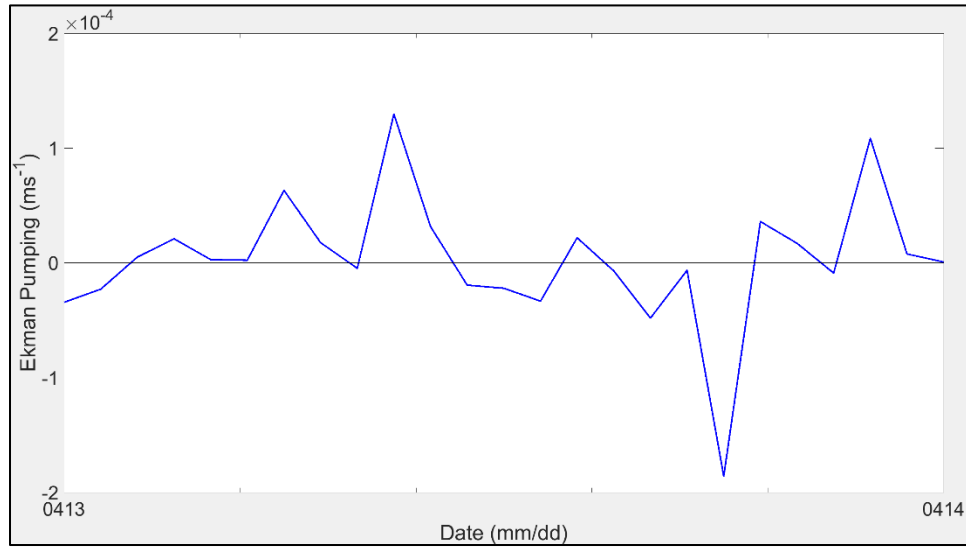


Figure 5.12 Ekman pumping rate between M4 and M5 on 13 April during the sixth highest tidal range and second lowest wind stress

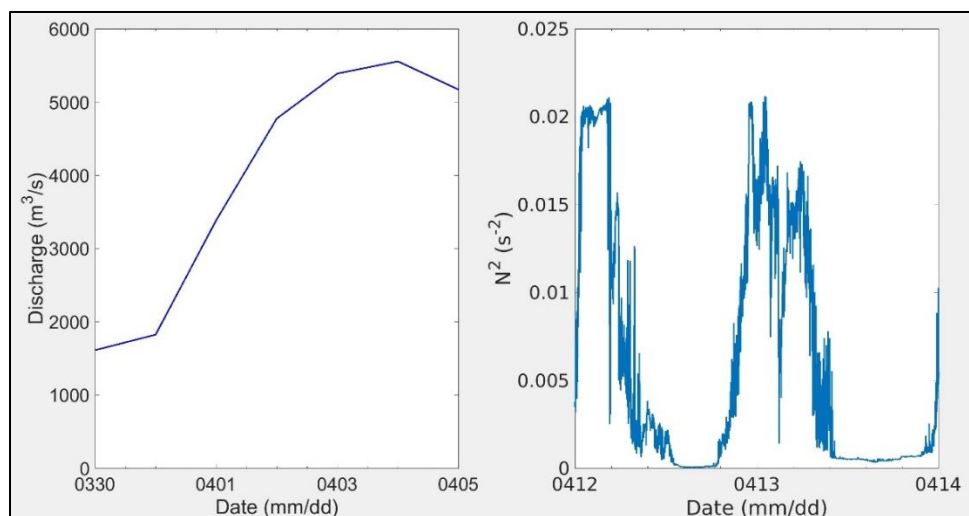


Figure 5.13 River discharge at Tombigbee/Alabama River gauges 7-14 days before 13 April (i) Brunt Vaisala frequency at M4 on 13 April. (ii).

The tide at M4 switched from ebb to flood at 0806 (UTC). Surface (bottom) water in situ alongshore and across shore current velocity switched to eastward (westward) and southward (northward) (Figure 5.11). Temperature decreased to 19.5 °C and salinity increased to 35 psu at 12 m, two hours after low tide and significantly reduced Brunt Vaisala (0.017 to 0.001 s^{-2}) between 12 and 15 m (Figure 5.13). A high salinity, low temperature water mass at a depth of 12 m suggests water propagated shoreward from the Bight during flood tide. SPM concentration decreased from 17 to 7 mgL^{-1} between 5 and 10 m, approximately two hours after low tide. SPM concentration in the river plume remained high (12 to 20 mgL^{-1}), but decreased to 7 mgL^{-1} between 5 and 10 m. SPM concentration also decreased to 3 mgL^{-1} at depths greater than 10 m during flood tide.

5.5 Discussion

5.5.1 SPM Concentration variation at M4 and M5 during cold front events and calm wind conditions

Maximum SPM concentration occurred in the fresh water surface plume exiting Mobile Bay as expected. It was not possible to quantify the SPM concentration within the river plume because the concentration exceeded the maximum in situ SPM concentration (20 mgL^{-1}) used to calibrate the ADCPs. Maximum SPM concentration (20 mgL^{-1}) within the water column occurred during the post cold front phase as the front moved away from the area. Post front northerly winds advected particulate matter from Mobile Bay to MS Bight through Main Pass. During calm wind conditions, southward bottom currents transport sediments into the Bight during ebb tide. Conversely, northward bottom currents transport sediment depleted water northward during flood tide and reduces the SPM concentration south of Main Pass.

5.5.2 SPM Concentration at M4 during Maximum Tidal Range and Minimum/Maximum Wind Stress

River discharge in Mobile Bay affected the concentration of particulate matter transported south into the Bight. It takes approximately 5-9 days for the discharge recorded at Alabama/Tombigbee River to deposit into Mobile Bay (Shroeder, 1979). Total river discharge decreased from $4300 \text{ m}^3\text{s}^{-1}$ within two weeks prior to 2 April, and increased from $1800 \text{ m}^3\text{s}^{-1}$ from 31 March to 6 April (Figures 5.10 and 5.13). The difference in river discharge caused higher SPM concentration in the surface

plume on 13 April during ebb tide. Maximum SPM concentration was observed for approximately 10 hours during ebb tide on 13 April compared to only 4 hours on 2 April.

It was not possible to ascertain the effect of the wind stress (magnitude) on SPM concentration in the Bight since minimum wind stress occurred during increased fresh water discharge from Mobile Bay. Subsequent reduction in the wind stress did not affect SPM concentration in the surface plume when both the tidal range and wind stress were initially high. Wind direction (upwelling favorable/downwelling favorable) and volume of river discharge had a more direct effect on the SPM concentration within the water column, compared to the magnitude of the wind stress.

5.6 Conclusion

During calm wind conditions, the tidal signal has a significant effect on SPM concentration south of Main Pass. The diurnal tide increases the SPM concentration in the Bight during ebb tide and northward advection of SPM depleted water decreases SPM concentration within the water column during flood tide. Post cold front northerly winds advect particulate matter from Mobile Bay south into the Bight and generates the highest SPM concentration during a cold front event. River discharge into Mobile Bay increases the SPM concentration throughout the water column, increases the density gradient in the bottom water, and results in a more stable water column.

CHAPTER VI

6.1 Conclusions

6.1.1 Chapter III

Observations from this study supported the primary hypothesis that the advection of cold saline bottom water resuspended sediments along the seabed and increased the sediment concentration during the cold front event. Southeasterly winds associated with the prefrontal phase of the cold front transported surface water shoreward in Lake Borgne and Mississippi Sound (MS Sound). Increased bed shear due to the offshore advection of high salinity bottom water suspended fine silt along the seabed in Mississippi Bight (MS Bight). Sediment concentration was limited to below the fresh surface water due to the stratified (spring fresh water plume) water column. Clockwise rotation of the winds to northerly resulted in the flushing of estuarine discharge from the Sound into the Bight through the tidal passes. Increased concentration of fine silt in MS Bight was associated with the estuarine discharge as fresh water moved offshore and the denser higher salinity water moved shoreward at depth.

6.1.2 Chapter IV

The primary hypothesis was not satisfied and results showed the suspended particulate matter (SPM) anomaly at Main Pass was negative in spring and summer 2016. The peak Alabama/Tombigbee River discharge was $2800 \text{ m}^3\text{s}^{-1}$ less in winter/spring 2015 compared with winter/spring 2016, but peak discharge occurred in April 2015 and January 2016 respectively. A considerable decline (49% less than 2012-2016 mean) in

summer 2016 discharge followed the early 2016 discharge. Summer 2015 discharge was 19% lower than the five-year mean. The timing of the peak river discharge had a more dominant effect on the SPM at Main Pass than the volume of the discharge in that year.

SPM anomaly was also negative in summer 2016 and positive in summer 2015 at the MS tidal passes. The prevalence of westerly winds in the Sound contributed to the particulate matter anomaly at the surface. A higher frequency and larger mean velocity of the westerly winds at the tidal passes, resulted in the advection of surface waters from the Sound into the Bight and the resuspension of a higher concentration of particulate matter.

6.1.3 Chapter V

Results from analysis of the backscatter derived SPM, in situ data and model data were inadequate to support the primary hypothesis that increased wind stress increases the concentration of SPM via Ekman transport during a cold front. Minimum wind stress coincided with increased fresh water discharge from Mobile Bay into the Bight. Increased discharge resulted in elevated SPM concentration in the river plume during ebb tide. Upwelling/downwelling favorable winds and river discharge volume were the main forcing factors driving the SPM concentration in the Bight.

6.2 Summary

Results presented in this dissertation show the variability of sediments and particulate matter concentrations in MS Sound, Mobile Bay and MS Bight due to river discharge, ocean currents, tides and meteorological parameters. Sediment concentration is maximum in the bottom water during the post cold front period due to the bed shear exerted by the bottom water on the seabed during northerly winds. River discharge and the wind direction (upwelling/downwelling favorable) are two dominant forcing factors for the dispersion of particulate matter in MS Bight during a cold front. The timing of the peak river discharge has important implications for the concentration of particulate matter present in Mobile Bay and Main Pass in spring and summer.

REFERENCES

- Agrawal, Y.C. & H.C. Pottsmith. (2000). Instruments for particle size and settling velocity observations in sediment transport. *Marine Geology*, 168: 89-114. doi: 10.1016/S0025-3227(00)00044-X
- Amante, C.J., M.R. Love, L.A. Taylor and B.W. Eakins. (2011). Digital Elevation Models of Mobile, Alabama: Procedures, Data Sources and Analysis (NESDIS NGDC-44). Boulder, CO: NOAA National Geophysical Data Center. Retrieved from <http://www.ngdc.noaa.gov/dem/squareCellGrid/download/673>
- Arnone, R. (1983). Water Optics of the Mississippi Sound. (Report 63). MS: Remote Sensing Branch, Oceanography Division, Naval Ocean Research Development Activity.
- Balsam, W.L. and J.P. Beeson. (2003). Sea-floor sediment distribution in the Gulf of Mexico. *Deep-Sea Research I*, 50: 1421-1444. doi: 10.1016/j.dsr.2003.06.001
- Bell, G., S. Goldenberg, E. Blake, C. Landsea, J. Schemm, R. Pasch and T. Kimberlain. (2012). The 2012 North Atlantic Hurricane Season a Climate Perspective. NOAA National Weather Service. Miami, FL: NOAA/National Weather Service, National Centers for Environmental Prediction, National Hurricane Center. Retrieved from http://www.cpc.ncep.noaa.gov/products/expert_assessment/hurrsummary_2011.pdf
- Bell, G., E. Blake, C. Landsea, T. Kimberlain, S. Goldenberg, J. Schemm and R. Pasch. (2011). The 2011 North Atlantic Hurricane Season a Climate Perspective. NOAA National Weather Service. NOAA National Weather Service. Miami, FL:

NOAA/National Weather Service, National Centers for Environmental Prediction,
National Hurricane Center. Retrieved from
[http://www.cpc.ncep.noaa.gov/products/expert_assessment/hurrsummary_2012.p
df](http://www.cpc.ncep.noaa.gov/products/expert_assessment/hurrsummary_2012.pdf)

Bryant, W.R., J.R. Bryant, M.H. Feeley and G.R. Simmons. (1990). Physiographic and bathymetric characteristics of the continental slope, northwest Gulf of Mexico. *Geo-Marine Letters*, 10:182-199.

Buczowski, B.J., J.A. Reid, C.J. Jenkins, J.M. Reid, S.J. Williams & J.G. Flocks. (2006). usSEABED: Gulf of Mexico and Caribbean (Puerto Rico and U.S. Virgin Islands) offshore surficial sediment data release: U.S. Geological Survey Data Series 146, version 1.0. Retrieved from <https://pubs.usgs.gov/ds/2006/146/>

Bue, B.G., S. Sharr & J.E. Seeb. (1998). Evidence of damage to Pink Salmon populations inhabiting Prince William Sound, Alaska, two generations after the Exxon Valdez oil spill. *Transactions of the American Fisheries Society*, 127: 35-43. doi: 10.1577/1548-8659(1998)<127, 0035:EODTPS>2.0.CO;2

Bunya, S., J.C. Dietrich, J.J. Westerink, B.A. Ebersole, J.M. Smith, J.H. Atkinson, R. Jensen, D.T. Resio, R.A. Luettich, C. Dawson, V.J. Cardone, A.T. Cox, M.D. Powell, H.J. Westerink and H.J. Roberts. (2010). A High-Resolution Coupled Riverine Flow, Tide, Wind, Wind Wave and Storm Surge Model for Southern Louisiana and Mississippi. Part I: Model Development and Validation. *American Meteorological Society*, 138:345-377.

- Burdin, W.W. (1992). General Design Memorandum Main Report: Pascagoula Harbor Channel Improvement, Pascagoula, Mississippi. Mobile, AL: U.S. Army Core of Engineers.
- Byrnes, M.R., J.D. Rosati, S.F. Griffiee & J.L. Berlinghoff. (2013). Historical sediment transport pathways and quantities for determining an operational sediment budget: Mississippi Sound barrier islands. *Journal of Coastal Research*, 63:166-183. doi: 10.2112/SI63-014.1
- Caress, D.W. and D.N. Chayes. (1996). Improved processing of Hydrosweep DS multibeam data on the R/V Maurice Ewing. *Marine Geophysical Research*, 18:631-650.
- Carlin, J.A., G. Lee, T.M. Dellapenna & P. Laverty. (2016). Sediment resuspension by wind, waves, and currents during meteorological frontal passages in a micro-tidal lagoon. *Estuarine, Coastal and Shelf Science*, 172: 24-33. doi: 10.1016/j.ecss.2016.01.029
- Chen, Q., L. Wang, H. Zhao and S.L. Douglass. (2007). Prediction of Storm Surges and Wind Waves on Coastal Highways in Hurricane-Prone Areas. *Journal of Coastal Research*, 23: 1208+1304-1317.
- Clarke, A.J. & K. Brink. (1985). The response of stratified, frictional flow of shelf and slope waters to fluctuating large-scale, low frequency wind forcing. *Journal of Physical Oceanography*, 15: 439-453.
- Colson, B.E. & E.H. Boswell. (1985). Water-resources overview of the Mississippi Gulf Coast area. MS: United States Geologic Survey.

- Cowen, R.K., A.T. Greer, C.M. Guigand, J.A. Hare, D.E. Richardson & H.J. Walsh. (2013). Evaluation of the In Situ Ichthyoplankton Imaging System (ISIIS): Comparison with the traditional (bongo net) sampler. *Fishery Bulletin*, 111:1-12, <http://dx.doi.org/10.7755/FB.111.1.1>.
- Cowen, R.K., & C.M. Guigand. (2008). In Situ Ichthyoplankton Imaging System (ISIIS): System design and preliminary results. *Limnology and Oceanography: Methods*, 6:126-132, <http://dx.doi.org/10.4319/lom.2008.6.126>
- Crone, T.J. & M. Toltstoy. (2010). Magnitude of the 2010 Gulf of Mexico oil leak. *Science*, 330: 634. doi: 10.1126/science.1195840
- Degens, E.T. (1970). Molecular nature of nitrogenous compounds in seawater and recent marine sediments. In Hood, D.W., *Organic matter in natural waters, Alaska*: University of Alaska
- Deines, K.L. (1999, March). Backscatter estimation using broadband Acoustic Doppler Current Profilers. Paper presented at the IEEE Sixth Working Conference on Current Measurements, San Diego, California, 249-253.
- De Ponca, M.S.F.V., G.S. Manikin, G. DiMego, S.G. Benjamin, D.F. Parrish, R.J. Purser, W.-S. Wu, J.D. Horel, D.T. Myrick, Y. Lin, R.M. Aune, D. Keyser, B. Colman, G. Mann & J. Vavra. (2011). The Real-Time Mesoscale Analysis at NOAA's National Centers for Environmental Prediction: Current status and development. *Weather Forecasting*, 26:593–612, <http://dx.doi.org/10.1175/WAF-D-10-05037.1>

- De Velasco, G.G. & C.D. Winant. (1996). Seasonal patterns of stress and wind stress curl over the Gulf of Mexico. *Journal of Geophysical Research*, 101(C8): 18127-18140. doi: 10.1029/96JC01442.
- Dietrich, J.C., S. Bunya, J.J. Westerink, B.A. Ebersole, J.M. Smith, J.H. Atkinson, R. Jensen, D.T. Resio, R.A. Luetlich, C. Dawson, V.J. Cardone, A.T. Cox, M.D. Powell, H.J. Westerink and H.J. Roberts. (2010). A High-Resolution Coupled Riverine Flow, Tide, Wind, Wind Wave and Storm Surge Model for Southern Louisiana and Mississippi. Part II: Synoptic Description and Analysis of Hurricanes Katrina and Rita. *American Meteorological Society*, 138:378-404.
- Dinnel, S.P., W.W. Schroeder & W.J. Wiseman, Jr. (1990). Estuarine-shelf exchange using Landsat images of discharge plumes. *Journal of Coastal Research*, 6(4): 789-799.
- D'Sa, E.J., R.L. Miller & B.A. McKee. (2007). Suspended particulate matter dynamics in coastal waters from ocean color: Application to the northern Gulf of Mexico. *Geophysical Research Letters*, 34: L23611. doi: 10.1029/2007GL031192
- D'sa, E.J., R.L. Miller & C. Del Castillo. (2006). Bio-optical properties and ocean color algorithms for coastal waters influenced by the Mississippi River during a cold front. *Applied Optics*, 45(28): 7410-7428. doi: 10.1364/AO.45.007410
- Duarte, C.M. (1991). Seagrass depth limits. *Aquatic Botany*, 40 (4): 363-377. doi: 10.1016/0304-3770(91)90081-F
- Dzwonkowski, B., A.T. Greer, C. Briseno-Avena, J.W. Krause, I.M. Soto, F.J. Hernandez, A.L. Deary, J.D. Wiggert, D. Joung, P.J. Fitzpatrick, S.J. O'Brien, S.L. Dykstra, Y. Lau, M.K. Cambazoglu, G. Lockridge, S.D. Howden, A.M.

- Shiller & W.M. Graham. (2017). Estuarine influence on biogeochemical properties of the Alabama shelf during the fall season. *Continental Shelf Research*, 140:96-109.
- Dzwonkowski, B., K. Park, J. Lee, B.M. Webb & A. Valle-Levinson. (2014). Spatial variability of flow over a river-influenced inner shelf in coastal Alabama during spring. *Continental Shelf Research*, 74: 25-34. doi: 10.1016/j.csr.2013.12.005
- Dzwonkowski, B. & K. Park. (2012). Subtidal circulation on the Alabama shelf during the Deepwater Horizon oil spill. *Journal of Geophysical Research*, 117 (C03027). doi: 10.1029/2011JC007664
- Dzwonkowski, B., K. Park, H.K. Ha, W.M. Graham, F.J. Hernandez & S.P. Powers. (2011a). Hydrographic variability on a coastal shelf directly influenced by estuarine outflow. *Continental Shelf Research*, 31:939-950. doi: 10.1016/j.csr.2011.03.001
- Dzwonkowski, B., K. Park & L. Jiang. (2011b). Subtidal across-shelf velocity structure and surface transport effectiveness on the Alabama shelf on the northern Gulf of Mexico. *Journal of Geophysical Research*, 116 (C10012). doi: 10.1029/2011JC007188
- Dzwonkowski, B. & K. Park. (2010). Influence of wind stress and discharge on the mean and seasonal currents on the Alabama shelf of the northeastern Gulf of Mexico. *Journal of Geophysical Research*, 115 (C12052). doi: 10.1029/2010JC006449
- Eisemann, E.R., D.J. Wallace, M.C. Buijsman & T. Pierce. (2018). Response of a vulnerable barrier island to multi-year storm impacts: LIDAR-data-inferred

morphodynamic changes on Ship Island, Mississippi, USA. *Geomorphology*, 313: 58-71. doi: 10.1016/j.geomorph.2018.04.001

Engle, V.D., J.L. Hyland & C. Cooksey. (2009). Effects of Hurricane Katrina on benthic macroinvertebrate communities along the northern Gulf of Mexico coast. *Environmental Monitoring Assessment*, 150:193-209. doi: 10.1007/s10661-008-0677-8

Fairall C. W., E. F. Bradley, J. E. Hare, A. A. Grachev & J. B. Edson. (2003). Bulk parameterization of air-sea fluxes: Updates and verification for the COARE algorithm. *Journal of Climate* 16:571-591.

Fitzpatrick, P. and Lau, Y. (2019) CONCORDE Meteorological Analysis (CMA) Data along the Northern Gulf Coast between April 2015 and December 2016. Distributed by: Gulf of Mexico Research Initiative Information and Data Cooperative (GRIIDC), Harte Research Institute, Texas A&M University-Corpus Christi. doi: 10.7266/N72F7KHX

Flocks, J, J. Kindinger, M. Marot & C. Holmes. (2009). Sediment characterization and dynamics in Lake Pontchartrain, Louisiana. *Journal of Coastal Research*, 54: 113-126. doi: 10.1012/SI54-011.1

Francois, R. E & G.R. Garrison. (1982a). Sound absorption based upon ocean measurements. Part I: pure water and magnesium sulphate contributions. *The Journal of the Acoustical Society of America*, 72: 896-907. doi: 10.1121/1.388170

Francois, R. E & G.R. Garrison. (1982b). Sound absorption based upon ocean measurements. Part II: boric acid contribution and equation for total absorption.

The Journal of the Acoustical Society of America, 72: 1870-1890. doi:
10.1121/1.388673

Fredsoe, J. & R. Deigaard. (1992). Mechanics of Coastal Sediment Transport. In Liu, P.L.F., Advanced Series on Ocean Engineering (Vol. 3). NJ, USA: World Scientific Publishing Co. Pte. Ltd.

Gartner, J.W. (2004). Estimating suspended solids concentrations from backscatter intensity measured by acoustic Doppler current profiler in San Francisco Bay, California. *Marine Geology*, 211: 169-187. doi: 10.1016/j.margeo.2007.07.001

Garvine, R.W. (1995). A dynamical system for classifying buoyant coastal discharge. *Continental Shelf Research*, 15:1585-1596.

Gelfenbaum, G. & R.P. Stumpf. (1993). Observations of currents and density structure across a buoyant plume front. *Estuaries* 16(1): 40-52. doi: 10.2307/1352762.

Glover, D.M., W.J. Jenkins & S.C. Doney. (2011). Modeling methods for Marine Science. Cambridge, UK: Cambridge University Press.

Gornitz, V.M., R.C. Daniels, T.W. White and K.R. Birdwell. (1994). The Development of a Coastal Risk Assessment Database: Vulnerability to Sea-Level Rise in the U.S. Southeast. *Journal of Coastal Research*, Special Issue No. 12:327-338.

Greer, A.T., A.M. Shiller, E.E. Hofmann, J.D. Wiggert, S.J. Warner, S.M. Parra, C. Pan, J.W. Book, D. Joung, S. Dykstra, J.W. Krause, B. Dzwonkowski, I.M. Soto, M.K. Cambazoglu, A.L. Deary, C. Briseno-Avena, A.D. Boyette, J.A. Kastler, V. Sanial, L. Hode, U. Nwankwo, L.M. Chiaverano, S.J. O'Brien, P.J. Fitzpatrick, Y.H. Lau, M.S. Dinniman, K.M. Martin, P. Ho, A.K. Mojziz, S.D. Howden, F.J. Hernandez, I. Church, T.N. Miles, S. Sponaugle, J.N. Moum, R.A. Arnone, R.K.

- Cowen, G.A. Jacobs, O. Schofield & W.M. Graham. (2018). Functioning of coastal river-dominated ecosystems and implications for oil spill response: From observations to mechanisms and models. *Oceanography*, 31(3). doi: 10.5670/oceanog.2018302
- Greer, A.T., R.K. Cowen, C.M. Guigand & J.A. Hare. (2015). Fine-scale planktonic habitat partitioning at a shelf-slope front revealed by a high resolution imaging system. *Journal of Marine Systems*, 142: 111-125. doi: 10.1016/j.jmarsys.2014.10.008
- Ha, H.K. & K. Park. (2012). High-resolution comparison of sediment dynamics under different forcing conditions in the bottom boundary layer of a shallow, micro-tidal estuary. *Journal of Geophysical Research*, 117: C06020. doi: 10.1029/2012JC007878.
- Hardin, J.D., C.D. Sapp, J.L. Emplaincourt & K.E. Ritcher. (1976). Shoreline and bathymetric changes in the coastal area of Alabama, a remote-sensing approach. (Alabama Geologic Survey Information Series 50). AL: Alabama Geologic Survey.
- Huang, W. & C. Li. (2017). Cold front driven flows through multiple inlets of Lake Pontchartrain Estuary. *Journal of Geophysical Research: Oceans*, 122: 8627-8645. doi: 10.1002/2017JC012977
- Hudson, P.F. & J. Mossa. (1997). Suspended sediment transport effectiveness of three large impounded rivers, U.S. Gulf Coast Plain. *Environmental Geology*, 32(4): 263-273. doi: 10.1007/s002540050216

- Huh, O.K., N.D. Walker & C. C. Moeller. (2001). Sedimentation along the eastern Chenier Plain coast: down drift impact of a delta complex shift. *Journal of Coastal Research*, 17:72-81.
- Hummell, J.P. (1990). Main Pass and ebb-tidal delta of Mobile Bay, Alabama. (Circular no. -146). AL: Geological Survey of Alabama.
- Imran, J. (2008). Sediment Transport. In Chaudhry, M.H., *Open-Channel Flow* (2nd ed.). MA, USA: Springer. doi: 10.1007/978-0-387-68648-6_16
- Ischen, M. (2009). Using two-dimensional numerical models to analyze hydraulic effects of constricted flows through the Rigolet Pass between Lake Pontchartrain and Lake Borgne (Master's thesis). Retrieved from Scholar Works, University of New Orleans.
- Isphording, W.C., F.D. Imsand & R.B. Jackson. (1996). Fluvial Sediment Characteristics of the Mobile River Delta. *Transactions of the Gulf Coast Association of Geological Societies*, 46: 185-191.
- Jacobs, W. (2004). Modelling the Rhine River Plume (Master's Thesis). Retrieved from TUDelf, Faculty of Civil Engineering and Geosciences, Hydraulic Engineering. uuid: cf8e752d-7ba7-4394-9a94-2b73e14f9949.
- Jarrell, J.P. (1981). Hydrodynamics of Mobile Bay and MS Sound-Pass exchange studies. (Report no. 271-112). AL: College of Engineering, University of Alabama.
- Jensen, J.R. (2007). *Remote Sensing of the Environment: An Earth Resource Perspective* (2nd Edition). NJ, U.S.A: Pearson Prentice Hall
- Jones, K.H. (1998). A comparison of algorithms used to compute hill slope as a property of the DEM. *Computers & Geosciences*, 24(4): 315-323.

- Kapucu, N. (2012). Disaster and emergency management systems in urban areas. *Cities*, 29:S41-S49. doi:10.1016/j.cities.2011.1.009
- Karpen, V., L. Thomsen & E. Suess. (2004). A new 'schlieren' technique application for fluid flow visualization at cold seep sites. *Marine Geology*, 204: 145-159. doi: 10.1016/S0025-3227(03)00370-0
- Keen, T.R. (2002). Waves and currents during a winter cold front in the Mississippi Bight, Gulf of Mexico: implications for barrier island erosion. *Journal of Coastal Research*, 18(4): 622-636.
- Kennicutt, M.C., W.W. Schroeder & J.M. Brooks. (1995). Temporal and spatial variations in sediment characteristics on the Mississippi-Alabama continental shelf. *Continental Shelf Research*, 15:1-18.
- Khelifa, A., P. Stoffyn-Egli, P.S. Hill & K. Lee. (2005). Effects of salinity and clay type on oil-mineral aggregation. *Marine Environmental Research*, 59: 235-254. doi: 10.1016/j.marenvres.2004.05.003
- Kim, Y.H., B. Gutierrez, T. Nelson, A. Dumars, M. Maza, H. Perales & G. Voulgaris. (2004). Using the acoustic Doppler current profiler (ADCP) to estimate suspended sediment concentration (CPSD #04-01). Columbia, S.C.: Coastal Processes Sediment Dynamics Laboratory, Department of Geological Sciences, University of South Carolina. Retrieved from http://seoe.sc.edu/gvoulgar/TechReports/CPSD_TechReport_04_02.pdf
- Kineke, G.C., E.E. Higgins, K. Hart & D. Velasco. (2006). Fine-sediment transport associated with cold-front passages on the shallow shelf, Gulf of Mexico. *Continental Shelf Research*, 26: 2073-2091. doi: 10.1016/j.csr.2006.07.023

- Kjerfve, B. & J.E. Sneed. (1984). Analysis and synthesis of oceanographic conditions in the Mississippi Sound offshore region (Volume 1). SC: University of South Carolina Department of Geology.
- Knabb, R.D., J.R. Rhome and D.P. Brown. (2005). Tropical Cyclone Report Hurricane Katrina 23-30 August 2005. NOAA National Hurricane Center. NOAA National Weather Service. NOAA National Weather Service. Miami, FL: NOAA/National Weather Service, National Centers for Environmental Prediction, National Hurricane Center. Retrieved from http://www.nhc.noaa.gov/pdf/TCR-AL122005_Katrina.pdf
- Knauss, J.A. (1997). Introduction to Physical Oceanography (2nd Edition). IL, U.S.A: Waveland Press Inc.
- Landers, M.N., T.D. Straub, M.S. Wood & M.M. Domanski. (2016). Sediment acoustic index method for computing continuous suspended-sediment concentrations: U.S. Geological Survey Techniques and Methods, 3-C5. Reston, Virginia: U.S. Geological Survey
- Liu, H., K.C. Jezek & B. Li. (1999). Development of an Antarctic digital elevation model by integrating cartographic and remotely sensed data: a geographic information system based approach. *Journal of Geophysical Research*, 104(B10): 23,199-23,213.
- Lohrmann, A. (2001). Monitoring sediment concentration with acoustic backscattering instruments (Report No. 003). Norway: Nortek.
- Love, M.R., C.J. Amante, B.W. Eakins and L.A. Taylor. (2012). Digital Elevation Models of the Northern Gulf Coast: Procedures, Data Sources and Analysis.

- (NESDIS NGDC-59). Boulder, CO: NOAA National Geophysical Data Center.
Retrieved from: <http://www.ngdc.noaa.gov/dem/squareCellGrid/download/742>
- Love, M.R., C.J. Amante, L.A. Taylor and B.W. Eakins. (2011). Digital Elevation Models of New Orleans, Louisiana: Procedures, Data Sources and Analysis (NESDIS NGDC-49). Boulder, CO: NOAA National Geophysical Data Center.
Retrieved from:
http://docs.lib.noaa.gov/noaa_documents/NESDIS/NCEI/TM/NOAA_TM_NESDIS_NCEI_49.pdf
- Lynch, J.F., J.D. Irish, C.R. Sherwood & Y.C. Agrawal. (1994). Determining suspended sediment particle size information from acoustical and optical backscatter measurements. *Continental Shelf Research*, 14: 1139-1165.
- Michel, J., E.H. Owens, S. Zenegel, A. Graham, Z. Nixon, T. Allard, W. Holton, P.D. Reimer, A. Lamache, M. White, N. Rutherford, C. Childs, G. Mauseth, G. Challenger & E. Taylor. (2013). Extent and degree of shoreline oiling: Deepwater Horizon Oil Spill, Gulf of Mexico, USA. *PLoS ONE*, 8(6): e65087. doi: 10.1371/journal.pone.0065087
- Mikkelsen, O.A., T.G. Milligan, P.S. Hill, R.J. Chant, C.F. Jago, S.E. Jones, V. Kristov & G. Mitchelson-Jacob. (2008). The influence of schlieren on in situ optical measurements used for particle characterization. *Limnology and Oceanography: Methods*, 6: 133-143. doi: 10.4319/lom.2008.6.133
- Miles, T., G. Seroka, J. Kohut, O. Schofield & S. Glenn. (2015). Glider observations and modeling of sediment transport in Hurricane Sandy. *Journal of Geophysical Research: Oceans*, 120: 1771-1791. doi: 10.1002/2014JC010474.

- Mitchum, G.T. & A.J. Clarke. (1986). The frictional nearshore response to forcing by synoptic scale winds. *Journal of Physical Oceanography*, 16:934-946
- Mobley, C.D. (1994). *Light and Water*. CA, USA: Academic Press.
- Moeller, C.C., O.K. Huh, H.H. Roberts, L.E. Gumley & W.P. Menzel. (1993). Response of Louisiana coastal environments to a cold front passage. *Journal of Coastal Research*, 9:434-447.
- Morey, S.L., J. Zavala-Hidalgo & J.J. O'Brien. (2005). The seasonal variability of continental shelf circulation in the northern and western Gulf of Mexico from a high-resolution numerical model. In Sturges, W. & A. Lugo-Fernandez, *Circulation of the Gulf of Mexico: Observations and Models*, Geophysical Monograph Series, vol. 161: 203-218. Washington, D.C., USA: American Geophysical Union.
- Morey, S.L., P.J. Martin, J.J. O'Brien, A.A. Wallcraft & J. Zavala-Hidalgo. (2003). Export pathways for river discharged fresh water in the northern Gulf of Mexico. *Journal of Geophysical Research*, 108 (C10): 3303. doi: 10.1029/2002JC001674.
- Moriarty, J.M., C.K. Harris & M.G. Hadfield. (2014). A hydrodynamic and sediment transport model for the Waipaooa Shelf, New Zealand: sensitivity of fluxes to spatially-varying erodibility and model nesting. *Journal of Marine Science and Engineering*, 2:336-369. doi: 10.3390/jmse2020336
- Murawski, S.A., J.W. Fleeger, W.F. Patterson III, C. Hu, K. Daly, I. Romero & G.A. Toro-Farmer. (2016). How did the Deepwater Horizon oil spill affect coastal and continental shelf ecosystems of the Gulf of Mexico? *Oceanography*, 29(3): 160-173. doi: 10.5670/oceanog.2016.80.

- Muschenheim, D.K. & K. Lee. (2002). Removal of oil from the sea surface through particulate interactions: review and prospectus. *Spill Science and Technology Bulletin*, 8(1): 9-18. doi: 10.1016/S1353-2561(02)00129-9
- NASA Goddard Space Flight Center, Ocean Biology Processing Group. (2016): Moderate Resolution Imagine Spectroradiometer (MODIS) Ocean Color Data, NASA OB.DAAC, Greenbelt, MD, USA.
<http://oceandata.sci.gsfc.nasa.gov/MODIS-Aqua/L1>. Accessed 2014/05/21.
Maintained by NASA Ocean Biology Distributed Active Archive Center (OB.DAAC), Goddard Space Flight Center, Greenbelt MD.
- National Geophysical Data Center. (2012). [Map of the NGDC Digital Elevation Models superimposed on the digital elevation model hillshades]. Retrieved 4 April 2012 from: <http://maps.ngdc.noaa.gov/viewers/bathymetry/>
- National Geophysical Data Center. (n.d). NGDC 3 Arc Second Coastal Relief Model Development. Boulder, CO. Retrieved 30 April 2012, from: <http://www.ngdc.noaa.gov/mgg/coastal/model.html>
- National Ocean Service. (2017). Hydrographic surveys specifications and deliverables. Retrieved from <https://nauticalcharts.noaa.gov/publications/docs/standards-and-requirements/specs/hssd-2017.pdf>
- Newcome, R., Jr., D.E. Shattles & C.P. Humphreys, Jr. (1968). Water for the growing needs of Harrison County Mississippi. Washington, D.C.: United States Geological Survey.
- Northern Gulf Coastal Hazards Collaboratory. (2012). Northern Gulf Coastal Hazards Collaboratory (NG-CHC) Second Annual Report to National Science Foundation

(2011/2012). Retrieved 2 May 2012 from:

http://ngchc.org/sites/default/files/public_files/NG-

[CHC%202ndAnnRpt_FINAL.pdf](#)

Passow, U., K. Ziervogel, V. Asper & A. Diercks. (2012). Marine snow formation in the aftermath of the Deepwater Horizon oil spill in the Gulf of Mexico.

Environmental Research Letters, 7(3): 035301. doi: 10.1088/1748-

9326/7/3/035301

Perez, B.C., J.W. Day, Jr., L.J. Rouse, R.F. Shaw & M. Wang. (2000). Influence of

Atchafalaya River discharge and frontal passage on suspended sediment

concentration and flux in Fourleague Bay, Louisiana. *Estuarine, Coastal and Shelf*

Science, 50:271-290. doi: 10.1006/ecss.1999.0564

Priddy, R.R., R.M. Crisler, C.P. Sebren, J.D. Powell & H. Burford. (1955). Sediments of

Mississippi Sound and inshore waters. (Bulletin 82). MS: Mississippi State

Geological Survey.

Reddy, C.M., J.S. Arey, J.S. Seewald, S.P. Sylva, K.L. Lemkau, R.K. Nelson, C.A.

Carmichael, C.P. McIntyre, J. Fenwick, G.T. Ventura & B.A. Van Mooy. (2012).

Composition and fate of gas and oil released to the water column during the

Deepwater Horizon oil spill. *Proceedings of the National Academy of Sciences of*

the United States of America, 109(50): 20229-20234. doi:

10.1073/pnas.1101242108

Richards, S.D., Heathershaw, A.D. & Thorne, P.D. (1996). The effects of suspended

particle matter on sound attenuation in seawater. *Journal of Acoustical Society of*

America, 100 (3), 1447-1450. doi: 10.1121/1.415991

- Roberts, H.H., O.K. Huh, L.J.Jr. Rouse & D. A. Rikman. (1989). Winter storm impacts on the Chenier Plain coast of southwestern Louisiana. *Gulf Coast Association of Geological Societies Transactions*, 39: 515-522.
- Ross, T & R. Lueck. (2003). Sound scattering from oceanic turbulence. *Geophysical Research Letters*, 30(6): 1344. doi: 10.1029/2002GL016733
- Ryan, J.J. (1969). A sedimentologic study of Mobile Bay, Alabama (Contribution no. 30). FL: Florida State University Department of Geology.
- Sackett, W. M. (1978). Suspended matter in seawater. In Riley, J.P. & R. Chester, *Chemical Oceanography* (Vol. 3). London, England: Academic Press.
- Sager, W.S., W.W. Schroeder, J.S. Laswell, K.S. Davis, R. Rezak and S.R. Gittings. (1992). Mississippi-Alabama outer continental shelf topographic features formed during the Late Pleistocene-Holocene Transgression. *Geo-Marine Letters*, 12:41-48.
- Salisbury, E.J., J.W. Campbell, E. Linder, L.D. Meeker, F.E. Muller-Karger & C.J. Vorosmarty. (2004). On the seasonal correlation of surface particle fields with wind stress and Mississippi discharge in the northern Gulf of Mexico. *Deep-Sea Research II*, 51:1187-1203.
- Sawyer, W.B., C. Vaughan, D. Lavoie, Y. Furukawa, N. Carnaggio, J. Maclean & E. Populis. (2001). Northern Gulf Littoral Initiative (NGLI), Geology and Physical Properties of Marine Sediments in the N.E. Gulf of Mexico: Data Report. MS: Naval Research Laboratory.
- Schardin, H. (1942). The schlieren process and their applications. *Ergebnisse Der Exakten Naturwissenschaften*, 20: 304-405.

- Schroeder, W.W. (1979). Dispersion and impact of Mobile River System waters in Mobile Bay, Alabama. Water Resources Institute Bulletin 37. Water Resources Research Institute, Auburn University, Auburn, Alabama, 48.
- Sequoia. (2013). Laser In Situ Scattering and Transmissometry-100X Particle Size Analyzer: User's Manual. WA: Sequoia Scientific Inc.
- Sheng, Y.P. (1983). Mathematical Modeling of three-dimensional coastal currents and sediment dispersion: model development and application (CERC-83-2). Princeton, NJ.
- Shields, I.A. (1936). Application of similarity principle and turbulence research to bed-load movement. (Publication No. 167). CA: United States Department of Agriculture, Soil Conservation Service.
- Sikora, W.B., & B. Kjerfve. (1985). Factors Influencing the Salinity Regime of Lake Pontchartrain, Louisiana, a Shallow Coastal Lagoon: Analysis of a Long-Term Data Set. *Estuaries*, 8:170-180.
- Smyth, W.D. & J.N. Moum. (2012). Ocean mixing by Kelvin-Helmholtz instability. *Oceanography*, 25(2): 140-149. doi: 10.5760/oceanog.2012.49
- Stokes, G.G. (1850). On the effects of the internal friction of fluids on the motion of pendulums. *Transactions of the Cambridge Philosophical Society*, 9: 8-106.
- Stumpf, R.P., G. Gelfenbaum & J.R. Pennock. (1993). Wind and tidal forcing of a buoyant plume, Mobile Bay, Alabama. *Continental Shelf Research*, 13: 1281-1301.
- Sullivan, M. (2008). *Fundamentals of Statistics* (2nd ed.). New Jersey: Pearson Education, Inc.

- Sumaila, U.R., A.M. Cisneros-Montemayor, A. Dyck, L. Huang, W. Cheung, J. Jacquet, K. Kleisner, V. Lam, A. McCrea-Strub, W. Swartz, R. Watson, D. Zeller & D. Pauly. (2012). Impact of the Deepwater Horizon well blowout on the economics of U.S. Gulf fisheries. *Canadian Journal of Fisheries and Aquatic Sciences*, 69:499-510. doi: 10.1139/F2011-171
- Taylor, L.A., B.W. Eakins, K.S. Carignan, R.R. Warnken, T. Sazonova and D.C. Schoolcraft. (2008). Digital Elevation Model of Biloxi, Mississippi: Procedures, Data Sources and Analysis. (NESDIS NGDC-9). Boulder, CO: NOAA National Geophysical Data Center. Retrieved from <http://www.ngdc.noaa.gov/dem/squareCellGrid/download/241>
- Taylor, K.E. (2001). Summarizing multiple aspects of model performance in a single diagram. *Journal of Geophysical Research*, 106: 7183-7192. doi: 10.1029/2000JD900719
- Thorne, P.D. & D.M. Hanes. (2002). A review of acoustic measurement of small-scale sediment processes. *Continental Shelf Research*, 22(4): 603-632. doi: 10.1016/S0278-4343(01)00101-7
- Thorne, P.D., C. Manley & J. Brimelow. (1993). Measurements of form function and total scattering cross section for a suspension of spheres. *Journal of Acoustical Society of America*, 93(1): 243-248. doi: 10.1121/1.405658
- Tolman, H.L. & WAVEWATCH III Development Group. (2014). User manual and system documentation of WAVEWATCH III version 4.18 (Report No. MMAB Contribution No. 316). MD: U.S.A.

- Topler, A. (1867). About the method of streaking observations as a microscopic tool and remarks on the theory of oblique lighting. *Poggendorf's Annalen der Physik and Chemie*, 127: 556-580.
- Twilley, R., S. Brandt, D. Breaux, J. Cartwright, J. Chen, G. Easson, P. Fitzpatrick, K. Fridley, S. Graves, S. Harper, C. Kaiser, A. Maestre, M. Maskey, W. McAnally, J. McCorquodale, E. Meselhe, T. Miller-Way, K. Park, J. Pereira, T. Richardson, J. Tao, A. Ward, J. Wiggert, and D. Williamson, Simulation Management Systems Developed by the Northern Gulf Coastal Hazards Collaboratory (NG-CHC): An Overview of Cyberinfrastructure to Support the Coastal Modeling Community in the Gulf of Mexico, in *Remote Sensing and Modeling*, edited by C. W. Finkl and C. Makowski, pp. 365-394, 10.1007/978-3-319-06326-3_15, Springer International Publishing, 2014.
- Uchupi, E. (1967). Bathymetry of the Gulf of Mexico. *Transactions-Gulf Coast Association of Geological Societies*, 17: 161-172.
- United States Army Corps of Engineers. (2018). Spillway Operation Information. New Orleans: LA. Department of Defense. Retrieved from <https://www.mvn.usace.army.mil/Missions/Mississippi-River-Flood-Control/Bonnet-Carre-Spillway-Overview/Spillway-Operation-Information/>
- United States Environmental Protection Agency. (1982). *Methods for the chemical analysis of water and wastes (EPA-600/4-79-020)*. Cincinnati, OH: Environmental Monitoring and Support Laboratory. Retrieved from https://www.wbdg.org/FFC/EPA/EPACRIT/epa600_4_79_020.pdf

- Urick, R.J. (1948). The absorption of sound in suspensions of irregular particles. *Journal of Acoustical Society of America*, 20: 283-289. doi: 10.1121/1.1906373
- Valle-Levinson, A. (2010). *Contemporary Issues in Estuarine Physics*. United Kingdom: Cambridge University Press.
- Virmani, J.I. & R.H. Weisberg. (2003). Features of the observed annual ocean-atmosphere flux variability on the west Florida shelf. *Journal of Climate*, 16: 734-745.
- Vincent, C.E. (2007). Measuring suspended sand concentration using acoustic backscatter: a critical look at the errors and uncertainties. Geological Society, London, *Special Publications*, 274:7-15. doi: 10.1144/GSL.SP.2007.274.01.02
- Walker, N.D., W. Wiseman Jr. & A. Babin. (2005). Effects of river discharge, wind stress and slope eddies on circulation and the satellite observed structure of the Mississippi River plume. *Journal of Coastal Research*, 21:1228-1244.
- Walker, N.D. & A. Hammack. (2000). Impacts of winter storms on circulation and sediment transport: Atchafalaya-Vermillion Bay region, Louisiana, U.S.A. *Journal of Coastal Research*, 16:996-1010.
- Walker, H.J., J.M. Coleman, H.R. Roberts & R.S. Tye. (1989). Wetland loss in Louisiana. *Geografiska Annaler*, 69A (1): 189-200.
- Warner, J.C., B. Armstrong, R. He & J.B. Zambon. (2010). Development of a coupled ocean atmosphere-wave-sediment transport (COAWST) modeling system. *Ocean Model*, 35:230-244. doi: 10.1016/j.ocemod.2010.07.010
- Warner, J.C., C.R. Sherwood, R.P. Signell, C.K. Harris & H.G. Arango. (2008a). Development of a three-dimensional, regional, coupled wave, current, and

- sediment-transport model. *Computers and Geosciences*, 34: 1284-1306. doi:
10.1016/j.cageo.2008.02.012
- Warner, J.C., B. Butman & P.S. Dayander. (2008b). Storm-driven sediment transport in
Massachusetts Bay. *Continental Shelf Research*, 28: 257-282. doi:
10.1016/j.csr.2007.08.008
- Weisberg, R.H., R. He, Y. Li & J.I. Virmani. (2005). West Florida shelf circulation on
synoptic, seasonal and interannual time scales. In Sturges W. & A. Lugo-
Fernandez, *Circulation in the Gulf of Mexico*. Washington, D.C., USA: The
National Academic Press
- Wentworth, C.K. (1922). A scale of grade and class terms for clastic sediments. *The
Journal of Geology*, 30 (5): 377-392.
- Wessel, P., W.H.F. Smith, R. Scharroo, J. Luis and F. Wobbe. (2013). *Generic Mapping
Tools: Improved version released*. *EOS, Transactions American Geophysical
Union*, 94 (45):409-410. doi: 10.1002/2013EO450001
- Wessel, P. and W.H.F. Smith. (1998). *New, improved version of the Generic Mapping
Tools released*. *EOS, Transactions American Geophysical Union*, 79 (47):579.
doi: 10.1029/98EO00426
- Wessel, P. and W.H.F. Smith. (1995). *New version of the Generic Mapping Tools
released*. *EOS, Transactions American Geophysical Union*, 76 (33):329. doi:
10.1029/95EO00198.
- Wessel, P. and W.H.F. Smith. (1991). *New software helps map and display data*. *EOS,
Transactions American Geophysical Union*, 72 (41):445-446. doi:
10.1029/90EO00319.

- Whitney, M.M., & R.W. Garvine. (2005). Wind influence on a coastal buoyant outflow. *Journal of Geophysical Research*, 110: C03014. doi: 10.1029/2003JC002261
- Wiberg, P.L. & C.R. Sherwood. (2008). Calculating wave-generated bottom orbital velocities from surface-wave parameters. *Computer & Geosciences*, 34 (10): 1243-1262. doi: 10.1016/j.cageo.2008.02.010
- Wiggert, J., S.J. O'Brien & D.W. Dodd. (2018a) Bathymetric Dynamic Digital Elevation Model for the Northern Gulf of Mexico. Distributed by: Gulf of Mexico Research Initiative Information and Data Cooperative (GRIIDC), Harte Research Institute, Texas A&M University-Corpus Christi. doi: 10.7266/N747488G.
- Wiggert, J.D., S.J. O'Brien, S. Dykstra, B. Dzwonkowski, D.J. Wallace & G. Lockridge. (2018b). LISST-100X (type B) grain size distribution, sediment distribution, Mobile Bay river plume, March-April 2016. Distributed by: Gulf of Mexico Research Initiative Information and Data Cooperative (GRIIDC), Harte Research Institute, Texas A&M University-Corpus Christi. doi: 10.7266/N7D798F3
- Wiggert, J.D., S.J. O'Brien, S. Dykstra, B. Dzwonkowski, D.J. Wallace & G. Lockridge. (2018c). Total Suspended Solids in situ data, northern Gulf of Mexico, Mobile Bay river plume, March-April 2016. Distributed by: Gulf of Mexico Research Initiative Information and Data Cooperative (GRIIDC), Harte Research Institute, Texas A&M University-Corpus Christi. doi: 10.7266/N74Q7S2Z
- Wiggert, J., Pan, C., Dinniman, M., Hofmann, E. and Cambazoglu, K. (2018d) Physical Model of the Mississippi Sound and Bight, from January 13 to February 13, 2016. Distributed by: Gulf of Mexico Research Initiative Information and Data

Cooperative (GRIIDC), Harte Research Institute, Texas A&M University-Corpus Christi. DOI: 10.7266/N7P55M4G.

Wiggert, J., Pan, C., Dinniman, M. and Hofmann, E. (2018e) Biogeochemical Model of the Mississippi Sound and Bight, from March 17 to April 18, 2016. Distributed by: Gulf of Mexico Research Initiative Information and Data Cooperative (GRIIDC), Harte Research Institute, Texas A&M University-Corpus Christi. doi: 10.7266/N7125R1V.

Wiggert, J., Pan, C., Dinniman, M., Hofmann, E. and Cambazoglu, K. (2018f) Physical Model of the Mississippi Sound and Bight, from July 14 to August 15, 2016. Distributed by: Gulf of Mexico Research Initiative Information and Data Cooperative (GRIIDC), Harte Research Institute, Texas A&M University-Corpus Christi. doi: 10.7266/N7ZP44QK.

Wiggert, J. and O'Brien, S. J. (2018g) Time series of MODIS-Aqua 8-days Suspended Particles Matter (SPM) composites from 2012 to 2016 for the northern Gulf of Mexico. Distributed by: Gulf of Mexico Research Initiative Information and Data Cooperative (GRIIDC), Harte Research Institute, Texas A&M University-Corpus Christi. DOI: 10.7266/N76W98FS.

Wiggert, J., Pan, C., Dinniman, M. and Hofmann, E. (2018h) Biogeochemical Model of the Mississippi Sound and Bight, from March 17 to April 18, 2016. Distributed by: Gulf of Mexico Research Initiative Information and Data Cooperative (GRIIDC), Harte Research Institute, Texas A&M University-Corpus Christi. doi: 10.7266/N7125R1V.

- Wiggert, J.D., R.R. Hood & C.W. Brown. (2017). Modeling Hypoxia and Its Ecological Consequences in Chesapeake Bay in Modeling Coastal Hypoxia: Numerical Simulations of Patterns, Controls and Effects of Dissolved Oxygen Dynamics, D. Justic, R.D. Hetland, K.A. Rose and K. Fennel, ed., Vol. Springer, 119-147.
- Wiseman, W.J., R.E. Turner, F.J. Kelly, L.J. Rouse & R.F. Shaw. (1986). Analysis of biological and chemical associations near a turbid coastal front during winter 1982. *Contributions in Marine Science*, 29: 141-151.
- Woodard, K.C. (2014). Exploration of biophysical interactions associated with mesoscale variability in the central Gulf of Mexico (Master's thesis). Retrieved from The Aquila Digital Community, The University of Southern Mississippi.
- Xu, K., R.C. Mickey, Q. Chen, C.K. Harris, R.D. Hetland, K. Hu & J. Wang. (2016). Shelf sediment transport during hurricanes Katrina and Rita. *Computer & Geosciences*, 90: 24-39. doi: 10.1016/j.cageo.2015.10.009
- Xu, J., E.P. Myers, I. Jeong and S.A. White. (2013). VDatum for the coastal waters of Texas and western Louisiana: tidal datums and topography of the sea surface (NOS CS 29). Silver Spring, MD: NOAA National Oceanic and Atmospheric Administration
- Yang, Z., E.P. Myers and S.A. White. (2010). VDatum for eastern Louisiana and Mississippi coastal waters: tidal datums, marine grids, and sea surface topography (NOS CS 19). Silver Spring, MD: NOAA National Oceanic and Atmospheric Administration

Zang, Z., Z.G. Xue, S. Bao, Q. Chen, N.D. Walker, A.S. Haag, Q. Ge & Z. Yao. (2018).

Numerical study of sediment dynamics during hurricane Gustav. *Ocean*

Modelling, 126:29-42. doi: 10.1016/j.ocemod.2018.04.002

Zhao, H., Q. Chen, N.D. Walker, Q. Zheng & H.L. Mac Intyre. (2011). A study of

sediment transport in a shallow estuary using MODIS imagery and particle

tracking simulation. *International Journal of Remote Sensing*, 32 (21): 6653-

6671.